Xi Li Unfolding the Early Fatigue Damage Accumulation for Cross-ply Laminates

Unfolding the Early Fatigue Damage Accumulation for Cross-ply Laminates

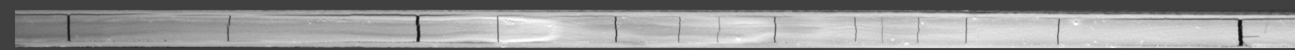

Xi Li

INVITATION

You are kindly invited to the public defence of my PhD dissertation entitlted

Unfolding the Early Fatigue Damage Accumulation for Cross-ply Laminates

On Thursday,
the 8th of September 2022
at 12:30 hrs

In the Senate Hall of the Aula Congress Centre of the Delft University of Technology, Mekelweg 5, 2628 CC, Delft, The Netherlands

Prior to the defence, at 12:00 hrs, I will give a brief overview of my PhD work.

Xi Li
Xi.Li@tudelft.nl

TU Delft

Propositions

accompanying the dissertation

UNFOLDING THE EARLY FATIGUE DAMAGE ACCUMULATION FOR CROSS-PLY LAMINATES

by

Xi LI

1. Involving multiple structural health monitoring techniques during mechanical testing is needed for achieving a reliable damage monitoring of non-transparent composites.
2. Instead of the non-interactive damage scheme, an interactive damage scheme should be used to describe the fatigue damage accumulation process of fibre-reinforced polymer laminates.
3. Modelling is not a necessity to experimental analysis, but experimental validation is a must for modelling.
4. Due to the corona pandemic, we know how to clean our hands in a professional way to get rid of germs.
5. Personal feeling is the best advisor for decision making.
6. To guarantee a pleasant biking trip during the wintertime in Netherlands, checking the weather forecast is highly recommended.
7. Knowledge is priceless but creating and accessing the knowledge has a price.
8. Replacing plastics to other ‘green’ alternatives is not eco-friendly, as the core to protect the environment should be how to reduce our human beings’ exploitation from the earth.
9. Fairness is not absolute but relative.
10. People should be educated that avoiding the waste of food becomes common sense.

These propositions are regarded as opposable and defendable, and have been approved as such by the promotor prof. dr. ir. R. Benedictus and the copromotor dr. ir. D. Zarouchas.

Stellingen

behorende bij het proefschrift

UNFOLDING THE EARLY FATIGUE DAMAGE ACCUMULATION FOR CROSS-PLY LAMINATES

door

Xi LI

1. Het betrekken van meerdere structurele gezondheidsbewakingstechnieken tijdens het mechanisch testen is nodig om tot een betrouwbare schademonitoring van niet-transparante composieten te komen.
2. In plaats van het niet-interactieve schadeschema, zou een interactief schadeschema moeten worden gebruikt om het accumulatieproces van vermoeidheidsschade van vezelversterkte polymeerlaminaten te beschrijven.
3. Modellering is geen noodzaak voor experimentele analyse, maar experimentele validatie is een must voor modellering.
4. Door de coronapandemie weten we hoe we onze handen professioneel moeten reinigen om ze te ontdoen van ziektekiemen.
5. Gevoel is de beste adviseur voor besluitvorming.
6. Om een aangename fietstocht in de Nederlandse winter te garanderen, is het zeer aan te bevelen de weersvoorspelling te raadplegen.
7. Kennis is onbetaalbaar, maar het creëren en verkrijgen van kennis heeft een prijs.
8. Het vervangen van plastic door andere 'groene' alternatieven is niet milieuvriendelijk, aangezien de kern van de bescherming van het milieu zou moeten zijn hoe we onze uitbuiting van de aarde kunnen verminderen.
9. Rechtvaardigheid is niet absoluut maar relatief.
10. Mensen moeten worden voorgelicht zodat het vermijden van voedselverspilling gemeengoed wordt.

Deze stellingen worden opponeerbaar en verdedigbaar geacht en zijn als zodanig goedgekeurd door de promotor prof. dr. ir. R. Benedictus en de copromotor dr. ir. D. Zarouchas.

Unfolding the early fatigue damage accumulation for cross-ply laminates

UNFOLDING THE EARLY FATIGUE DAMAGE ACCUMULATION FOR CROSS-PLY LAMINATES

Dissertation

for the purpose of obtaining the degree of doctor
at Delft University of Technology
by the authority of the Rector Magnificus, Prof. dr. ir. T. H. J. J. van der Hagen
chair of the Board for Doctorates
to be defended publicly on
Thursday 8 September 2022 at 12:30 o'clock

by

Xi LI

Master of Engineering in Solid Mechanics,
Northwestern Polytechnical University, China
born in Weinan, China

This thesis has been approved by the promotors.

Composition of the doctoral committee:

Rector Magnificus,	Chairperson
Prof. dr. ir. R. Benedictus,	Delft University of Technology, promotor
Dr. ir. D. Zarouchas,	Delft University of Technology, copromotor

Independent members:

Prof. dr. C. Zhang	Northwestern Polytechnical University, China
Prof. dr. ir. D. van Hemelrijck	Vrije Universiteit Brussel, Belgium
Prof. dr. T. Loutas	University of Patras, Greece
Dr. ir. F. P. Van der Meer	Delft University of Technology, Netherlands
Prof. dr. ir. J. G. Rots	Delft University of Technology, Netherlands
Prof. C. A. Dransfeld	Delft University of Technology, reserve member

Keywords: Fatigue; Composites; Stochastic matrix cracking; Delamination; Damage interaction; Stiffness degradation; Poisson's ratio; Acoustic emission; Digital image correlation; Image processing; In-situ monitoring; Probabilistic damage model;

Printed by: Ipskamp printing

Front & Back: Beautiful cover that captures the content of this thesis.

ISBN (E-book) 978-94-6384-364-5
ISBN (Paperback) 978-94-6384-363-8

An electronic version of this dissertation is available at
http://repository.tudelft.nl/.

路漫漫其修远兮，吾将上下而求索。
Long the road as it is, I will keep my initiative to search.

屈原
Qu Yuan

Contents

SUMMARY

FATIGUE damage of composite laminates has attracted considerable attention from research community and industry, in view that laminated structures are inevitable to suffer from fatigue loading during their service life. It is rather complicated to understand and explain, what governs the initiation, accumulation, interaction (synergy or competition) of different damage mechanisms. Intrinsic and extrinsic scatter sources are hard to eliminate during the fatigue testing of laminates, which produce significant dispersion of laboratory data and further hinder our understanding about the progressive accumulation process of fatigue damage. Consequently, most of fatigue damage models for laminates are mathematically fitted to existing experimental data, rather than being related to the mechanisms of damage accumulation process.

Considering the majority of stiffness is degraded during the early fatigue life before the final failure of laminates, the objective of this thesis is to investigate the accumulation of matrix-dominant damage, mainly off-axis cracks and delamination, with the possible scatter phenomena taken into account. Carbon fibre/polymer laminates were selected as the research target as they have been increasingly used for aerospace structures due to the light weight, and two types of cross-ply configurations were designed and manufactured as $[0/90_2]_s$ and $[0_2/90_4]_s$. Experimental set-up involving multiple damage monitoring systems, i.e. edge observation by digital cameras, digital image correlation (DIC) and acoustic emission (AE), was developed to in-situ characterise and quantify the initiation and accumulation of transverse cracks and delamination.

To evaluate the capabilities of proposed experimental methods, cross-ply laminates with thick 90 ply block were firstly tested under static loading at different rates. Besides images captured from the edge view, DIC-based axial strain concentration and cumulative AE energy of acoustic signals within the low peak frequency band both provide sufficient information related to the accumulation of transverse cracks. Based on the experimental findings and analysis under static loading, tension-tension fatigue tests under different stress levels were further performed for cross-ply laminates with thin and thick 90 ply blocks. The evolution of mechanical properties, i.e. stiffness and Poisson's ratio, and the accumulation of transverse cracks and delamination, during the fatigue loading, were investigated and compared between both ply configurations.

Although sharing the same longitudinal stiffness, a bi-linear trend of stiffness degradation was presented for the $[0/90_2]_s$ laminates, which hardly reach the plateau like the $[0_2/90_4]_s$ laminates. For the $[0/90_2]_s$ laminates, transverse cracks are the dominant damage mechanism with almost non-existed delamination, while delamination initiates before the saturation of transverse cracks, and both damage mechanisms interact in a competitive way for the $[0_2/90_4]_s$ laminates. Therefore, opposite trends of Poisson's ratio as a function of fatigue cycles were observed between both ply configurations. It deceases due to the dominance of transverse cracks for the $[0/90_2]_s$ laminates during the testing. However, an increase of Poisson's ratio was presented for the $[0_2/90_4]_s$ laminates which is attributed to the significant transverse strain concentration induced at the delaminated region. Accordingly, the correlation among delamination area, transverse strain concentration area and Poisson's ratio is explored, which is then used for quantifying the delamination growth inside the $[0_2/90_4]_s$ laminates.

For both cross-ply laminates, after initiating at edges, most of transverse cracks propagated through the width direction within 500 cycles, based on the axial strain concentration from DIC analysis. Cumulative AE energy is found to be a helpful indicator of crack density under fatigue loading. As for the differences of crack evolution between both ply configurations, the saturated crack density is about 2-5 times larger for the $[0/90_2]_s$ laminates than that for the $[0_2/90_4]_s$ laminates. Severer interaction among transverse cracks occurs for the $[0/90_2]_s$ laminates and it slows down the growth rate of crack density. To quantify the interaction among transverse cracks, dependent crack ratio is proposed based on a critical crack spacing which varies between two ply configurations and can be obtained from finite element modelling. Besides, the accumulation of transverse cracks with the increase of fatigue cycles scatters among the $[0_2/90_4]_s$ laminates that share the similar stiffness degrading trends. Specimens presenting a higher saturated crack density spent less fatigue cycles and produced less delamination at the characteristic damage state, which indicates the existence of different interactive levels between transverse cracks and delamination. To further investigate this scattering of crack evolution among specimens, a strength-based probabilistic model is developed, and the distribution of local strength at 90 plies is found to be the scatter source.

In conclusion, this thesis provides a clear picture about the interactive scheme of early fatigue damage accumulation of cross-ply laminates, based on the developed in-situ damage monitoring methods.

SAMENVATTING

VERMOEIDHEIDSSCHADE van composietlaminaten heeft veel aandacht getrokken van de onderzoeksgemeenschap en de industrie, aangezien gelamineerde constructies onvermijdelijk te lijden hebben van vermoeidheidsbelasting tijdens hun levensduur. Het is nogal ingewikkeld om te begrijpen en uit te leggen wat de initiatie, accumulatie, interactie (synergie of competitie) van verschillende schademechanismen regelt. Intrinsieke en extrinsieke verstrooiingsbronnen zijn moeilijk te elimineren tijdens het vermoeiingstests van laminaten, die een aanzienlijke verspreiding van laboratoriumgegevens veroorzaken en ons begrip van het progressieve accumulatieproces van vermoeidheidsschade verder belemmeren. Bijgevolg zijn de meeste modellen voor vermoeidheidsschade voor laminaten wiskundig aangepast aan bestaande experimentele gegevens, in plaats van gerelateerd te zijn aan de mechanismen van het proces van schadeaccumulatie.

Aangezien de meeste stijfheid afneemt tijdens de vroege vermoeiingslevensduur voordat het laminaat uiteindelijk bezwijkt, is het doel van dit proefschrift om de accumulatie van matrix-dominante schade te onderzoeken, voornamelijk off-axis scheuren en delaminatie, rekening houdend met mogelijke verstrooiingsverschijnselen. Koolstofvezel/polymeerlaminaten werden gekozen als onderzoeksdoel vanwege hun lichte gewicht en worden steeds vaker gebruikt in de lucht- en ruimtevaartconstructie, en er zijn twee soorten kruislaagconfiguraties ontworpen en vervaardigd als $[0/90_2]_s$ en $[0_2/90_4]_s$. Experimentele opstelling met meerdere schadebewakingssystemen, d.w.z. randobservatie door digitale camera's, digitale beeldcorrelatie (DIC) en akoestische emissie (AE), werd ontwikkeld om de initiatie en accumulatie in-situ van transversale scheuren en delaminatie.

Om de mogelijkheden van voorgestelde experimentele methoden te evalueren, werden kruislaaglaminaten met dik 90-laags blok eerst getest onder statische belasting met verschillende snelheden. Naast beelden die zijn vastgelegd vanuit de randweergave, bieden op DIC gebaseerde axiale spanningsconcentratie en cumulatieve AE-energie van akoestische signalen binnen de lage piekfrequentieband beide voldoende informatie met betrekking tot de accumulatie van transversale scheuren. Op basis van de experimentele bevindingen en analyse onder statische belasting werden verder spannings- en vermoeiingstests bij verschillende spanningsniveaus uitgevoerd voor kruislaaglaminaten met dunne en dikke 90-laags blokken. De evolutie van mechanische eigenschappen, d.w.z. stijfheid en Poisson-verhouding, en de accumulatie van transversale scheuren en delaminatie, tijdens de vermoeiingsbelasting, werden onderzocht en vergeleken tussen beide laagconfiguraties.

Hoewel ze dezelfde longitudinale stijfheid delen, werd een bi-lineaire trend van stijfheidsdegradatie gepresenteerd voor de $[0/90_2]_s$ laminaten, die het plateau nauwelijks bereiken zoals de $[0_2/90_4]_s$ laminaten. Voor de $[0/90_2]_s$-laminaten zijn transversale scheuren het dominante schademechanisme met bijna onbestaande delaminatie, terwijl delaminatie begint vóór de verzadiging van transversale scheuren, en beide scha-

demechanismen werken op een concurrerende manier samen voor de $[0_2/90_4]_s$ laminaat. Daarom werden tegengestelde trends van de Poisson-verhouding als functie van vermoeiingscycli waargenomen tussen beide laagconfiguraties. Het sterft door de dominantie van transversale scheuren voor de $[0/90_2]_s$ laminaten tijdens het testen. Er werd echter een toename van de Poisson-ratio gepresenteerd voor de $[0_2/90_4]_s$ laminaten, die wordt toegeschreven aan de significante transversale spanningsconcentratie die wordt geïnduceerd in het gedelamineerde gebied. Dienovereenkomstig wordt de correlatie tussen het delaminatiegebied, het transversale spanningsconcentratiegebied en de Poisson-verhouding onderzocht, die vervolgens wordt gebruikt voor het kwantificeren van de delaminatiegroei binnen de $[0_2/90_4]_s$ laminaten.

Voor beide cross-ply laminaten, na het initiëren aan de randen, plantten de meeste transversale scheuren zich voort in de breedterichting binnen 500 cycli, gebaseerd op de axiale spanningsconcentratie van DIC-analyse. Cumulatieve AE-energie blijkt ook een nuttige indicator te zijn voor de scheurdichtheid onder vermoeiingsbelasting. Wat betreft de verschillen in scheurontwikkeling tussen beide laagconfiguraties, is de verzadigde scheurdichtheid ongeveer 2-5 keer groter voor de $[0/90_2]_s$ laminaten dan die voor de $[0_2/90_4]_s$ laminaten. Bij de $[0/90_2]_s$-laminaten vindt een grotere interactie tussen transversale scheuren plaats en dit vertraagt de groeisnelheid van de scheurdichtheid. Om de interactie tussen transversale scheuren te kwantificeren, wordt een afhankelijke scheurverhouding voorgesteld op basis van een kritische scheurafstand die varieert tussen twee laagconfiguraties en kan worden verkregen uit eindige-elementenmodellering. Bovendien verspreidt de accumulatie van transversale scheuren met de toename van vermoeiingscycli zich onder de $[0_2/90_4]_s$ laminaten die dezelfde stijfheidsverlagende trends delen. Exemplaren met een hogere verzadigde scheurdichtheid hebben gewoonlijk minder vermoeiingscycli en produceren minder delaminatie bij de karakteristieke schadetoestand, wat wijst op het bestaan van verschillende interactieve niveaus tussen transversale scheuren en delaminatie. Om deze verstrooiing van scheurevolutie tussen specimens verder te onderzoeken, is een op sterkte gebaseerd probabilistisch model ontwikkeld, en de verdeling van lokale sterkte bij 90 lagen blijkt de verstrooiingsbron te zijn.

Samenvattend, dit proefschrift geeft een duidelijk beeld van het interactieve schema van vroege accumulatie van vermoeiingsschade van dwarslaagse laminaten, gebaseerd op de ontwikkelde in-situ schademonitoringmethode.

Nomenclature

Latin symbols

A	Parameter of P-S-N curves
a_0, a_1, a_2	Fitting parameters in the function of axial stress state at the cracked region of 90 plies
A_C	Normalised area of transverse strain concentration
A_d	Normalised delamination area
A_{dL}	Local normalised delamination area
A_{loss}	Loss of amplitude
B	Parameter of P-S-N curves
d	Crack spacing
$d_{average}$	Average crack spacing
d_{max}	Maximum crack spacing
d_{min}	Minimum crack spacing
E_0	Initial axial stiffness of the laminate
E_N	Degraded axial stiffness of the laminate at the cycle N
F	Load from the testing machine
f_p	Peak frequency of the AE signal
F_{max}	Maximum load from the testing machine
I_r	Interlaminar crack ratio
L	Gauge length
L_{l1}, L_{l2}	Total length of inter-laminar cracks located at each interface of the left edge
L_{r1}, L_{r2}	Total length of inter-laminar cracks located at each interface of the right edge
M	Number of transverse cracks generated on both edges
N	Number of fatigue cycles
N_a	The number of cycles when the independent crack initiates
N_i	Fatigue life up to final failure under the axial stress of σ_{pi}
n_i	Consumed fatigue cycles under the axial stress of σ_{pi} at an interactive region
P	Cumulative probability of the statistical distribution
P_{peak}	Cumulative probability at the peak of probabilistic density function
R	Stress (strain) ratio
r_d	Dependent crack ratio
S	Local strength of 90 plies
S_a	Local strength of 90 plies where the independent crack initiates
S_b	Local strength of 90 plies where the dependent crack initiates
T_a	Number of independent cracks
T_b	Number of dependent cracks

U_{AE}	Cumulative AE energy
X	Location at the gauge region of specimens along the loading direction
Greek symbols	
β	Shape parameter of Weibull distribution
η	Scale parameter of Weibull distribution
$\bar{\epsilon}_{xx}$	Average axial strain of the laminate at the gauge region
$\bar{\epsilon}_{yy}$	Average transverse strain at the gauge region
$\overline{\sigma}_{applied}$	Maximum cyclic stress applied at the laminate (averaged through the thickness)
ρ	Crack density
ρ_L	Local crack density
ρ_S	Saturated crack density
ρ_{max}	Crack density before failure under static loading
σ_{90_i}	The axial stress of the laminate when the first crack initiates under static loading
σ_{pi}	Axial stress at 90 plies averaged by the thickness at an interactive region (i=1 is the applied one; i=2 is the redistributed one)
σ_r	Residual strength of 90 plies
σ_{ult}	Ultimate strength
σ_{xx}	Axial stress of the laminate
υ	Poisson's ratio
Abbreviations	
AE	Acoustic emission
CDS	Characteristic Damage State
$CFRP$	Carbon fibre reinforced polymer
DIC	Digital image correlation
FRP	Fibre reinforced polymer
$G1$	Group 1
$G2$	Group 2
IR	Infrared thermography
$SLERA$	Strength Life Equal Rank Assumption
UD	Unidirectional
UTS	Ultimate tensile strength

List of Figures

List of Tables

1

Introduction

1

1.1. COMPOSITES UNDER FATIGUE LOADING

COMPOSITES contain two or more distinct constituents or phases with different physical or chemical properties [1]. Among different types of composites, fibre reinforced polymer (FRP) composites, which have the polymer as the matrix phase and the fibre as the filling phase, become increasingly attractive in engineering applications. This thesis focuses on the laminated FRP composites which have an identical fibre orientation at each ply.

The advantages of laminates over traditional metallic materials are attributed to their high ratio of strength to weight [2], high resistance to corrosion and high fatigue limit [3]. Here, fatigue is a time-dependent varying load whose maximum amplitude would be insufficient to cause catastrophic failure of composites if it was monotonically applied [4]. As being designated as fatigue insensitive, laminates were once considered as the materials that never suffer from fatigue [5]. However, laminates do fail under fatigue loading and the research community still has open scientific questions about the fatigue behaviour of these structures.

The basics of laminate fatigue are similar to metals, but it is rather more complex to understand. Due to the inhomogeneous and anisotropic nature of laminates, load transfers from one fibre to another through the matrix and interface, which could cause the fatigue damage in laminates accumulating in a way that is different from metals [3, 6]. To be specific, many damage mechanisms (e.g. matrix cracking, delamination, and fibre breakage) [7] coexist and interact, not only for multidirectional, but also for unidirectional laminates; besides, it is challenging to develop a commonly accepted method, which considers the significant variances about the type of fibres, matrices, manufacturing methods, stacking sequences, etc. [8].

Accompanied with the above-mentioned complexities, one more concern, which needs to be urgently highlighted, is the significant scatter phenomenon of data from laboratory tests for laminates under fatigue loading. For instance, the fatigue life for crack initiation could show a large scatter of more than two orders of magnitude [9], while the spreading range of fatigue life when the final failure occurs could be even larger [10]. As summarised in [5], scatter sources can be divided into the intrinsic ones (e.g. inhomogeneous material morphology and process variability, manufacture defects, etc.) and the extrinsic ones (e.g. variation geometry size and cutting quality of specimens, operator experiences and test set-up of fatigue machine, etc.). They are hard to quantify in test campaigns, especially the intrinsic sources. Therefore, the analysis about damage and failure of laminates under fatigue loading remains a challenge.

1.2. EARLY FATIGUE DAMAGE

AMONG mechanical [11, 12], thermal [13, 14], acoustic [15, 16], and optical properties [17, 18] of laminates which may be affected by the progressive damage process, stiffness becomes one of preferable indicators to reflect damage severity. It is relatively easily to measure, and it has been well-correlated to the damage accumulation in a variety of load cases [19–21].

A three-stage process in a rapid-slow-rapid manner has been reported as the representative trend of stiffness degradation for laminates under fatigue loading [22, 23]. To illustrate this process, take as an example a cross-ply laminate, Stage I shows the significant decrease of stiffness within a short duration of fatigue life, followed by Stage II that occupies most of fatigue life where the stiffness almost remains constant and Stage III with sudden drop of stiffness, as presented in Figure 1.1. Considering most of stiffness reduction before the final failure is presented in Stage I, attentions should be drawn on the accumulation of fatigue damage during the early fatigue life, which is referred as early fatigue damage in this thesis.

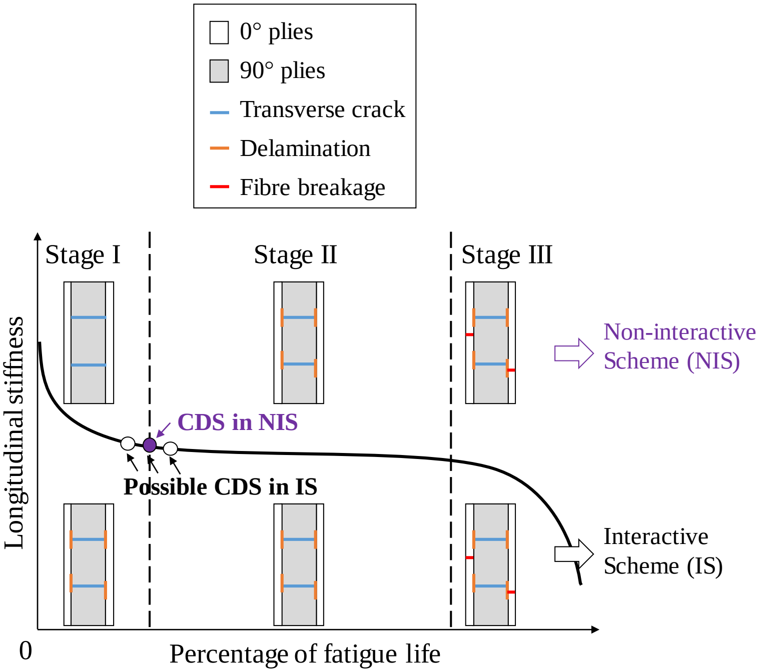

Figure 1.1: Stiffness degradation and damage accumulation process for cross-ply laminates.

Off-axis cracks are usually regarded as the main damage mechanism at Stage I, after which delamination becomes dominant at Stage II, followed by the occurrence of fibre breakage at Stage III [14, 22, 23]. It is widely agreed that fatigue damage accumulation of laminates is controlled by the matrix, in view that the degradation of the laminae under fatigue loading firstly occurs in the matrix, and fibre damage is the result of matrix degradation [8]. Sun and Chim [24] also concluded that the limiting factor in fatigue is not the fibre but the interface and the matrix. These statements stress the importance of the analysis on the accumulation of early fatigue damage which is matrix-dominant. Further, it may also help to gain a better insight of the significant scatter phenomenon about fatigue life for composites and pave the way for probabilistic predictions of fatigue life with physics of damage involved.

1.3. RESEARCH GOAL AND SCOPE

DURING the early fatigue life, as the non-interactive illustrates (see Figure 1.1), the accumulation of fatigue damage contains the initiation, evolution and the saturation of off-axis cracks. The saturation occurs at the transition moment from Stage I to Stage II. However, when considering the interactive scheme, as shown in Figure 1.1, it is possible that multiple damage mechanisms like matrix cracks and delamination occur within Stage I. Then, it is unclear when the saturation of matrix cracks happens: within Stage I, at the transition moment from Stage I to Stage II, or within Stage II. What might happen is that different interactive levels between matrix cracks and delamination exist among tested specimens, which could later affect the scatter of failure life. Besides, how off-axis cracks and delamination contribute to stiffness degradation within this interactive scheme also need to be explored.

Therefore, this thesis aims at unfolding the accumulation of matrix-dominant damage (i.e. off-axis cracks and delamination) during the early fatigue life of laminated composites, with the possible scatter phenomena taken into account, in order to understand:

- which damage mechanism(s) initiate(s) and how it(they) accumulate(s);
- if more than one damage mechanism coexist, how they interact;
- how its(their) accumulation affects the stiffness degradation of a laminate.

By answering these three questions, we can have a clear picture about the progressive damage accumulation process of laminates as well as its contribution on the stiffness degradation in the early fatigue life. These achievements will enhance our understanding about the development of physical-based fatigue damage models for FRP laminates. As mentioned in [8], even today, the fatigue theories are basically empirical in nature, which are literally "fitted" to existing experimental data. Therefore, it is meaningful to contribute our effort and knowledge in this field.

The way to address these questions in this thesis is mainly based on the experimental analysis with the involvement of in-situ damage monitoring techniques, to appropriately characterise the initiation, accumulation and saturation of related damage mechanisms. Besides, the phenomenological modelling method in a probabilistic style is included to help uncover the stochastic nature of damage accumulation.

1.4. THESIS OUTLINE

THE analysis and understanding of fatigue damage of FRP laminates, mainly matrix cracks and delamination, is reviewed in Chapter 2. Besides, different in-situ damage monitoring techniques that have been applied during the experimental campaign for measuring the matrix cracks and delamination are discussed. Furthermore, current knowledge gap related to the fatigue damage accumulation of laminates is stressed, and the research targets as well as the techniques applied for in-situ damage monitoring in this thesis are briefly concluded.

In Chapter 3, the experimental methods are described in detail, including information of the PrePreg materials, the manufacturing process of laminated panels, and the test set-up with different in-situ damage monitoring systems involved. Then, the verification of proposed experimental methods is firstly carried out under static loading, by analysing the monitored damage accumulation process. Finally, experimental campaign under fatigue loading is introduced and the changes of mechanical properties during testing are presented.

Chapter 4 analyses the initiation, accumulation and saturation of transverse cracks. Based on the experimental findings, the stochastic nature of crack formation is also explored with the assistance of a strength-based probabilistic model.

In Chapter 5, delamination growth along both length and width directions is characterised, according to measurements from edge damage monitoring system, digital image correlation system and C-scanner. Then, interaction between transverse cracks and delamination is discussed.

As different maximum stress levels and two types of ply configurations with different thickness are involved in the experimental campaigns, the effect of stress level and ply-block size on the accumulation of transverse cracks and delamination is also investigated in Chapter 4 and Chapter 5.

Finally, Chapter 6 presents the main conclusions of this thesis and offers some suggestions for future work.

REFERENCES

[1] X. S. Yi, S. Du, and L. Zhang, *Composite materials engineering, Volume 1: Fundamentals of Composite Materials* (Springer Singapore, 2018).

[2] P. Alam, D. Mamalis, C. Robert, C. Floreani, and C. M. Ó Brádaigh, *The fatigue of carbon fibre reinforced plastics - A review,* Composites Part B: Engineering **166**, 555 (2019).

[3] R. C. Alderliesten, *Critical review on the assessment of fatigue and fracture in composite materials and structures,* Engineering Failure Analysis **35**, 370 (2013).

[4] D. Dew-Hughes and J. L. Way, *Fatigue of fibre - reinforced plastics: a review,* Composites **4**, 167 (1973).

[5] R. C. Alderliesten, A. J. Brunner, and J. A. Pascoe, *Cyclic fatigue fracture of composites : What has testing revealed about the physics of the processes so far ?* Engineering Fracture Mechanics **203**, 186 (2018).

[6] K. Boller, *Fatigue fundamentals for composite materials,* in *Composite materials: testing and design* (ASTM International, 1969).

[7] R. Talreja, *DAMAGE DEVELOPMENT IN COMPOSITES: MECHANISMS AND MODELLING,* The Journal of Strain Analysis for Engineering Design **24**, 215 (1989).

[8] A. P. Vassilopoulos, *The history of fiber-reinforced polymer composite laminate fatigue,* International Journal of Fatigue **134**, 105512 (2020).

1

[9] J. A. Glud, J. M. Dulieu-Barton, O. T. Thomsen, and L. C. Overgaard, *Fatigue damage evolution in GFRP laminates with constrained off-axis plies,* Composites Part A: Applied Science and Manufacturing **95**, 359 (2017).

[10] N. H. Tai, C. C. Ma, and S. H. Wu, *Fatigue behaviour of carbon fibre/PEEK laminate composites,* Composites **26**, 551 (1995).

[11] P. Shabani, F. Taheri-Behrooz, S. Maleki, and M. Hasheminasab, *Life prediction of a notched composite ring using progressive fatigue damage models,* Composites Part B: Engineering **165**, 754 (2019).

[12] F. Taheri-Behrooz, M. M. Shokrieh, and L. B. Lessard, *Residual stiffness in cross-ply laminates subjected to cyclic loading,* Composite Structures **85**, 205 (2008).

[13] J. Huang, M. L. Pastor, C. Garnier, and X. J. Gong, *A new model for fatigue life prediction based on infrared thermography and degradation process for CFRP composite laminates,* International Journal of Fatigue **120**, 87 (2019).

[14] Y. Li, R. Zhang, L. Li, P. Bao, W. Zhang, Z. Yang, G. Tian, and A. Ming, *Temperature variation and damage characteristic of impacted CFRP laminate using infrared thermography: Experimental investigation,* International Journal of Fatigue **112**, 130 (2018).

[15] M. Saeedifar and D. Zarouchas, *Damage characterization of laminated composites using acoustic emission: A review,* Composites Part B: Engineering **195**, 108039 (2020).

[16] J. A. Pascoe, D. S. Zarouchas, R. C. Alderliesten, and R. Benedictus, *Using acoustic emission to understand fatigue crack growth within a single load cycle,* Engineering Fracture Mechanics **194**, 281 (2018).

[17] S. Korkiakoski, P. Brøndsted, E. Sarlin, and O. Saarela, *Influence of specimen type and reinforcement on measured tension-tension fatigue life of unidirectional GFRP laminates,* International Journal of Fatigue **85**, 114 (2016).

[18] A. V. Movahedi-Rad, T. Keller, and A. P. Vassilopoulos, *Fatigue damage in angle-ply GFRP laminates under tension-tension fatigue,* International Journal of Fatigue **109**, 60 (2018).

[19] J. Maeck, M. Abdel Wahab, B. Peeters, G. De Roeck, J. De Visscher, W. De Wilde, J.-M. Ndambi, and J. Vantomme, *Damage identification in reinforced concrete structures by dynamic stiffness determination,* Engineering Structures **22**, 1339 (2000).

[20] X. Li, D. Ma, H. Liu, W. Tan, X. Gong, C. Zhang, and Y. Li, *Assessment of failure criteria and damage evolution methods for composite laminates under low-velocity impact,* Composite Structures **207**, 727 (2019).

[21] E. J. Barbero and D. H. Cortes, *A mechanistic model for transverse damage initiation, evolution, and stiffness reduction in laminated composites,* Composites Part B **41**, 124 (2010).

[22] K. L. Reifsnider and R. Jamison, *Fracture of fatigue-loaded composite laminates,* International Journal of Fatigue **4**, 187 (1982).

[23] H. Pakdel and B. Mohammadi, *Stiffness degradation of composite laminates due to matrix cracking and induced delamination during tension-tension fatigue,* Engineering Fracture Mechanics **216**, 106489 (2019).

[24] C. Sun and E. Chim, *Fatigue retardation due to creep in a fibrous composite,* in *Fatigue of fibrous composite materials* (ASTM International, 1981).

2

Literature review

2.1. INTRODUCTION

FATIGUE loading used in literature and in this thesis is described in Section 2.2. Then, damage accumulation process of FRP laminates under fatigue loading is reviewed in Section 2.3. In Section 2.4 and 2.5, studies about off-axis cracks and delamination, which could initiate and accumulate in the early fatigue life, are summarised. Besides, damage monitoring techniques that have been applied for measuring the accumulation of off-axis cracks and delamination are introduced and discussed in Section 2.6. Later, the material, the design of specimens, and the in-situ damage monitoring techniques, which are used for the experimental campaigns of this thesis, are discussed and concluded in Section 2.7.

2.2. BASICS ABOUT FATIGUE LOADING

IN reality, fatigue loading shows a random load spectrum, while for laboratory tests, it is usually simplified as the cyclic sinusoidal wave, as presented in Figure 2.1. It has either a constant amplitude, or variable amplitudes containing different load blocks. Beside the minimum and maximum stress (strain), another basic parameter that determines this simplified cyclic loading is frequency, and it describes the number of cycles per second. The ratio of the minimum to the maximum cyclic stress(strain), also named as stress (strain) ratio R, classifies the fatigue loading: tension-tension ($0 < R < 1$), tension-compression ($-\infty < R < 0$), or compression-compression ($1 < R < \infty$).

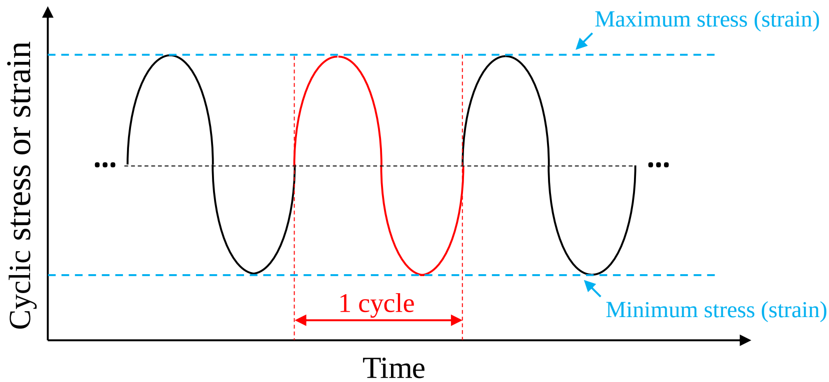

Figure 2.1: Fatigue load profile for laboratory tests.

The research scope of this thesis is under tension-tension fatigue with a constant amplitude. The fatigue damage reviewed in Section 2.3 - 2.5 relates to this type of fatigue loading.

2.3. FATIGUE DAMAGE ACCUMULATION PROCESS OF FRP LAMINATES

MECHANICAL properties of FRP laminates are usually degraded during the damage accumulation process under fatigue loading. Accordingly, phenomenological models, related to mechanical properties (i.e. residual stiffness and residual strength) as a function of fatigue cycles, have been proposed to implicitly represent the damage accumulation process [1]. Experimental tests could not be avoided to obtain related fitting parameters of these models which may be different from materials and ply configurations.

On the other hand, mechanism-involved analysis has been performed to explicitly explore the sequential initiation and accumulation of off-axis cracks, delamination and fibre damage during the entire fatigue life of laminates. Coupled with the three-stage degrading trend of stiffness presented in Figure 1.1, it was once recognised that each stage is dominated by one damage mechanism: Stage I - off-axis cracks; Stage II - delamination, Stage III - fibre damage [2, 3]. At the transition from Stage I to Stage II, the generation of off-axis cracks should reach a saturated state[2]. Based on this non-interactive damage scheme, a gradual stiffness degradation of 90 plies was performed to reflect the transverse crack evolution of cross-ply laminates within Stage I, which was then terminated by a sudden 90-ply discount when reaching CDS in the progressive damage model proposed by Shokrieh and Taheri-Behrooz [4].

However, as mentioned in Section 1.3, it might happen that multiple mechanisms coexist and interact in a synergistic or competitive way. For instance, delamination could initiate within the Stage I, even before the initiation of off-axis cracks [3, 5]; both delamination and fibre damage could occur within Stage III which may form either delamination dominant or fibre dominant damage state[6]. Therefore, the analysis of the fatigue damage accumulation process of FRP laminates should be performed with the establishment of an interactive damage scheme, which is rarely considered in literature. Considering the focus of this thesis is the early fatigue damage, current understandings about off-axis cracks and delamination as well as their interaction from literature are presented in Section 2.4 and 2.5.

2.4. OFF-AXIS CRACKS OF FRP LAMINATES UNDER FATIGUE

A large number of studies have been conducted for off-axis cracks inside a laminate, including the initiation and propagation of each single crack, the accumulation and saturation in the formation of multiple cracks, and the stochastic nature of crack generation. Hereafter, a review of relevant findings in literature is presented, in order to comprehensively grasp which parts have been understood and which parts need to be studied further.

2.4.1. INITIATION AND PROPAGATION OF A SINGLE CRACK

FOR coupon-level FRP laminates, an off-axis crack usually originates at the free edge [7, 8], as a result of random microcracks that formed and coalesced [9]. Watanabe et al. [10] observed two competing nanoscale mechanisms that generate a macroscale crack, i.e. fibre/epoxy interface debonding at the "thin" epoxy region and in-resin cracking at the "thick" epoxy region. Carraro and Quaresimin [11] proposed that local hydrostatic stress and local maximum principal stress, based on the concept of local nucleation plane, can be considered as representative of the driving forces at the micro level for initiating an off-axis crack. The initiation of an off-axis crack under fatigue loading can be affected by matrix toughness, load parameters and ply configurations of laminates.

The effect of the toughness of matrix on the fatigue behaviour of FRP composites has been studied by Gassan and Dietz [12], and Zhao et al. [13]. They both found that the crack resistance is high for composites with tough matrix, the fatigue life of which is thus enhanced in comparison to composites with brittle matrix.

Regarding the load parameters, when the maximum stress under fatigue loading is higher than the threshold stress to induce off-axis cracks under quasi-static loading, the first off-axis crack appears at the first few cycles; otherwise, its initiation delays [7, 8]. At low stress ratios, a rapid initiation of the off-axis crack is presented [14, 15]. The delay of crack initiation is also observed with the increase of frequency before self-heating becomes dominant [16, 17].

As for the ply configuration, beside the fibre orientation, the thickness of off-axis plies is a key factor, as it determines the in-situ strength [18]. An off-axis crack can easily generate in thick plies, while thin plies may suppress its initiation [19, 20]. Hosoi and Kawada [21] observed that fatigue life of transverse crack initiation is 30 times longer for $[0_2/90_6]_s$ laminates than that of $[0_2/90_{12}]_s$ laminates when the same stress level is imposed on laminates. The constraining effect of adjacent plies also plays a role here. The fibre orientation of constraining plies affects the crack plane at off-axis plies. For instance, as shown in Figure 2.2, the crack plane is normal to the loading axis in the case that the cracked 90 plies are constrained by 0 plies, while it is tilted if the outer layers are ±45 oriented, reported by Lafarie-Frenot et al. [8]. In addition, Lim and Hong [22] observed a slight increase of the onset strain for transverse cracking at the middle 90 plies with a constant thickness, when the thickness of outer 0 plies increases. Similar finding about the improvement of constraining effect for $[0_n/90_4]_s$ laminates on the crack formation was also reported by Shen et al. [19], as n changes from one to two.

After initiating from free edges, the off-axis crack could rapidly propagate parallel to the fibre direction, or show a slow propagating process and then arrest in the middle of off-axis plies, or just concentrate near edges [9]. How it propagates depends on the lay-up and far-field loading; however, the average growth rate is not only dependent on the crack length like homogeneous materials and crack spacing could also play a role [7, 23]. Off-axis plies with a large thickness and a fibre orientation which has a large deviation away from the loading direction usually present a rapid crack propagation [19, 24]. On the contrary, partial cracks may form due to the slow crack propagation [24]. Three states of crack propagation, i.e.initiation-controlled state, steady state, crack interaction and saturation state, have been described by Jagannathan et al. [23]. The crack growth rate at the first state is lower than that at the steady state, and the crack length is less than around two times of the ply thickness. Then, with the increase of crack length, the growth rate remains constant at the steady state. When the crack spacing is 4-5 times of the ply thickness, the crack growth turns to the last state and the growth rate decreases. After the crack spacing reaches about the ply thickness, no further crack growth can be observed. Quite frequently variations of the Paris-law have been used to describe the propagation of an off-axis crack in composites under fatigue loading [25].

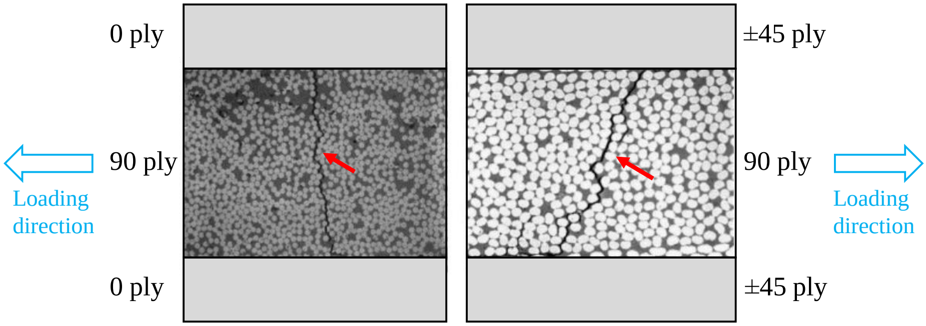

Figure 2.2: Crack morphology from the edge view under fatigue loading, regenerated from [8].

2.4.2. ACCUMULATION AND SATURATION OF MULTIPLE CRACKS

As fatigue cycles increase, multiple cracks generate at off-axis plies, and crack density is usually used to quantify their accumulation process. Matrix toughness, load parameters and ply configurations also affect the growth rate of crack density, which is similar to the crack initiation as mentioned in Section 2.4.1.

A significant increase of crack density is usually observed at the early fatigue cycles, followed by a gradual decrease of the growth rate. When the crack density is high, interaction among cracks may be triggered, and the stress state between adjacent cracks redistributes to a lower value than the applied [26, 27]. After the growth rate of crack density decreases to a certain level, a saturated state occurs and the crack density becomes constant. This saturated state is also named as Characteristic Damage State (CDS) [2]. A Paris-law based function is usually used to describe the growth rate of crack density as a function of fatigue cycles, under the assumption that the increase in the crack density is proportional to the increase in the crack extension [28]. However, the Paris-law type of crack density growth has not been verified theoretically, and it is difficult to explain the crack density growth under low stress level where no cracks initiate at the very early fatigue cycles [29].

As for the analysis about CDS, it has been proposed that the CDS is independent of loading conditions, as the crack density at saturation was observed to be similar under fatigue loading with different maximum stress and stress ratio [2, 3]. Laminate layups, geometries and material properties show a significant effect on the CDS. Off-axis plies with a fibre orientation which has a large deviation away from the loading direction present high crack density at the CDS [3]. Besides, matrix cracks in thinner off-axis plies saturate with higher densities [3, 30]. Pakdel and Mohammadi [3, 31] proposed that the moment of the onset of matrix crack saturation can be identified as the moment of the initiation of delamination which releases higher energy than the multiplication of matrix cracks. Based on this statement, a competition criterion considering different damage modes is formulated to predict the saturated crack density of laminates. However, what needs to be clear is when the saturation of matrix cracks happens: at, before, or after the moment of delamination initiation, as illustrated in Figure 1.1.

Until the saturation is reached, it is possible to observe the significant effect of multiple matrix cracks on the mechanical properties like the degradation of stiffness and Poisson's ratio [30]. The correlation between crack density and mechanical properties for the cracked laminate can be derived based on the stress state analysis using unit cell approaches such as variational, shear lag or finite element analysis [15]. These approaches are under the assumption that matrix cracks distribute uniformly along the length of a laminate and the new crack will initiate at the middle of two prior cracks.

Apparently, quite some analysis about accumulation and saturation of matrix cracks in literature is deterministic which does not consider the stochastic nature of crack generation regarding both temporal and spatial variations [26, 27, 32]. For instance, the unit cell approaches as mentioned above simplify the fact that the distribution of off-axis cracks is actually non-uniform and the position of the new crack is random rather than in the middle of two prior cracks. It has been concluded that the uniform distribution of cracks overestimates the stiffness degradation of cracked laminates in comparison with the non-uniform cases [33, 34]. Therefore, the probabilistic analysis about off-axis cracks should be proposed, with the stochastic crack formation taken into account.

2.4.3. STOCHASTIC ANALYSIS

IT was found that defects in local microstructures at off-axis plies, i.e. matrix porosity, debonded fibres, local volume fraction of fibre and matrix, and their spatial distributions, affect when and where an off-axis crack would initiate [35, 36]. Due to the current manufacturing processes, these local defects are hard to control [37–39], posing challenges to uncover the mechanisms of off-axis crack initiation. Efforts have been made to quantify the stochastic fibre architectures and defects by using image analysis techniques; based on this, representative volume element models were built, producing the microlevel structure-local material property connection [35, 40, 41]. Accordingly, the randomness of crack initiation caused by the variations of local microstructures at off-axis plies can be related to the variations of local material properties.

The growing trend of crack density as a function of fatigue cycles can be interpreted when taking the variations of local material properties into account. Initiation and accumulation of matrix cracks at a low density happen at the relatively weak positions of off-axis plies, which contributes to a significant increase of crack density during the early fatigue cycles; Later, the growth rate of crack density gradually decreases due to the occurrence of crack interaction and high crack resistance of remaining positions at off-axis plies [29].

Probabilistic models have been developed to predict the stochastic evolution of multiple matrix cracks with the variations of local strength or local fracture toughness, which can be then categorised into: strength based and energy based. For the strength-based approach, crack initiation is checked by a point failure criterion: a new crack is generated when the applied stress is equal to the strength at the local position of off-axis plies. The energy-based approach assumes a micro-crack or a flaw exists along the anticipated new crack plane, while its growth is analysed by considering the balance of energy [42, 43]. For the matrix cracking at thick plies which propagates immediately through the width direction, the strength-based approach is preferable. As for the matrix cracking at thin plies, it is mainly propagation-governed, thus the energy-based approach should apply [44].

Between these two types of approaches, the energy-based approach could consider the effect of ply thickness on the crack evolution [45]. However, the size and the pattern of the micro-cracks need to be obtained precisely so as to determine the variations of local fracture toughness [46]. Instead, the variations of local strength at off-axis plies employed in the strength-based approach can be directly obtained by performing tensile tests of unidirectional lamina. To further account for the in-situ effect of off-axis strength, band models by dividing the off-axis plies into multiple elements, as shown in Figure 2.3, were proposed and axial stresses when the off-axis crack initiate at each discretised region can be collected to obtain the distribution of in-situ local strengths in one/few tensile tests [7, 23]. Probabilistic strength-based models have showed the capabilities to describe the stochastic initiation of off-axis cracks in both low and high densities. For the low crack density, the model accounts for a statistical distribution of the local strength [29]. Considering the high density, the model accounts for, not only the local strength variation, but also the stress redistribution around the cracked region [26, 47]; both the strength and stress state at the local region of off-axis plies determine the fatigue cycles to initiate a new crack.

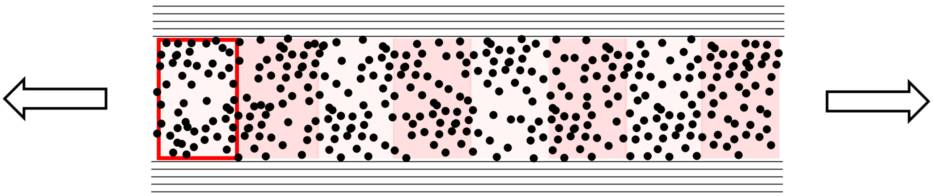

Figure 2.3: Discretisation of the off-axis plies to obtain the distributed static transverse strength.

2.5. DELAMINATION OF FRP LAMINATES UNDER FATIGUE

COMPARED to the off-axis cracks, delamination of FRP laminates is less investigated under tension-tension fatigue loading. It is hard to in-situ monitor during the testing and its growth could be affected by the accumulation of other damage mechanisms like off-axis cracks and fibre damage. Section 2.5.1 and 2.5.2 summarise the understandings so far about the initiation and growth of delamination, as well as its interaction with off-axis cracks.

2.5.1. INITIATION AND GROWTH

DELAMINATION usually originates from the tips of off-axis cracks or free edges due to the high interlaminar stress concentration [2, 48]. Afterwards, it grows in several ways, as presented in Figure 2.4. For the matrix crack induced delamination, it could form a uniform delamination front across the width of a laminate or an angled delamination front bounded with one free edge [49]. For the free edge delamination, it could be considered as the mode-I delamination propagating towards the centre of a laminate [50, 51]. O'Brien [52] observed that the growth rate of free edge delamination as a function of fatigue cycles is constant once the delamination has propagated over the entire length of the laminate edge.

2

Crossman and Wang [53] studied the effect of the ply clustering thickness on delamination for $[\pm 25/90_n]_s$ laminates ($n = 0.5$ to 8). They found that matrix crack induced delamination happens when $n \geqslant 4$, while laminates with $n \leqslant 3$ exhibit the free edge delamination. Therefore, laminates with the thick ply clustering have high chances to initiate the matrix crack induced delamination, while free edge delamination is prone to occur in the case with the thin ply clustering. Furthermore, a rapid growth rate of delamination is presented for the thick ply clustering, as reported by Takeda et al. [54].

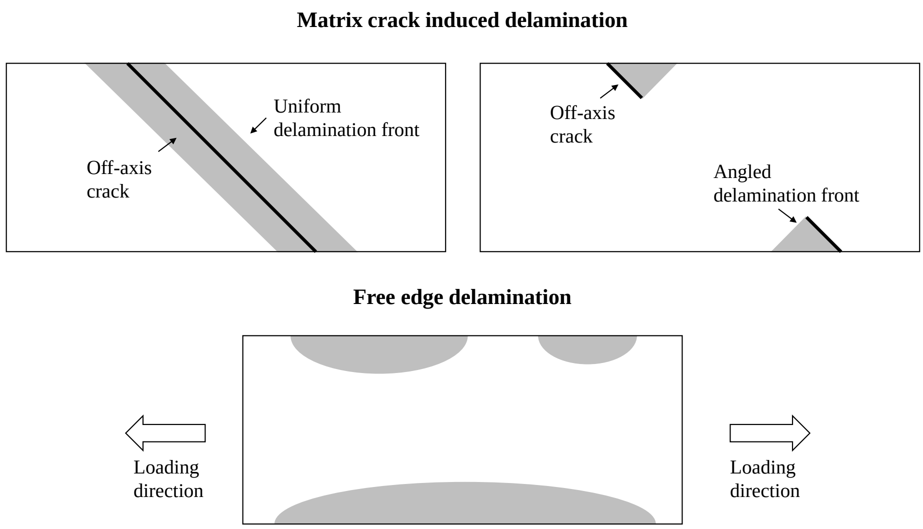

Figure 2.4: Delamination growth from an off-axis crack or free edges.

2.5.2. INTERACTION WITH OFF-AXIS CRACKS

IT has been hypothesised that delamination initiates at or after CDS [2], however, experimental observations [3] showed that before reaching CDS, delamination may appear especially at regions with high density of off-axis cracks. Furthermore, Hosoi et al. [5] reported that edge delamination initiates and propagates before or simultaneously with the initiation of off-axis crack under low stress level. These different occurring sequences of the off-axis crack initiation, saturation and delamination initiation reflect multiple levels of interaction between these damage mechanisms. Xu et al. [55] proposed that the constraining effect of uncracked plies and material properties of cracked plies determine whether off-axis cracks would initiate before or after the onset of delamination.

Delamination could postpone or prevent further generation of off-axis cracks at the neighbouring regions, as concluded by Pakdel and Mohammadi [3] and Shen et al. [19]. Based on the stress state analysis of co-existing off-axis cracks and delamination, Talreja [56] found that the maximum axial stress in the middle of adjacent cracks at the off-axis plies decreases with the increase of delamination length, causing the reduction of driving force for producing new off-axis cracks. However, how to describe or quantify the severity of interaction between off-axis cracks and delamination, or the severity of the constraining effect of delamination on the off-axis cracking has not been explored so far, which hinders our understanding on the interactive level between off-axis cracks and delamination.

2.6. Damage monitoring

To gain a better understanding of off-axis cracks and delamination which could initiate and accumulate during the early fatigue life of FRP laminates, experimental analysis is more straightforward once the characterisation of each damage mechanism and the quantification of their accumulation can be successfully achieved. Therefore, the damage monitoring, mainly for matrix cracks and delamination, by using different techniques based on the mechanical and thermal behaviours, as well as acoustic and optical properties of FRP laminates [57], is reviewed hereafter.

For the transparent FRP laminates like glass fibre/polymer laminates, transmitted light photography in combination with the image processing can achieve the in-situ monitoring of off-axis cracks and delamination [19, 30]. For the non-transparent FRP laminates like carbon/polymer laminates, an in-situ damage monitoring is not easy to perform, especially for delamination. In early studies, edge replica [2, 55] or electron microscopy [58, 59] was used to observe off-axis cracks and delamination from the edge view, while the delamination distribution was also obtained by X-radiography [54, 55, 59]. However, specimens need to be removed from the testing machine, or tests need to be interrupted for these ex-situ/in-situ damage inspections, which can induce the stress relaxation and further affect the cracking process [35]. Cho et al. [60] found that the crack density during the loading and unloading phase of tensile tests was strongly dependent on the particular loading sequence, and a time-dependent increase in matrix cracks occurred throughout the hold period.

Later, digital cameras were employed [61, 62] to automatically capture the crack evolution from the edge view of laminated specimens. However, how damage accumulates inside the specimen cannot be observed in this way. Besides, in view that high resolution and large observation window are usually hard to achieve simultaneously, in-situ crack characterisation in a large size view window by using digital cameras remains a challenge for non-interrupted tests of thin laminates. Recently, advanced in-situ monitoring techniques, like acoustic emission (AE), digital image correlation (DIC), infrared thermography (IR), lamb wave and fibre optics, have also shown the great potentials to identify different damage mechanisms and monitor their accumulation process.

Among these different techniques, AE is one of the most popular techniques to uncover the initiation and accumulation of different damage mechanisms [63]. Intensive efforts have been made on the interpretations of AE activities by analysing multiple AE features with clustering algorithms involved. Figure 2.5 shows a typical AE waveform, where some important AE features are defined. Amplitude and frequency are treated as the most preferred AE features to classify different AE activities [62, 64–67].

To correlate AE clusters to different damage mechanisms, some researchers have executed destructive tests on the individual constituent materials, for example coupons made of pure resin or fibre bundles, to obtain the AE feature of each damage mechanism separately. These AE features were then used as the reference patterns to correlate each AE cluster to a specific damage mechanism [65–67]. A general trend has been established which relates AE waveform with low peak frequency and amplitude to matrix-cracking-related damage mechanisms [65–67]. However, doubts exist in view that AE features for each damage mechanism might be different for composite samples with different dimensions [68] or stacking sequences [62]. Therefore, it is necessary to combine AE and other monitoring systems during the tests to provide a reliable interpretation of AE activities and corresponding features. Oz et al. [62] correlated AE clusters obtained from k-means ++ algorithm to different damage mechanisms (e.g. matrix cracks at the surface and inner 90 plies, micro and macro delamination, etc.) monitored from optical edge observation and DIC. They found that the depth of damage source can affect the corresponding AE features and high frequency could also be induced by the matrix cracking when 90 plies approach the mid-section of specimens. Baker et al. [69] concluded that waveform-based AE energy can be used to identify matrix crack initiation observed by the optical microscope from the edge. These observations indicate AE activities could be comprehensively interpreted to identify different damage mechanisms, and the evolution of AE features from different clusters is expected to act as the indicators to quantitatively represent the accumulation of different damage mechanisms in the future.

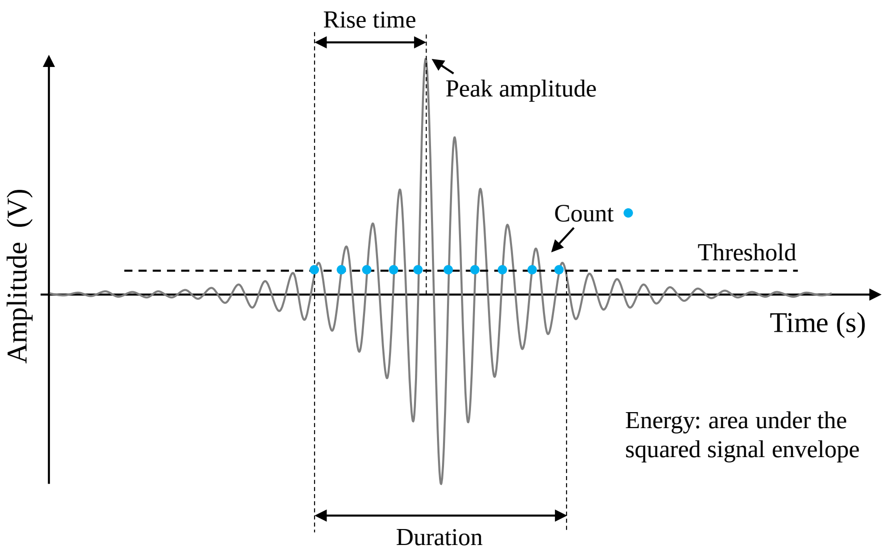

Figure 2.5: A typical AE waveform and some important features [63].

Beside the in-situ damage monitoring based on acoustic properties, a full-field measurement of deformation by DIC can also provide some damage information. Tessema et al. [70] investigated the matrix crack initiation and gradual propagation of quasi-isotropic laminates using the local concentration of axial and shear strain as damage indicators of intralaminar and interlaminar cracks. Mehdikhani et al. [35] quantified the evolution of transverse matrix cracks of cross-ply laminates by counting the peaks of the strain profile via both macro and meso scale DIC analysis. Furthermore, Miskdjian et al. [71] achieved an automatic edge detection of ply cracks via multi-scale digital image correlation, and found that displacement fields delivered better results than strain fields in crack density calculation and individual crack characterisation. However, detecting the damage accumulation in this way can be highly affected by the ply thickness and the stacking sequence of laminates [62].

Considering the other three techniques, infrared thermography (IR), lamb wave and fibre optics, they have also been successfully applied in the damage diagnostic of FRP laminates [72–74]. For IR, the variation of surface temperature is used to reflect the degrading and dissipating mechanisms of a material [75]. It can be classified into passive and active IR based on the difference of heat sources. The intensity of infrared images from passive IR can be affected by the infrared source attenuation caused by environmental absorption, while active IR requires a thermal excitation [76]. Regarding lamb wave, the damage identification is essentially subject to the interpretation of the captured wave signals, while diverse noise, interference from natural structural vibration, confusion of multiple modes and bulkiness of sampled data may happen during the extraction of key features from these wave signals [77]. As for fibre optics, plastic optical fibres and fibre Bragg grating sensors are two of the representative. They are usually embedded into laminates to monitor the crack evolution, based on the loss of optical power and the change of reflection spectra, respectively [78]. However, the embedding process may affect the health of the optical fibre itself, and may also change the fatigue behaviours of laminates [79].

Although some progress has been made to in-situ monitor the damage accumulation process of FRP laminates by using these advanced techniques, most of studies only focus on the identification of matrix cracks. For the case involving the delamination or the co-existed matrix cracks and delamination, it remains a challenge to characterise and quantify the damage initiation and accumulation, and a new experimental approach should be developed.

2.7. DISCUSSIONS AND CONCLUSIONS

BASED on the literature review, quite some studies have been conducted to understand the evolution of off-axis cracks and delamination for FRP laminates under fatigue loading. Besides, different ex-situ/in-situ techniques have been developed for a better monitoring of damage accumulation process. Apparently, more efforts have been made on the analysis of off-axis cracking than delamination, including the initiation and propagation of a single crack as well as the accumulation of multiple cracks in a laminate. As for the delamination, it is rather complicated to investigate in view of the challenges of detection and its interaction with other damage mechanisms.

In summary, there are still some open questions which need to be explored further. For the analysis about off-axis crack evolution, it is less studied how to quantify the interaction between adjacent cracks and how to describe the phenomena that stochastic crack evolution may scatter across multiple specimens under the same stress level. As for the analysis of delamination, it is necessary to figure out how to describe the severity of interaction with off-axis cracks, or the severity of its constraining effect on the off-axis cracking. Moreover, the analysis including both damage mechanisms, especially a progressive fatigue damage process where they initiate, accumulate and interact, with the possible scatter among tested specimens taken into account, is quite inadequate. Therefore, the focus of this thesis is put on the early fatigue damage, from the characterisation to the quantification, aiming at unfolding the initiation, accumulation and saturation of off-axis cracks, initiation and growth of delamination, as well as the interaction between both damage mechanisms.

The FRP composites of interest in this thesis are CFRP laminates, and they have been increasingly applied in the field of aerospace engineering due to their light weight. Considering the potential slow-growth approach for analysing the damage tolerance of composites used in aircraft, as advocated by Pascoe [80], damage growth might be allowed in the design phase if it is slow, stable and predictable. Therefore, it is meaningful to contribute our efforts towards the damage accumulation of CFRP laminates. However, this type of composites imposes an extra challenge on the damage characterisation within the laminate as they are non-transparent. Thus they have been studied less in comparison to transparent composites, i.e. glass-fibre reinforced composites. To address this challenge, a tough matrix is used in this thesis for the CFRP laminates, which could help provide a relatively high fatigue resistance and a relatively slow damage accumulation process during the early fatigue life, in order to obtain sufficient measurement points [12, 13]. On top of that, a cross-ply configuration, with a 90 ply block in the middle and 0 plies outside, is selected as it could form transverse cracks which are prone to propagate rapidly across the width of the laminate [19, 24]. To consider the size effect about the ply-block of 90 plies, this cross-ply configuration with two types of ply-block thickness is designed. In addition, three of the most widely-used techniques, AE, DIC and digital cameras for the edge observation, are employed in the experimental campaigns of this thesis, to achieve the in-situ damage monitoring. It is expected that the selected material, designed ply configurations and damage monitoring techniques could serve for the research aim of this thesis.

REFERENCES

[1] P. Alam, D. Mamalis, C. Robert, C. Floreani, and C. M. Ó Brádaigh, *The fatigue of carbon fibre reinforced plastics - A review,* Composites Part B: Engineering **166**, 555 (2019).

[2] K. L. Reifsnider and R. Jamison, *Fracture of fatigue-loaded composite laminates,* International Journal of Fatigue **4**, 187 (1982).

[3] H. Pakdel and B. Mohammadi, *Characteristic damage state of symmetric laminates subject to uniaxial monotonic-fatigue loading,* Engineering Fracture Mechanics **199**, 86 (2018).

[4] M. M. Shokrieh and F. Taheri-Behrooz, *Progressive fatigue damage modeling of cross-ply laminates, I: Modeling strategy,* Journal of Composite Materials **44**, 1217 (2010).

[5] A. Hosoi, K. Takamura, N. Sato, and H. Kawada, *Quantitative evaluation of fatigue damage growth in CFRP laminates that changes due to applied stress level,* International Journal of Fatigue **33**, 781 (2011).

[6] A. D'Amore and L. Grassia, *Phenomenological approach to the study of hierarchical damage mechanisms in composite materials subjected to fatigue loadings,* Composite Structures **175**, 1 (2017).

[7] J.-M. Berthelot, A. Ei Mahi, and J.-F. Le Corre, *Development of transverse cracking in cross-ply laminates during fatigue tests,* Composites science and technology **61**, 1711 (2001).

[8] M. C. Lafarie-Frenot, C. Hénaff-Gardin, and D. Gamby, *Matrix cracking induced by cyclic ply stresses in composite laminates,* Composites Science and Technology **61**, 2327 (2001).

[9] S. Abrate, *Matrix cracking in laminated composites: A review,* Composites Engineering **1**, 337 (1991).

[10] T. Watanabe, Y. Takeichi, Y. Niwa, M. Hojo, and M. Kimura, *Nanoscale in situ observations of crack initiation and propagation in carbon fiber/epoxy composites using synchrotron radiation X-ray computed tomography,* Composites Science and Technology **197**, 108244 (2020).

[11] P. A. Carraro and M. Quaresimin, *A damage based model for crack initiation in unidirectional composites under multiaxial cyclic loading,* Composites Science and Technology **99**, 154 (2014).

[12] J. Gassan and T. Dietz, *Fatigue behavior of cross-ply glass-fiber composites based on epoxy resins of different toughnesses,* Composites Science and Technology **61**, 157 (2001).

[13] X. Zhao, X. Wang, Z. Wu, and J. Wu, *Experimental study on effect of resin matrix in basalt fiber reinforced polymer composites under static and fatigue loading,* Construction and Building Materials **242**, 118121 (2020).

[14] K. Ogi, M. Takahashi, and S. Yashiro, *Empirical Models for Matrix Cracking in a CFRP Cross-Ply Laminate Under Static- and Cyclic-Fatigue Loadings,* Polymer Composites **32**, 1652 (2011), 1206.4529 .

[15] H. Pakdel and B. Mohammadi, *Stiffness degradation of composite laminates due to matrix cracking and induced delamination during tension-tension fatigue,* Engineering Fracture Mechanics **216**, 106489 (2019).

[16] C. Henaff-Gardin and M. C. Lafarie-Frenot, *Specificity of matrix cracking development in CFRP laminates under mechanical or thermal loadings,* International Journal of Fatigue **24**, 171 (2002).

[17] M. Eftekhari and A. Fatemi, *On the strengthening effect of increasing cycling frequency on fatigue behavior of some polymers and their composites: Experiments and modeling,* International Journal of Fatigue **87**, 153 (2016).

[18] P. P. Camanho, C. G. Dávila, S. T. Pinho, L. Iannucci, and P. Robinson, *Prediction of in situ strengths and matrix cracking in composites under transverse tension and in-plane shear,* Composites Part A: Applied Science and Manufacturing **37**, 165 (2006).

[19] H. Shen, W. Yao, W. Qi, and J. Zong, *Experimental investigation on damage evolution in cross-ply laminates subjected to quasi-static and fatigue loading,* Composites Part B:Engineering **120**, 10 (2017).

[20] B. Kötter, J. Endres, J. Körbelin, F. Bittner, H. J. Endres, and B. Fiedler, *Fatigue and fatigue after impact behaviour of Thin- and Thick-Ply composites observed by computed tomography,* Composites Part C: Open Access **5**, 100139 (2021).

[21] A. Hosoi and H. Kawada, *Fatigue life prediction for transverse crack initiation of CFRP cross-ply and quasi-isotropic laminates,* Materials **11**, 1182 (2018).

[22] S. G. Lim and C. S. Hong, *Prediction of Transverse Cracking and Stiffness Reduction in Cross-Ply Laminated Composites,* Journal of Composite Materials **23**, 695 (1989).

[23] N. Jagannathan, S. Gururaja, and C. M. Manjunatha, *Probabilistic strength based matrix crack evolution model in multi-directional composite laminates under fatigue loading,* International Journal of Fatigue **117**, 135 (2018).

[24] J. A. Glud, J. M. Dulieu-Barton, O. T. Thomsen, and L. C. Overgaard, *A stochastic multiaxial fatigue model for off-axis cracking in FRP laminates,* International Journal of Fatigue **103**, 576 (2017).

[25] M. May, R. Pullin, M. Eaton, C. Featherston, and S. R. Hallett, *An advanced model for initiation and propagation of damage under fatigue loading - part II: Matrix cracking validation cases,* Composite Structures **93**, 2350 (2011).

[26] J. A. Glud, J. M. Dulieu-Barton, O. T. Thomsen, and L. C. Overgaard, *Fatigue damage evolution in GFRP laminates with constrained off-axis plies,* Composites Part A: Applied Science and Manufacturing **95**, 359 (2017).

[27] V. V. Silberschmidt, *Matrix cracking in cross-ply laminates: Effect of randomness,* Composites Part A: Applied Science and Manufacturing **36**, 129 (2005).

[28] J. Llobet, P. Maimí, Y. Essa, and F. M. De, *Progressive matrix cracking in carbon / epoxy cross-ply laminates under static and fatigue loading,* International Journal of Fatigue **119**, 330 (2019).

[29] H. Ben Kahla, Z. Ayadi, F. Edgren, A. Pupurs, and J. Varna, *Statistical model for initiation governed intralaminar cracking in composite laminates during tensile quasi-static and cyclic tests,* International Journal of Fatigue **116**, 1 (2018).

[30] P. A. Carraro, L. Maragoni, and M. Quaresimin, *Characterisation and analysis of transverse crack-induced delamination in cross-ply composite laminates under fatigue loadings,* International Journal of Fatigue **129**, 105217 (2019).

[31] H. Pakdel and B. Mohammadi, *Prediction of outer-ply matrix crack density at saturation in laminates under static and fatigue loading,* International Journal of Solids and Structures **139-140**, 43 (2018).

[32] V. V. Silberschmidt, *Effect of micro-randomness on macroscopic properties and fracture of laminates,* Journal of Materials Science **41**, 6768 (2006).

[33] M. S. Loukil, J. Varna, and Z. Ayadi, *Applicability of solutions for periodic intralaminar crack distributions to non-uniformly damaged laminates,* Journal of Composite Materials **47**, 287 (2013).

[34] M. Hajikazemi, L. N. McCartney, W. Van Paepegem, and M. H. Sadr, *Theory of variational stress transfer in general symmetric composite laminates containing non-uniformly spaced ply cracks,* Composites Part A: Applied Science and Manufacturing **107**, 374 (2018).

[35] M. Mehdikhani, E. Steensels, A. Standaert, K. A. Vallons, L. Gorbatikh, and S. V. Lomov, *Multi-scale digital image correlation for detection and quantification of matrix cracks in carbon fiber composite laminates in the absence and presence of voids controlled by the cure cycle,* Composites Part B: Engineering **154**, 138 (2018).

[36] M. Mehdikhani, N. A. Petrov, I. Straumit, A. R. Melro, S. V. Lomov, and L. Gorbatikh, *The effect of voids on matrix cracking in composite laminates as revealed by combined computations at the micro- and meso-scales,* Composites Part A: Applied Science and Manufacturing **117**, 180 (2019).

[37] J. M. Berthelot and J. F. Le Corre, *Statistical analysis of the progression of transverse cracking and delamination in cross-ply laminates,* Composites Science and Technology **60**, 2659 (2000).

[38] L. Maragoni, P. A. Carraro, and M. Quaresimin, *Effect of voids on the crack formation in a [45/-45/0]s laminate under cyclic axial tension,* Composites Part A: Applied Science and Manufacturing **91**, 493 (2016).

[39] S. Koley, P. M. Mohite, and C. S. Upadhyay, *A micromechanical study and uncertainty quantification for effective properties of unidirectional fibre reinforced composites,* Composite Structures **225**, 111141 (2019).

[40] L. Maragoni, P. A. Carraro, and M. Quaresimin, *Development, validation and analysis of an efficient micro-scale representative volume element for unidirectional composites,* Composites Part A: Applied Science and Manufacturing **110**, 268 (2018).

[41] D. Ma, S. Campos Amico, M. Giglio, and A. Manes, *Effect of fibre bundle uncertainty on the tensile and shear behaviour of plain-woven composites,* Composite Structures **259**, 113440 (2021).

[42] C. V. Singh and R. Talreja, *Evolution of ply cracks in multidirectional composite laminates,* International Journal of Solids and Structures **47**, 1338 (2010).

2

[43] C. Singh, *Evolution of multiple matrix cracking,* in *Modeling Damage, Fatigue and Failure of Composite Materials* (Elsevier, 2016) pp. 143–171.

[44] J. Andersons, R. Joffe, and E. Spārniņš, *Statistical model of the transverse ply cracking in cross-ply laminates by strength and fracture toughness based failure criteria,* Engineering Fracture Mechanics **75**, 2651 (2008).

[45] J. Montesano and C. V. Singh, *Predicting evolution of ply cracks in composite laminates subjected to biaxial loading,* Composites part B **75**, 264 (2015).

[46] Y. Huang, J. Varna, and R. Talreja, *Statistical methodology for assessing manufacturing quality related to transverse cracking in cross ply laminates,* Composites Science and Technology **95**, 100 (2014).

[47] P. A. Carraro, L. Maragoni, and M. Quaresimin, *Prediction of the crack density evolution in multidirectional laminates under fatigue loadings,* Composites Science and Technology **145**, 24 (2017).

[48] G. Guillamet, A. Turon, J. Costa, and P. Linde, *A quick procedure to predict free-edge delamination in thin-ply laminates under tension,* Engineering Fracture Mechanics **168**, 28 (2016).

[49] M. Kashtalyan and C. Soutis, *Analysis of local delaminations in composite laminates with angle-ply matrix cracks,* International Journal of Solids and Structures **39**, 1515 (2002).

[50] P. Johnson and F.-K. Chang, *Characterization of Matrix Crack-Induced Laminate Failure — Part I : Experiments,* Journal of Composite Materials **35**, 2009 (2001).

[51] P. Johnson and F.-K. Chang, *Characterization of Matrix Crack-Induced Laminate Failure — Part II : Analysis and Verifications,* Journal of Composite Materials **35**, 2037 (2001).

[52] T. O'brien, *Characterization of delamination onset and growth in a composite laminate,* in *Damage in composite materials: basic mechanisms, accumulation, tolerance, and characterization* (ASTM International, 1982).

[53] F. Crossman and A. Wang, *The dependence of transverse cracking and delamination on ply thickness in graphite/epoxy laminates,* in *Damage in composite materials: basic mechanisms, accumulation, tolerance, and characterization* (ASTM International, 1982).

[54] N. Takeda, S. Ogihara, and A. Kobayashi, *Microscopic fatigue damage progress in CFRP cross-ply laminates,* Composites **26**, 859 (1995).

[55] L. Y. Xu, *Interaction between matrix cracking and edge delamination in composite laminates,* Composites Science and Technology **50**, 469 (1994).

[56] R. Talreja, *Damage and fatigue in composites – A personal account,* Composites Science and Technology **68**, 2585 (2008).

[57] A. V. Movahedi-Rad, T. Keller, and A. P. Vassilopoulos, *Fatigue damage in angle-ply GFRP laminates under tension-tension fatigue,* International Journal of Fatigue **109**, 60 (2018).

[58] C. Li, F. Ellyin, and A. Wharmby, *On matrix crack saturation in composite laminates,* Composites Part B: Engineering **34**, 473 (2003).

[59] T. Yokozeki, T. Aoki, and T. Ishikawa, *Fatigue growth of matrix cracks in the transverse direction of CFRP laminates,* Composites Science and Technology **62**, 1223 (2002).

[60] C. Cho, J. W. Holmes, J. R. Barber, and A. Arbor, *Distribution of Matrix Cracks in a Uniaxial Ceramic Composite,* Journal of the Americun Ceramic Society **75**, 316 (1992).

[61] L. Zubillaga, A. Turon, J. Renart, J. Costa, and P. Linde, *An experimental study on matrix crack induced delamination in composite laminates,* Composite Structures **127**, 10 (2015).

[62] F. E. Oz, N. Ersoy, M. Mehdikhani, and S. V. Lomov, *Multi-instrument in-situ damage monitoring in quasi-isotropic CFRP laminates under tension,* Composite Structures **196**, 163 (2018).

[63] M. Saeedifar and D. Zarouchas, *Damage characterization of laminated composites using acoustic emission: A review,* Composites Part B: Engineering **195**, 108039 (2020).

[64] V. Munoz, B. Valès, M. Perrin, M. L. Pastor, H. Welemane, A. Cantarel, and M. Karama, *Damage detection in CFRP by coupling acoustic emission and infrared thermography,* Composites Part B **85**, 68 (2016).

[65] C. Huang, S. Ju, M. He, Q. Zheng, Y. He, J. Xiao, J. Zhang, and D. Jiang, *Identification of failure modes of composite thin-ply laminates containing circular hole under tension by acoustic emission signals,* Composite Structures **206**, 70 (2018).

[66] R. Mohammadi, M. Ahmadi, M. Saeedifar, J. Youse, and G. Minak, *Correlation of acoustic emission with finite element predicted damages in open-hole tensile laminated composites,* Compoistes Part B **108**, 427 (2017).

[67] V. Arumugam, K. Saravanakumar, and C. Santulli, *Damage characterization of stiffened glass-epoxy laminates under tensile loading with acoustic emission monitoring,* Composites Part B **147**, 22 (2018).

[68] M. G. Sause, S. Schmitt, and S. Kalafat, *Failure load prediction for fiber-reinforced composites based on acoustic emission,* Composites Science and Technology **164**, 24 (2018).

[69] C. Baker, G. N. Morscher, V. V. Pujar, and J. R. Lemanski, *Transverse cracking in carbon fiber reinforced polymer composites : Modal acoustic emission and peak frequency analysis,* Composites Science and Technology **116**, 26 (2015).

2

[70] A. Tessema, S. Ravindran, and A. Kidane, *Gradual damage evolution and propagation in quasi-isotropic CFRC under quasi-static loading,* Composite Structures **185**, 186 (2018).

[71] I. Miskdjian, M. Hajikazemi, and W. V. Paepegem, *Automatic edge detection of ply cracks in glass fiber composite laminates under quasi-static and fatigue loading using multi-scale Digital Image Correlation,* Composites Science and Technology **200**, 108401 (2020).

[72] J. Berthe and M. Ragonet, *Passive infrared thermography measurement of transverse cracking evolution in cross-ply laminates,* Strain **54**, e12293 (2018).

[73] N. Toyama, S. Yashiro, J. Takatsubo, and T. Okabe, *Stiffness evaluation and damage identification in composite beam under tension using Lamb waves,* Acta Meterialia **53**, 4389 (2005).

[74] A. Rajabzadeh, R. Heusdens, R. C. Hendriks, and R. M. Groves, *Characterisation of Transverse Matrix Cracks in Composite Materials Using Fibre Bragg Grating Sensors,* Journal of Lightwave Technology **37**, 4720 (2019).

[75] J. Huang, M. L. Pastor, C. Garnier, and X. J. Gong, *A new model for fatigue life prediction based on infrared thermography and degradation process for CFRP composite laminates,* International Journal of Fatigue **120**, 87 (2019).

[76] D. Li, J. Zhou, and J. Ou, *Damage , nondestructive evaluation and rehabilitation of FRP composite-RC structure : A review,* Construction and Building Materials **271**, 121551 (2020).

[77] Z. Su, L. Ye, and Y. Lu, *Guided Lamb waves for identification of damage in composite structures : A review,* Journal of Sound and Vibration **295**, 753 (2006).

[78] N. Takeda, *Characterization of microscopic damage in composite laminates and real-time monitoring by embedded optical fiber sensors,* International Journal of Fatigue **24**, 281 (2002).

[79] B. Benchekchou and N. S. Ferguson, *The effect of embedded optical fibres on the fatigue behaviour of composite plates,* Composite Structures **41**, 113 (1998).

[80] J. A. Pascoe, *Slow-growth damage tolerance for fatigue after impact in FRP composites: Why current research won't get us there,* Theoretical and Applied Fracture Mechanics **116**, 103127 (2021).

3

Design of experiments

3.1. INTRODUCTION

As has been discussed in Section 2.7, CFRP cross-ply laminates with the ply configuration $[0_m/90_n]_s$ are used in this thesis. Details about the material and manufacturing properties of laminated panels, as well as the design of specimens are described in Section 3.2. Besides, the experimental set-up, with in-situ damage monitoring techniques involved, is introduced in Section 3.3. To check the availability of proposed experimental methods and to provide guidance for the fatigue testing, static tensile tests at different loading rates were carried out and results about damage accumulation are presented in Section 3.4. Finally, Section 3.5 summaries basic information about the fatigue test campaign related to this thesis: load condition and data acquisition, tested specimens and measured fatigue mechanical properties.

3.2. MATERIAL, MANUFACTURE AND SPECIMEN DESIGN

UNIDIRECTIONAL(UD) carbon fibre Prepreg is used during the manufacture of specimens, which is named as Hexply®F6376C–HTS(12 K)-5–35%. This Prepreg system contains high tenacity carbon fibres (Tenax®-E-HTS45) and tough epoxy matrix with high performance (Hexply®6376). The nominal fibre weight ratio and thickness of the Pregreg are 65% and 0.125 mm, respectively. The material properties of the UD-Prepreg layer in cured condition can be found in Table 3.1.

Table 3.1: Material properties of UD lamina manufactured by Hexply®F6376C-HTS(12 K)-5-35% Prepreg [1].(T - tension; C - compression)

Material properties	Values
Longitudinal modulus	E_{11T} = 142 GPa
Transverse modulus	$E_{22T} = E_{33T}$ = 9.1 GPa
In-plane shear modulus	$G_{12} = G_{13}$ = 5.2 GPa
Transverse shear modulus	G_{23} = 3.5 GPa
Longitudinal strength	X_T = 2274 MPa, X_C = 1849 MPa
Transverse strength	Y_T = 102 MPa, Y_C = 255 MPa
In-plane shear strength	$S_{12} = S_{13}$ = 63 MPa
Transverse shear strength	S_{23} = 35 MPa
In-plane Poisson ratio	$\nu_{12} = \nu_{13}$ = 0.27
Transverse Poisson ratio	ν_{23} = 0.30

Two types of cross-ply laminated panels were manufactured, with the stacking sequences of $[0/90_2]_s$ and $[0_2/90_4]_s$. After fabricating the two lay-ups, the laminates were inserted into an autoclave for the curing process. As recommended by the manufacturer [2], the temperature was 177 °C and the pressure was 7 bar for two hours during the curing cycle. Then, based on ASTM D3039/D3039M standard [3], the panels were cut, using a water-cooling diamond saw, into rectangular specimens of 250 mm × 25 mm, as shown in Figure 3.1(a). Thick paper tabs were glued on both ends of the specimen in 50 mm length, by using cyanoacrylate adhesive in order to increase clamping grip. Additionally, both edges of the specimen were covered with thin white paint to enhance the quality for the damage monitoring with the edge cameras. Finally, a white base coat was painted on the front surface of specimen and then designed speckle pattern with the dot size of 0.18 mm were printed on the surface.

3.3. EXPERIMENTAL SET-UP

TESTS campaigns were carried out on a 60 kN fatigue machine with hydraulic grips at room temperature, as shown in Figure 3.1(b). During the testing, edge observation, digital image correlation and acoustic emission systems were synchronised with the fatigue machine to create a synergistic work environment among different devices. Details about the setting of each system are introduced hereafter.

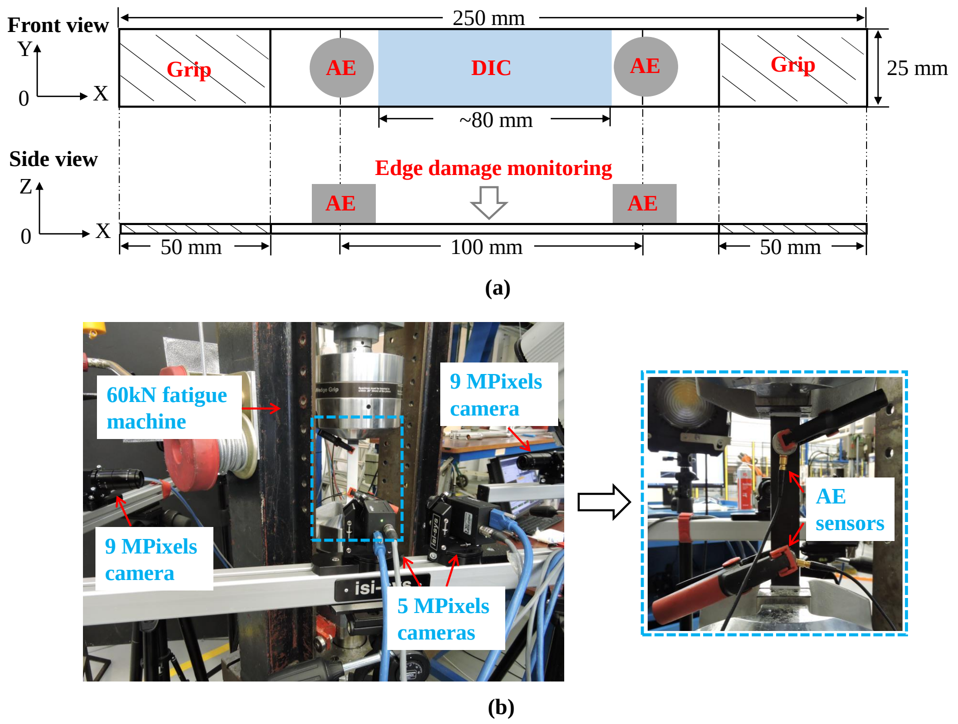

Figure 3.1: The schematic diagram of specimen dimensions, AE sensors' locations, measurement area of DIC and clamping regions (a); Experimental equipment (b).

3.3.1. EDGE OBSERVATION SYSTEM

A pair of 9 Megapixel cameras with 50 mm lens was placed at the left and right side of the clamped specimen to monitor transverse cracks from the edge view, as shown in Figure 3.1(b). After testing, the damage at edges was quantified through a user-defined MATLAB code. Here, for an example of quantifying the number and position of transverse cracks, the main steps of image processing are described as following. Figure 3.2 shows the original image **I0** which is a local region of 90 plies for one of the $[0_2/90_4]_s$ laminates captured during the fatigue testing, and processed images **I1**-**I3** after each step. By using this image processing algorithm, both transverse cracks at 90 plies and interlaminar cracks at 0/90 interfaces, can be automatically identified with less time cost.

Step 1: The captured image **I0** in Figure 3.2 is initially processed using a bottom-hat filtering to produce **I1**. This image filtering functions as computing the morphological closing (e.g. cracks in the current case) of the original image and then subtracting the original image from the result of computed morphological closing. Here, according to a structuring element SE, a dilation followed by an erosion is operated to obtain the morphological closing.

I1 = imbothat (**I0**, SE);

Step 2: The processed image **I1** is converted to the binary image **I2** based on a threshold T of luminance value, which ranges from zero to one. The aim here is to create a better contrast of crack and uncracked regions.

I2 = imbinarize (**I1**, T);

Step 3: The noise of the binary image **I2**, which has connected components(objects) fewer than P pixels, as marked in Figure 3.2 with red circles, is removed, thus producing another binary image **I3**.

I3 = bwareaopen (**I2**, P);

Step 4: The connected components in the binary image **I3** are labelled, where the number of transverse cracks (connected white pixels) can be obtained by **N** and the labelled image is stored in **L** .

[**L**, **N**] = bwlabel (**I3**);

Step 5: The position properties for each connected component(object) in **L** can be measured in this step, thus the recognised cracks can be localised.

Position = regionprops (**L**, 'BoundingBox');

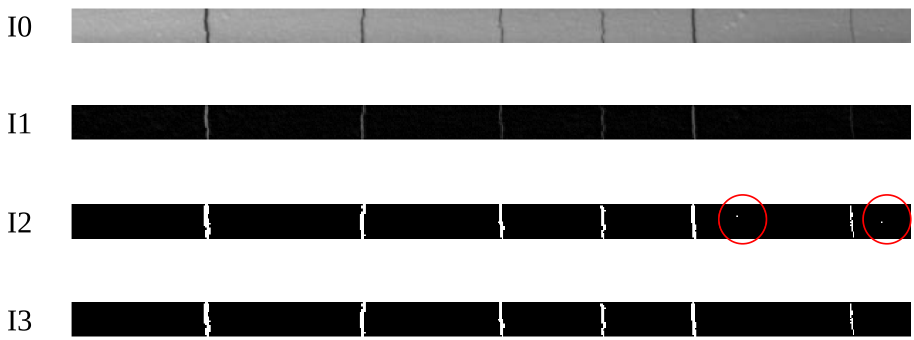

Figure 3.2: Image processing for monitoring transverse cracks.

3.3.2. DIGITAL IMAGE CORRELATION SYSTEM

DIC was employed to measure the displacement and strain distributions of the exterior 0 ply. In fact, two different positions of a specimen can be applied with DIC system to monitor the strain/displacement distributions during the test, i.e. the edge and the exterior 0 ply. Considering the thickness of the specimens (~0.75 mm for $[0/90_2]_s$ laminates and ~1.5 mm for $[0_2/90_4]_s$ laminates), it is extremely difficult to monitor the entire edge with accurate measurements. The speckle pattern, applied on the edges, could affect the contrast of edge images and disturb the identification of transverse cracks during the post image processing. Therefore, a pair of 5 Megapixel cameras with 23 mm lens was placed in the front side of the specimen, as shown in Figure 3.1(b), to measure the global axial deformation and the strain distribution close to the cracked regions of 90 plies. Post-processing was performed using the commercial software VIC-3D by Correlated Solutions™. A subset size of 29 pixels and step size of 7 pixels were selected for correlation analysis. The length of the view field for in-situ strain measurement was approximately 80 mm. Based on the experimental findings in [4–6], it is expected that strain concentration at the DIC measurement region due to the damage accumulated inside specimens may be used to provide the information about transverse cracks and delamination.

3.3.3. ACOUSTIC EMISSION SYSTEM

TWO broadband VS900-M AE sensors with a diameter of 20.3 mm and a frequency range of 100–900 kHz were clamped on the specimen. The distance between two sensors was fixed to 100 mm for all tests, as shown in Figure 3.1. Vacuumed silicon grease was used between the AE sensor and the specimen surface to create good acoustical coupling. The AMSY-6 4(8)-channel Vallen system was used to record the AE activity. Two pre-amplifiers with gain of 34 dB and band-pass filter of 20–1200 kHz were used to connect the sensors to the AE system. Before each test, pencil lead breaks were performed to calibrate the data acquisition system. In all tests, the sampling rate was set as 2 MHz, while the threshold of amplitude was set as 45 dB for static tests and 50 dB for fatigue tests. The AE features were recorded during testing, in order to correlate with the damage accumulation process.

3.4. VERIFICATION OF EXPERIMENTAL METHODS UNDER STATIC LOADING

AS the very first step of research activities in this thesis, $[0_2/90_4]_s$ laminates were tested under static loading with different loading rates. The aim is to evaluate the capabilities of established experimental methods, including the design of specimens and the test set-up, for monitoring the evolution of matrix damage during different testing periods.

The observed damage accumulation under static loading could provide knowledge for the further investigations of early fatigue damage, which is more complex to understand and time-consuming to monitor and quantify.

3.4.1. LOAD CONDITION AND DATA ACQUISITION

DIFFERENT loading rates were involved for static tests, under load or displacement control mode, as listed in Table 3.2. 100 mm gauge length was monitored from the edge view for measuring the damage occurred at edges. The image acquisition for edge damage monitoring and digital image correlation systems is 5-150 frame-per-second, depending on the loading rate. Beside basic features of AE signals like amplitude, energy, duration, rise time, etc., the waveform was recorded during testing.

Table 3.2: The control mode and loading rate under static loading.

Control mode	Loading rate
Load	0.019 kN/s
	0.19 kN/s
	1.9 kN/s
	19 kN/s
Displacement	1 mm/min

3.4.2. TRANSVERSE CRACKS

BASED on the image processing algorithm mentioned in Section 3.3.1, the number and location of transverse cracks generated at 90 plies can be obtained for each time interval of image acquisition under static loading.

TABLE 3.3 and 3.4 list the load level F/F_{max} and location X when and where the first transverse crack initiates under each loading condition. Here, the load level F/F_{max} is represented as the percentage of the current load F to the maximum load F_{max}. Besides, $X = 0$ mm is at the fixed side of the specimen, while $X = 100$ mm is near the loading side.

Among three specimens of each loading rate, the first transverse crack occurred at an arbitrary position of the inner 90 plies and the corresponding load level was distributed in the range from 52.50% to 87.12%, as shown in Table 3.3 and 3.4. As is the inherent material defects distributed inside the specimen that highly affect the origins of transverse matrix crack [7], these differences about the first crack initiation actually reflect the hardly-unified material/manufacturing defects among specimens.

Table 3.3: Load level when the transverse matrix crack initiated.

Loading rate	Load level F/F_{max} (%)		
	Specimen #1	Specimen #2	Specimen #3
0.019 kN/s	81.88	61.32	85.66
0.19 kN/s	82.43	52.50	66.07
1.9 kN/s	83.24	85.00	78.79
19 kN/s	73.02	75.01	87.12
1 mm/min	76.30	69.51	81.00

Table 3.4: Location of the first transverse matrix crack initiated.

Loading rate	Location X (mm)		
	Specimen #1	Specimen #2	Specimen #3
0.019 kN/s	79.49	29.15	88.95
0.19 kN/s	35.42	71.59	24.75
1.9 kN/s	91.33	66.26	38.67
19 kN/s	67.94	44.50	18.77
1 mm/min	61.13	73.07	16.05

DURING the testing, the number of transverse cracks at both left and right sides was nearly the same at each time interval of image acquisition, supporting the fact that the transverse matrix cracks might rapidly propagated through the entire width direction. This statement is later supported by the DIC analysis in Section 3.4.4.

Beside the initiation, the accumulation of transverse cracks also slightly varies among specimens. Table 3.5 lists the deviation of ρ_{max} which is the crack density before the failure. Crack density ρ here can be calculated as $M/2L$, where M is the number of transverse cracks generated on both edges and L is the gauge length 100 mm. In fact, the stochastic phenomena about transverse crack formation under static loading, not only exits among specimens presented as varying density and load levels, but also visualised within one specimen where a random distribution of transverse cracks along the length direction is showed at 90 plies. To further describe this randomness of the spatial distribution in each specimen, crack-spacing d between every two adjacent cracks before the failure is measured. Then, the average, minimum and maximum crack spacing, $d_{average}$, d_{min}, d_{max}, are summarised, see Table 3.5. Due to this nonuniform crack distribution, the difference of local crack density ρ_L every 20 mm length is significant, as shown in Figure 3.3. Therefore, it is necessary to guarantee a large view field for the edge damage monitoring, as the small gauge region might not be sufficient to represent the damage state of the entire specimen.

Table 3.5: Crack density and crack spacing of 90 plies before the final failure of specimens.

Loading rate	Crack density	Crack spacing d (mm)		
	ρ_{max} (mm^{-1})	$d_{average}$	d_{min}	d_{max}
0.019 kN/s	0.24 ± 0.02	3.64 ± 0.15	1.12±0.75	9.07 ± 1.05
0.19 kN/s	0.30 ± 0.04	3.33 ± 0.47	0.57±0.26	10.03 ± 3.59
1.9 kN/s	0.16 ± 0.01	5.59 ± 0.32	0.63±0.19	16.43 ± 6.03
19 kN/s	0.14 ± 0.02	5.84 ± 0.47	0.44±0.06	19.57 ± 7.71
1 mm/min	0.25 ± 0.02	3.84 ± 0.37	0.91±0.67	14.24 ± 3.89

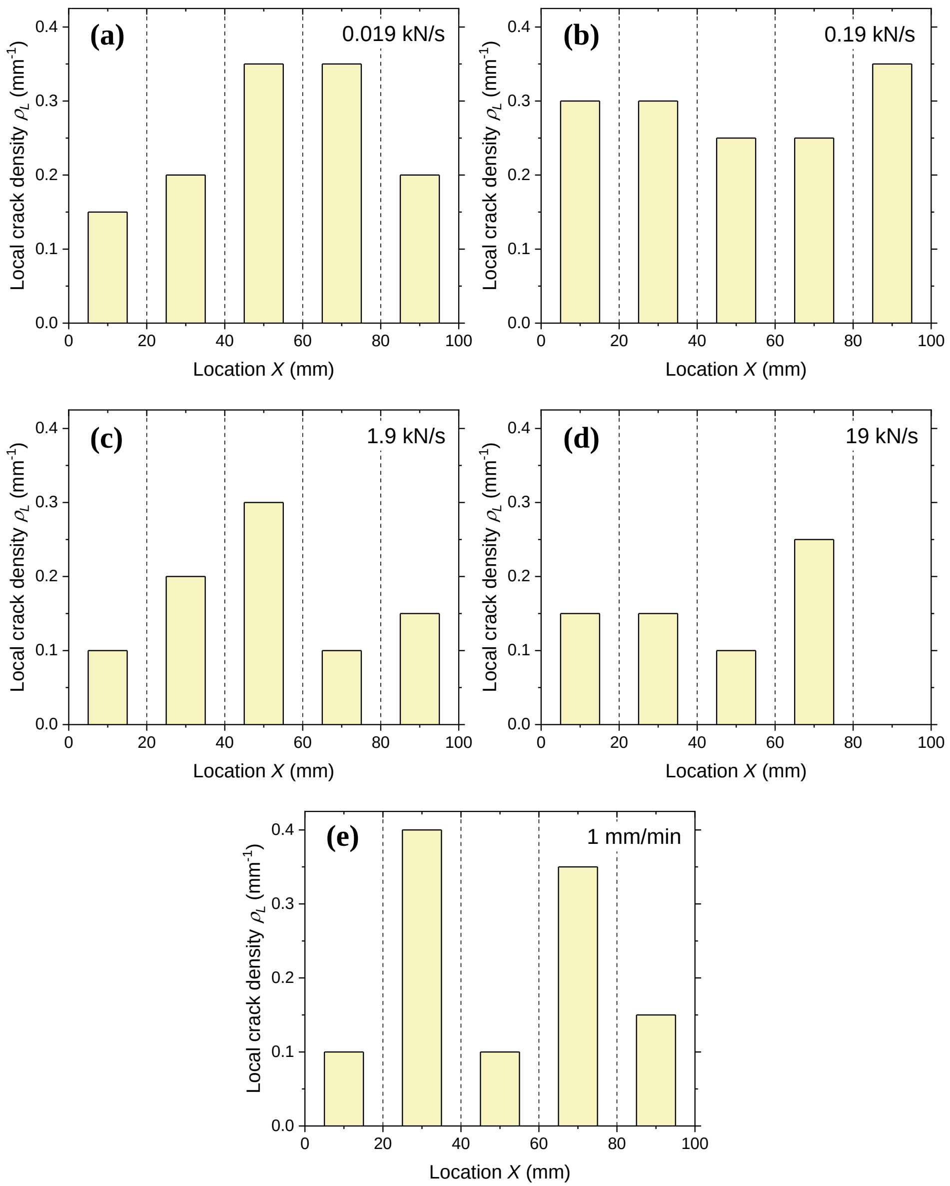

Figure 3.3: The local crack density at every 20 mm region of edges before the final failure.

3.4.3. INTERLAMINAR CRACKS

FROM the edge view, interlaminar cracks, originating at the tips of transverse cracks, were observed at 0/90 interfaces. Figure 3.4 presents two local regions along the loading direction (i.e. $0 \leqslant X \leqslant 25$ mm and $50 \leqslant X \leqslant 75$ mm), where typical morphology of the co-existing of transverse and interlaminar cracks before the failure is highlighted, shaping as H, L and T. Besides these three types, Carraro et al. [8] also found Z-shaped and mixed-shaped crack morphology. They reported that H shape presents the highest chance to be formulated in specimens since the two interfaces are nominally subjected to the same stress fields in the presence of a transverse crack.

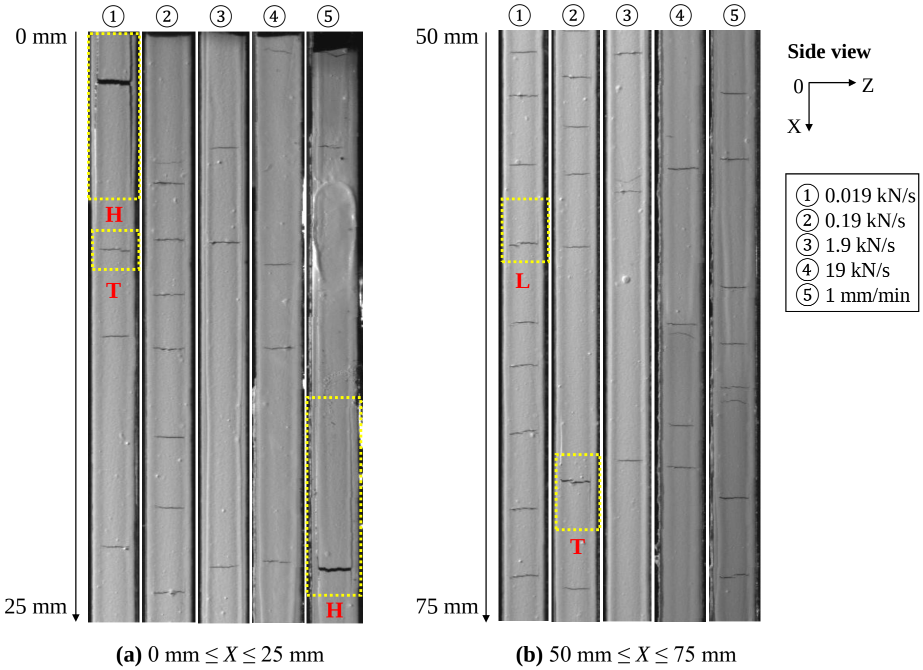

Figure 3.4: The distribution patterns of co-existing transverse and inter-laminar cracks at two local regions of the specimen edge before the failure.

The observation of interlaminar cracks provides a way to measure the delamination propagating along edges using the present test set-up. However, how to measure delamination propagation through the width is unclear as the delamination growth is insignificant for the designed specimens under static loading.

3.4.4. CORRELATION AMONG DIFFERENT SYSTEMS

BESIDES damage information from edge cameras, acoustic emission signals and DIC results are also analysed to check the correlation among these systems.

1. EDGE OBSERVATION AND AE ANALYSIS

AS waveform of AE signals was recorded, Fast Fourier Transform is used to obtain the peak frequency f_p, as presented in Figure 3.5, which is usually regarded as a representative feature to interpret the AE activity.

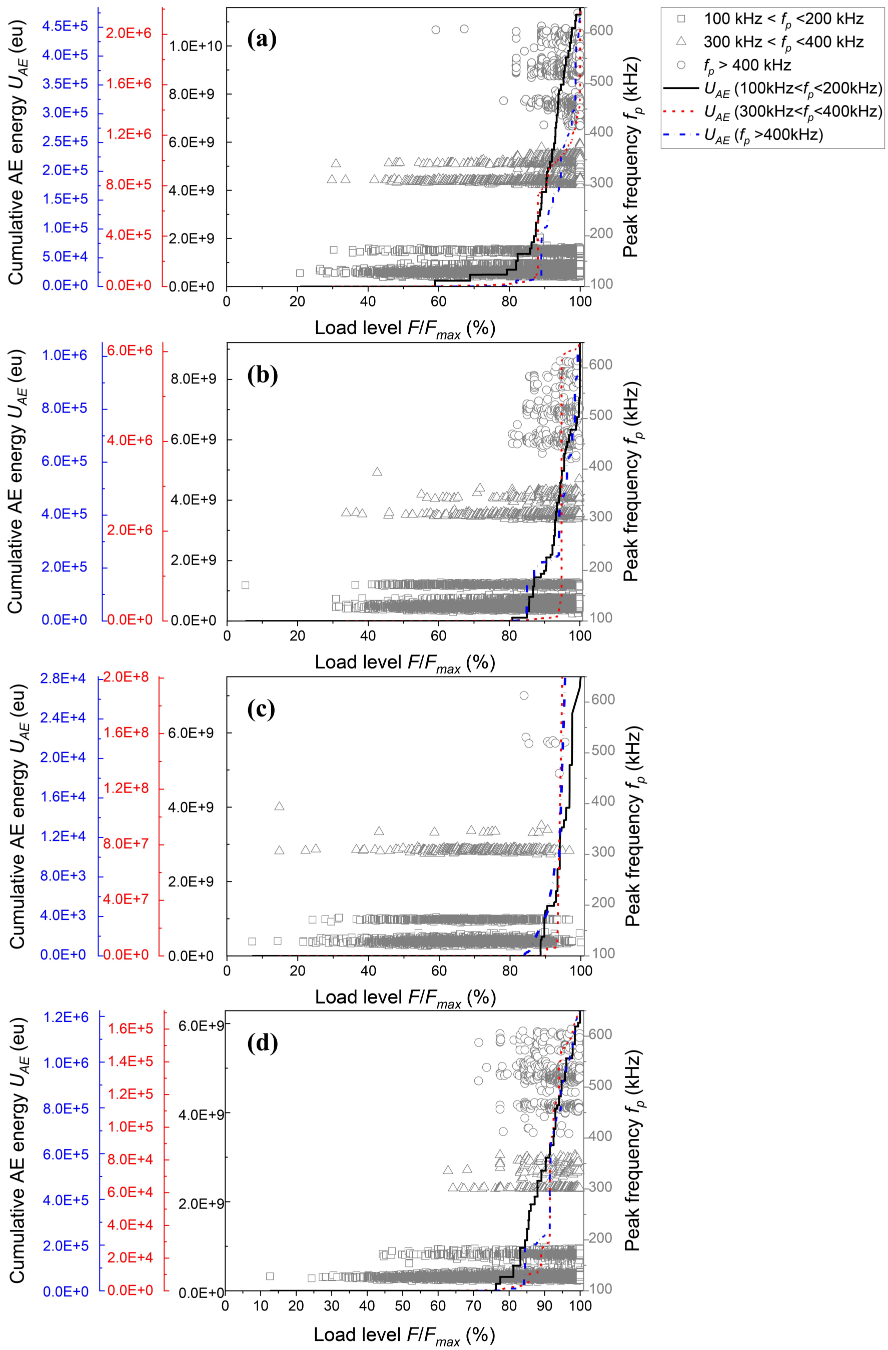

Figure 3.5: Three bands of peak frequency among AE activities and the related cumulative energy plotted with the increase of load level at different loading rates: (a) 0.019 kN/s, (b) 0.19 kN/s, (c) 1.9 kN/s, (d)1 mm/min. *Note*: 1 eu × 10000 Ω = 10^{-18} J [9].

The reason for choosing peak frequency is because it is less affected by the attenuation happened during the wave propagation, compared with amplitude, duration, etc. [10]. Figure 3.5 presents three bands of peak frequency (i.e. 100–200 kHz, 300–400 kHz and > 400 kHz) among AE activities, and the corresponding growing trends of cumulative energy U_{AE} with the increase of the load level. Here, the energy of each AE activities is defined as the area under the squared signal envelope [11], as shown in Figure 2.5. 19 kN/s were not analysed because almost 95% of AE activities occurred near the failure phases. The AE activity started at around 10% to 30% of the failure load, while the cumulative energy began to increase at the load level around 60% to 80%. The origin of the early AE activity with negligible cumulative energy indicates the development of micro-cracks before transverse cracks initiated. The highest cumulative energy during the tests is provided by AE activity in the peak frequency range from 100 kHz to 200 kHz.

Among three groups of AE activity classified by peak frequency, similar growing trends of crack density and cumulative energy as a function of the load level F/F_{max} were observed for the low frequency band (100–200 kHz), as presented in Figure 3.6. Here, both crack density and cumulative energy are normalised by their values at the peak load, as expressed as ρ/ρ_{max} and $U_{AE}/U_{AE_{max}}$, respectively. Each jump of ρ/ρ_{max} can sufficiently correlate to certain stepping increase of $U_{AE}/U_{AE_{max}}$.

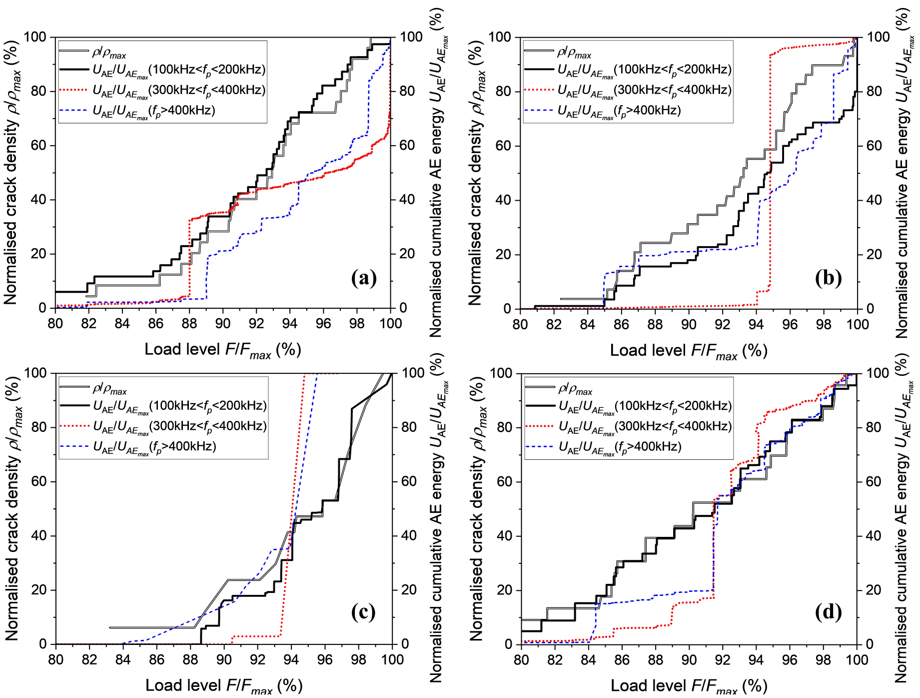

Figure 3.6: The normalised crack density and normalised cumulative energy of AE activities located at different frequency bands as a function of the load level under loading rates: (a) 0.019 kN/s, (b) 0.19 kN/s, (c) 1.9 kN/s, (d)1 mm/min

Therefore, AE activities in the low frequency level are dominantly related to transverse cracks. This conclusion is in agreement with the majority findings in literature [12–14], but it does not match with what Oz et al. reported [15]. The authors observed that matrix cracks at the inner 90 plies usually generate AE activity with peak-frequency of higher ranges and they explained that the depth of the damage source can affect the AE characteristics. In the present study, the thickness of exterior 0 plies for $[0_2/90_4]_s$ laminates is only 0.25 mm, thus the through thickness distance of a transverse crack to AE sensors can barely affect the corresponding AE characteristics.

Furthermore, the normalised crack density is plotted against the normalised cumulative AE energy of low-frequency AE activities (i.e. 100–200 kHz), where a linear correlation is found, see Figure 3.7. This plot demonstrates that the cumulative energy of low-frequency AE activities can describe the accumulation of transverse cracks for $[0_2/90_4]_s$ laminates, which further paves a promising way for the real-time quantification of transverse crack evolution based on AE features.

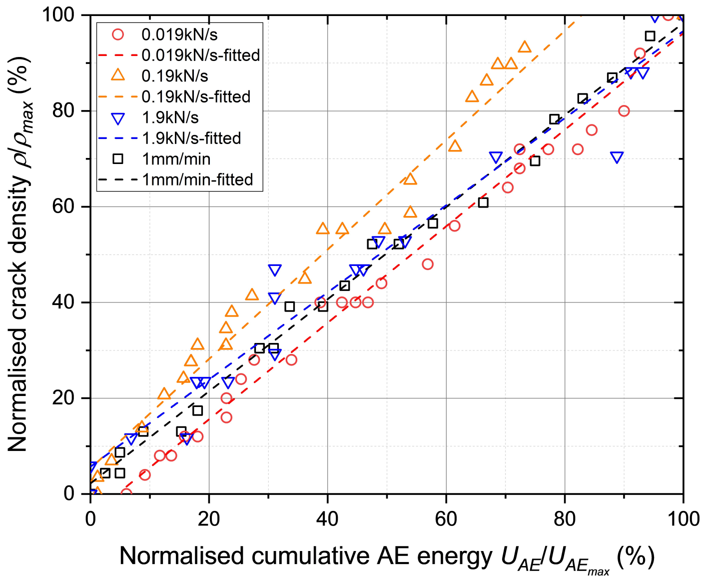

Figure 3.7: The relationship between normalised crack density and normalised cumulative energy of low-frequency AE activities at different loading rates.

2. EDGE OBSERVATION AND DIC ANALYSIS

REGARDING DIC analysis, axial strain distributions at the exterior 0 ply under four different loading levels (i.e. 85%, 90%, 95% and 100% of the maximum load) are presented in Figure 3.8. When transverse cracks started to initiate, strain concentrations with narrow strips (2.8 mm to 5.2 mm) occurred through the width of the specimens. As the load increased, some of these strips expanded or connected with their neighbours to form large strain concentrations. Further, the distribution of transverse cracks, obtained from edge observations, is compared with axial strain distributions measured by DIC at the peak load, as shown in Figure 3.9.

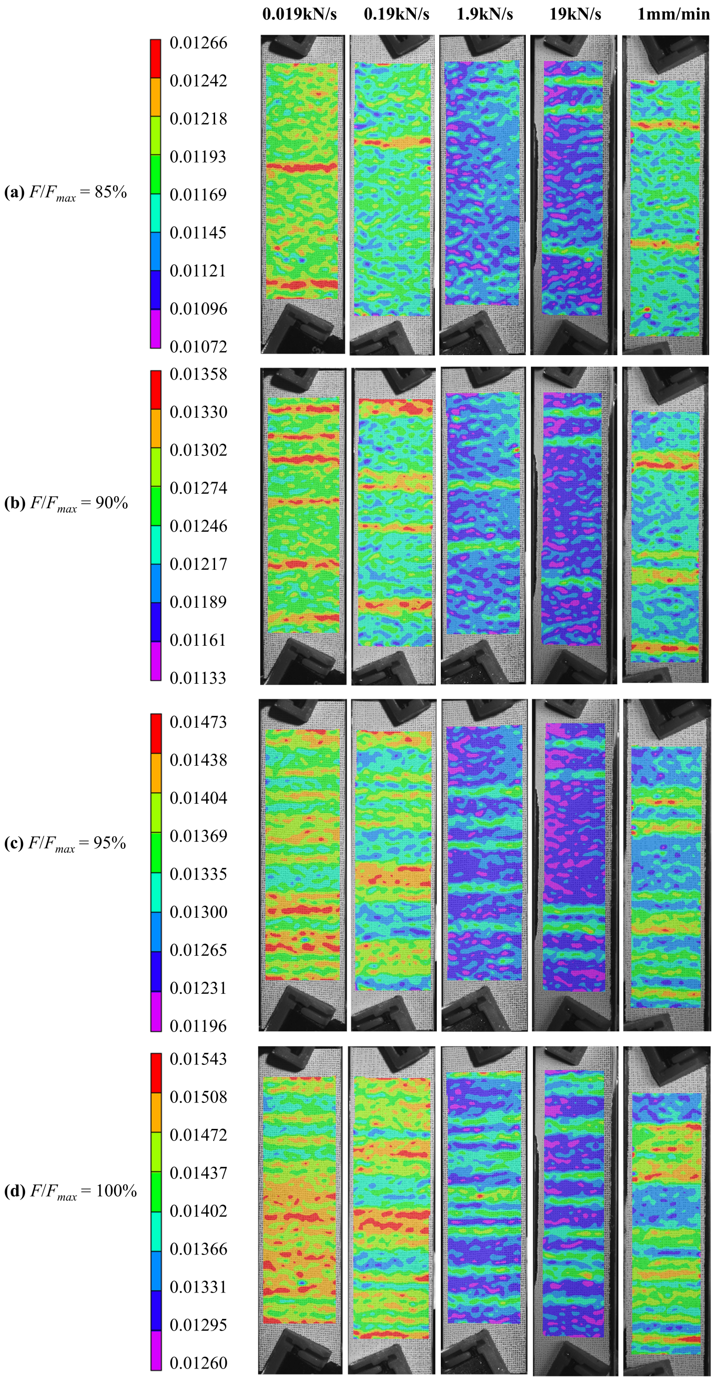

Figure 3.8: Axial strain distributions at the outer 0 ply under different load levels.

3

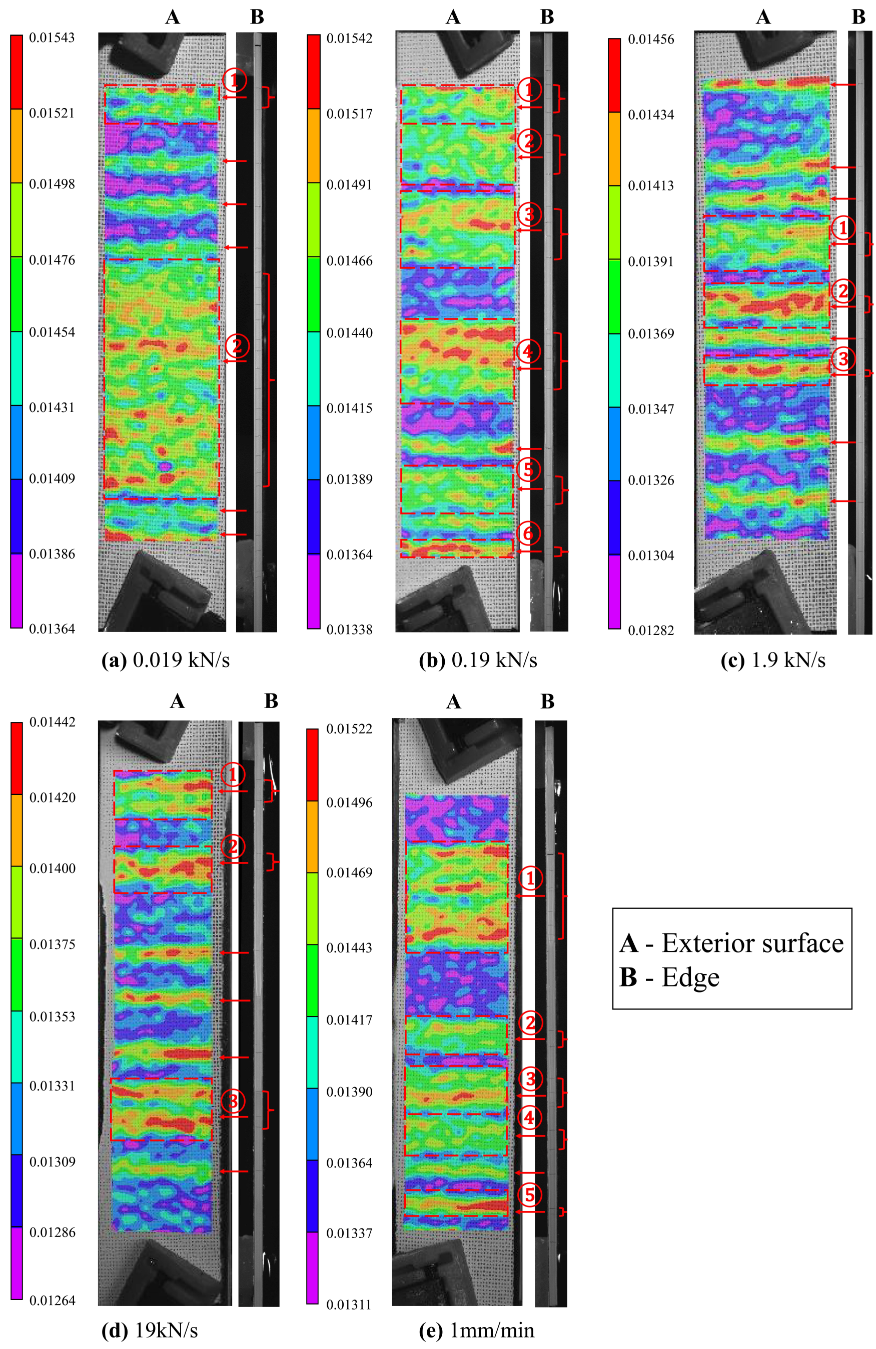

Figure 3.9: Correlation between strain concentrations at the exterior 0 ply and transverse cracks generated from the edge view at the maximum load.

Figure 3.9 shows a good correlation of transverse cracks at the inner 90 plies and strain concentrations at the exterior 0 ply. The red dash boxes at the front surface of specimens were used to label the strain concentration regions and the transverse cracks generated at the related local region were marked by the curly brackets at edges. It can be concluded that the uneven distribution of strain at the 0 plies is caused by transverse cracks at 90 plies. Besides, as the strain concentration distributed across the width, it further indicates that transverse cracks propagated through the width immediately once being initiated in $[0_2/90_4]_s$ laminates. In view that the interlaminar cracks were not widely distributed along the edge and they did not propagate broadly inside the specimens under tensile loading, their effects on the distributions pattern of axial strain are negligible for $[0_2/90_4]_s$ laminates under tensile loading.

3

3.4.5. DISCUSSIONS

ACCORDING to the monitoring and analysis about damage accumulation process of $[0_2/90_4]_s$ laminates under tensile loading, the present experimental methods show the capabilities for providing sufficient information about the accumulation of transverse cracks in varying loading rates and testing periods. Not only edge damage images, but also DIC strain distribution and acoustic emission energy provide the crack-related information during the loading process.

Significant stochastic initiation and accumulation of transverse cracks were presented within one specimen or among specimens, which are due to the manufacturing inhomogeneity. The following analysis about the transverse cracks generated under fatigue loading should take this phenomena into account.

Besides, whether the delamination propagating inside the specimens can be in-situ measured is not clear yet. This is because that nearly no significant delamination propagation is induced under tensile loading which is probably not the case for fatigue loading. However, as interlaminar cracks have been observed from the edge view, the current test set-up should be able to capture the delamination propagating along the length.

3.5. EXPERIMENTAL CAMPAIGN UNDER FATIGUE LOADING

BASED on the knowledge and experience obtained from the static testing, fatigue experimental campaign of this thesis is further conducted for both the $[0/90_2]_s$ and the $[0_2/90_4]_s$ laminates. The focus is firstly put on the laminates with thin 90 plies, as literature [8, 16, 17] shows that thin plies are prone to constrain the material/manufacturing defects and formation of delamination. When the early fatigue damage for laminates with thin 90 plies is understood, the analysis will further move to the laminates with thick 90 plies which have the high chances of the interaction of both transverse cracks and delamination.

Section 3.5.1 describes the details about load condition and data acquisition. Then, tested specimens are summarised in Section 3.5.2 and the mechanical properties changing with the increase of fatigue cycles are analysed in Section 3.5.3.

3.5.1. LOAD CONDITION AND DATA ACQUISITION

DURING fatigue testing, cyclic loading with sinusoidal waves at the constant amplitude was imposed on clamped specimens under load control mode. The stress ratio and frequency were fixed at 0.1 and 5 Hz, respectively. For each lay-up, different stress levels were applied during testing. After every 500 cycles, a tensile unloading-loading ramp was performed in two seconds where image acquisitions were triggered and images for edge damage monitoring and DIC systems were taken every 50 ms or 100 ms. The load profile is visualised in Figure 3.10. Acoustic emission signals were recorded during the entire loading process. Different from the static testing, waveform of AE signals was not recorded to reduce the size of AE data. Besides, the gauge region for the edge damage monitoring system is reduced from 100 mm to 80 mm length. One reason is to keep the same gauge area as the DIC system for later an accurate analysis about the stiffness degraded by transverse cracks. Another reason is to improve the resolution of the measurements of transverse cracks for $[0/90_2]_s$ laminates, as the thickness of 90 plies is ~0.5 mm.

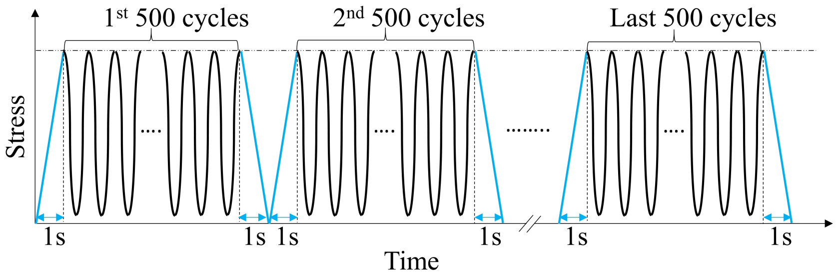

Figure 3.10: Load profile of tension-tension fatigue.

Considering the focus of this thesis is on the early fatigue damage, tests executed when the evolution of transverse cracks reached a saturated state for $[0/90_2]_s$ laminates. As for $[0_2/90_4]_s$ laminates, tests stopped when the stiffness degradation went through the first stage and approached the stable phase of the second stage. Besides, the run-off of all fatigue tests was set to ~1e6 cycles.

3.5.2. SUMMARY OF TESTED SPECIMENS

DETAILS about tested specimens under fatigue loading are summarised in Table 3.6. Two to seven tests were repeated for each load case. Here, the values of maximum cyclic stress and the corresponding percentage of ultimate tensile strength (UTS) for two ply configurations are listed. The ultimate tensile strength is obtained from static tests at 1mm/min, which is is 723.8 MPa and 800 MPa for $[0/90_2]_s$ and $[0_2/90_4]_s$ laminates, respectively. Besides, the axial stress of the first crack initiation σ_{90_i} is also obtained from static tests, which is 509.94 MPa and 626.43 MPa for the thick and thin laminates, accordingly. Thus, the percentage of σ_{90_i} for each stress level can be calculated, as shown in Table 3.6.

Table 3.6: Maximum stress levels and number of specimens for fatigue tests.

Stacking sequence	$[0/90_2]_s$			$[0_2/90_4]_s$				
Maximum cyclic stress (MPa)	613	560	507	533	507	480	453	400
Percentage of UTS (%)	77	70	63	74	70	66	63	55
Percentage of σ_{90_i} (%)	98	89	81	105	99	94	89	78
Number of specimens	2	2	2	3	7	6	4	3

3.5.3. FATIGUE MECHANICAL PROPERTIES

STRESS/STRAIN hysteresis loops are usually used to obtain secant stiffness and dynamic stiffness (also termed as fatigue stiffness [18]) with and without considering the creep effect, respectively [19]. Here, dynamic stiffness along the loading direction was calculated every 500 cycles, based on the slope of σ_{xx} and $\bar{\epsilon}_{xx}$ for each tensile loading ramp (see Figure 3.10), where σ_{xx} is the axial stress of the laminate and $\bar{\epsilon}_{xx}$ is the average axial strain at the gauge region of the exterior 0 ply calculated by DIC.

According to the classical lamination theory, both ply configurations have the same longitudinal stiffness due to the same ratio of 0-ply thickness to the 90-ply thickness. However, Figure 3.11 and Figure 3.12 show the differences about the degradation of normalised longitudinal stiffness E_N/E_0 in function of number of cycles N for both ply configurations.

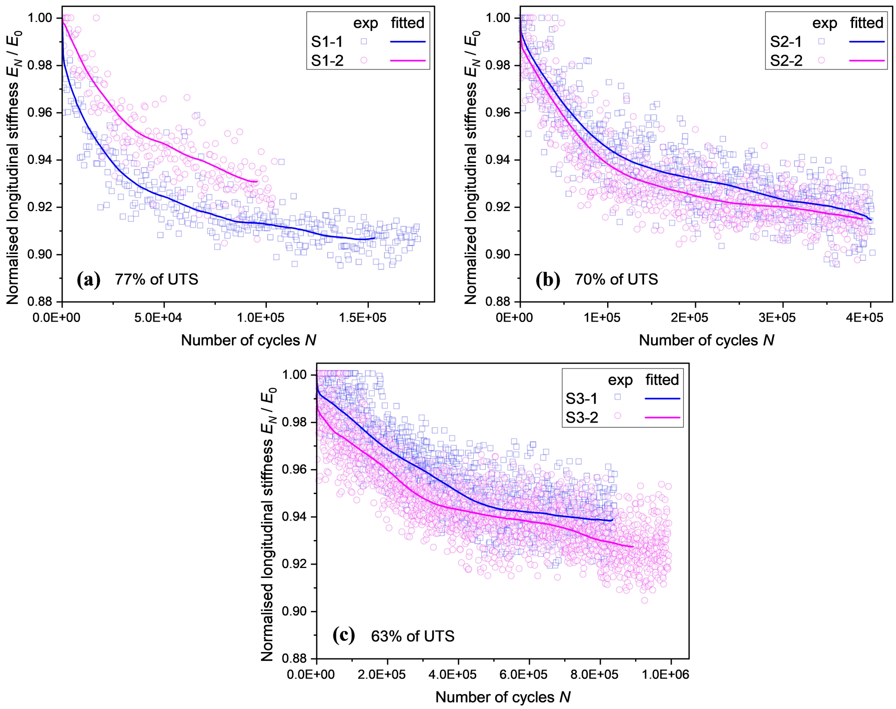

Figure 3.11: Normalised longitudinal stiffness versus number of cycles for $[0/90_2]_s$ laminates.

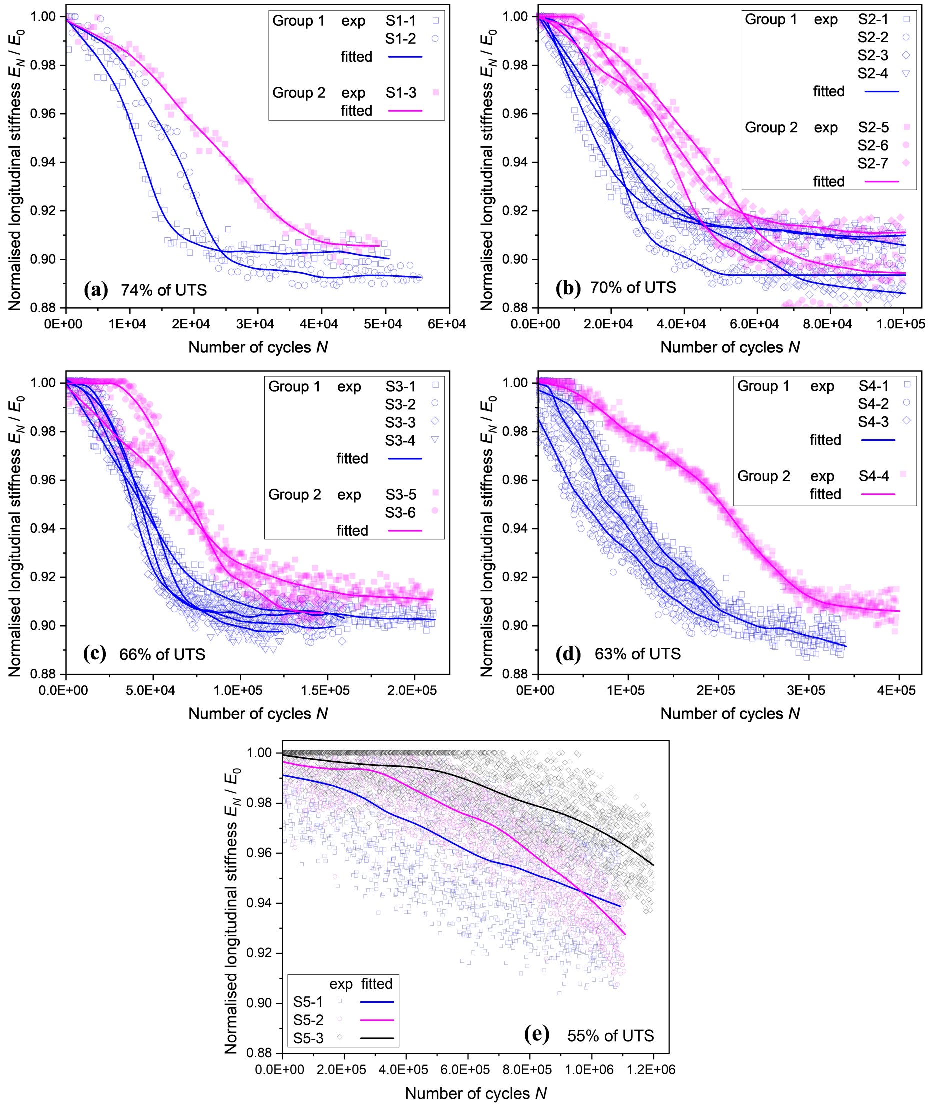

Figure 3.12: Normalised longitudinal stiffness versus number of cycles for $[0_2/90_4]_s$ laminates.

Here, E_0 is the initial axial stiffness obtained from the first tensile loading ramp (see Figure 3.10) and E_N is the degraded axial stiffness at the cycle N.

For the $[0/90_2]_s$ laminates, stiffness degradation trends are similar for a certain stress level, as thin plies restrain the manufacturing inhomogeneity [16]. 6%-10% drop of stiffness is exhibited in the end of tests. A bi-linear decrease of stiffness is presented in a rapid-slow manner, which can hardly reach a constant state of stiffness degradation (see Figure 3.11).

Regarding the $[0_2/90_4]_s$ laminates, the degrading trends of stiffness for the $[0_2/90_4]_s$

laminates are different from those for the $[0/90_2]_s$ laminates, indicating the different damage accumulation process. For the stress level at 55% of UTS, as shown in Figure 3.12 (e), the stiffness until the run-off (~1e6 cycles) did not degrade to a plateau like other stress levels. Therefore, the following analysis about the stiffness and Poisson's ratio excludes this load case.

In Figure 3.12 (a)-(d), two groups of specimens, classified by the decreasing rate of the stiffness within Stage I, are presented under the stress level at 74%, 70%, 66% and 63% of UTS. Group 1 shows a faster trend of stiffness degradation at Stage I than Group 2. This is due to the manufacturing inhomogeneity that two levels of fatigue resistance are performed among specimens. As the stress level decreases, the difference of degrading rates between two groups is increasingly significant, which means that the manufacturing inhomogeneity is magnified under low stress level. Until the stiffness reaches the plateau, the loss of stiffness in the early fatigue life is about 8-12% of initial stiffness, no matter which stress level is applied.

As for the changes of Poisson's ratio during the fatigue loading for both ply configurations, they are presented in Figure 3.13 and Figure 3.14. Here, Poisson's ratio v is calculated as $-\bar{\epsilon}_{yy}/\bar{\epsilon}_{xx}$, where $\bar{\epsilon}_{yy}$ is the average transverse strain within the gauge region from DIC measurements.

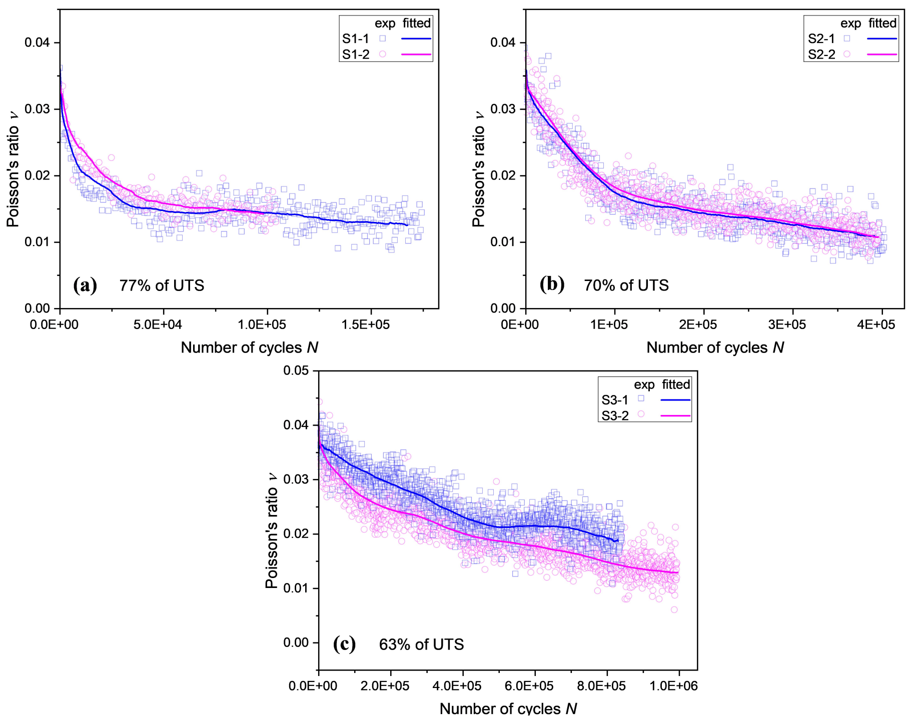

Figure 3.13: The change of Poisson's ratio for the exterior 0 ply as fatigue cycles increase for $[0/90_2]_s$ laminates.

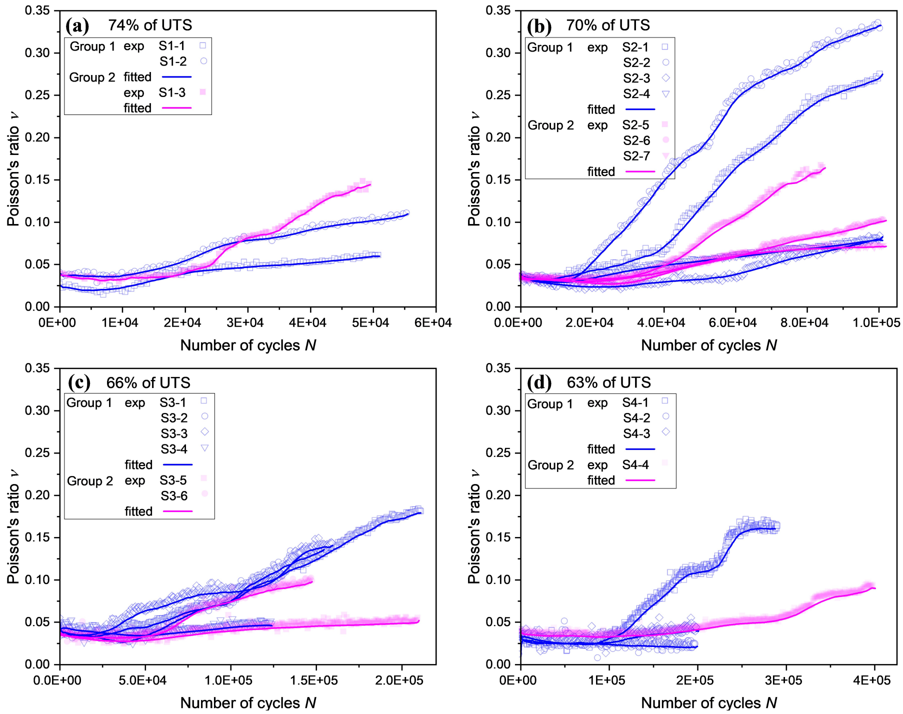

Figure 3.14: The change of Poisson's ratio for the exterior 0 ply as fatigue cycles increase for $[0_2/90_4]_s$ laminates.

With the increase of fatigue cycles, a decrease of υ is observed for the $[0/90_2]_s$ laminates in Figure 3.13, while most of the $[0_2/90_4]_s$ laminates show the opposite in Figure 3.14. Oz et al. [15] has found the significant transverse strain concentration and Poisson contraction from DIC at the delaminated region of laminates. Therefore, it is inferred that delamination inside the $[0_2/90_4]_s$ laminates should be the source to increase the absolute transverse strain which further induces the increase of Poisson's ratio υ. Besides, a scattering evolution of Poisson's ratio is observed almost for each group of $[0_2/90_4]_s$ specimens which share the similar degrading trends of stiffness. This scatter phenomenon of υ indicates that accumulation of delamination may vary among specimens of each group. However, for the $[0/90_2]_s$ laminates, the absolute values of transverse strains at the 0 plies decrease with the increase of fatigue cycles. In view that this decrease is negligible, transverse strains can be regarded as constant during the fatigue tests. Thus, it is mainly the increase of the axial strain causes the decrease of Poisson's ratio as fatigue cycles increase. It can also be inferred that no significant delamination grew at the interface between 0 and 90 plies for the $[0/90_2]_s$ laminates.

As a result, transverse cracks govern the decrease of Poisson's ratio for the $[0/90_2]_s$ laminates, while the increase of Poisson's ratio for the $[0_2/90_4]_s$ laminates is attributed to delamination. From this point of view, Poisson's ratio could be considered to identify whether the early fatigue damage of a cross-ply laminate is dominant by transverse cracks or involves delamination.

3.6. CONCLUSIONS

OVERALL, the designed experimental methods are verified under static loading. They are then applied in the fatigue test campaign and the changes of mechanical properties during the fatigue loading are successfully measured. Based on the image analysis of edge damage under static loading, the accumulation of transverse cracks should also be traceable and measurable for the fatigue testing, which is presented in Chapter 4. As for the delamination propagation, challenge for the in-situ monitoring exists which needs the seek of related damage indicators from applied techniques, and details are described in Chapter 5.

REFERENCES

[1] J. Kupski, S. Teixeira de Freitas, D. Zarouchas, P. P. Camanho, and R. Benedictus, *Composite layup effect on the failure mechanism of single lap bonded joints,* Composite Structures **217**, 14 (2019).

[2] Hexcel, *HexPly®6376 - Product Data Sheet - EU Version* (2016).

[3] ASTM, *D3039/D3039M: Standard test method for tensile properties of polymer matrix composite materials* (ASTM international, 2014).

[4] A. Tessema, S. Ravindran, and A. Kidane, *Gradual damage evolution and propagation in quasi-isotropic CFRC under quasi-static loading,* Composite Structures **185**, 186 (2018).

[5] M. Mehdikhani, E. Steensels, A. Standaert, K. A. Vallons, L. Gorbatikh, and S. V. Lomov, *Multi-scale digital image correlation for detection and quantification of matrix cracks in carbon fiber composite laminates in the absence and presence of voids controlled by the cure cycle,* Composites Part B: Engineering **154**, 138 (2018).

[6] I. Miskdjian, M. Hajikazemi, and W. V. Paepegem, *Automatic edge detection of ply cracks in glass fiber composite laminates under quasi-static and fatigue loading using multi-scale Digital Image Correlation,* Composites Science and Technology **200**, 108401 (2020).

[7] J. M. Berthelot, P. Leblond, A. El Mahi, and J. F. Le Corre, *Transverse cracking of cross-ply laminates: Part 1. Analysis,* Composites Part A: Applied Science and Manufacturing **27**, 989 (1996).

[8] P. A. Carraro, L. Maragoni, and M. Quaresimin, *Characterisation and analysis of transverse crack-induced delamination in cross-ply composite laminates under fatigue loadings,* International Journal of Fatigue **129**, 105217 (2019).

[9] Vallen Systeme GmbH, *Verification of the AE signal processor, parametric input channels and system performance according to EN 13477-2:2010,* (2019).

[10] Q. Q. Ni and M. Iwamoto, *Wavelet transform of acoustic emission signals in failure of model composites,* Engineering Fracture Mechanics **69**, 717 (2002).

[11] M. Saeedifar and D. Zarouchas, *Damage characterization of laminated composites using acoustic emission: A review,* Composites Part B: Engineering **195**, 108039 (2020).

[12] R. Mohammadi, M. A. Najafabadi, M. Saeedifar, J. Yousefi, and G. Minak, *Correlation of acoustic emission with finite element predicted damages in open-hole tensile laminated composites,* Composites Part B: Engineering **108**, 427 (2017).

[13] C. Huang, S. Ju, M. He, Q. Zheng, Y. He, J. Xiao, J. Zhang, and D. Jiang, *Identification of failure modes of composite thin-ply laminates containing circular hole under tension by acoustic emission signals,* Composite Structures **206**, 70 (2018).

[14] V. Arumugam, K. Saravanakumar, and C. Santulli, *Damage characterization of stiffened glass-epoxy laminates under tensile loading with acoustic emission monitoring,* Composites Part B **147**, 22 (2018).

[15] F. E. Oz, N. Ersoy, M. Mehdikhani, and S. V. Lomov, *Multi-instrument in-situ damage monitoring in quasi-isotropic CFRP laminates under tension,* Composite Structures **196**, 163 (2018).

[16] R. Amacher, J. Cugnoni, J. Botsis, L. Sorensen, W. Smith, and C. Dransfeld, *Thin ply composites: Experimental characterization and modeling of size-effects,* Composites Science and Technology **101**, 121 (2014).

[17] B. Kötter, J. Endres, J. Körbelin, F. Bittner, H. J. Endres, and B. Fiedler, *Fatigue and fatigue after impact behaviour of Thin- and Thick-Ply composites observed by computed tomography,* Composites Part C: Open Access **5**, 100139 (2021).

[18] A. V. Movahedi-Rad, T. Keller, and A. P. Vassilopoulos, *Fatigue damage in angle-ply GFRP laminates under tension-tension fatigue,* International Journal of Fatigue **109**, 60 (2018).

[19] J. Maier and G. Pinter, *Stiffness-based approach to fatigue-life prediction of composite materials,* in *Fatigue Life Prediction of Composites and Composite Structures* (Elsevier, 2020) pp. 539–568.

3

4

TRANSVERSE CRACKS UNDER FATIGUE LOADING

4.1. INTRODUCTION

TRANSVERSE cracks, as one of the dominant damage mechanisms that usually occur in the early fatigue life of cross-ply laminates, are analysed in this chapter, and their stochastic nature is taken into account from both spatial and temporal perspectives. Section 4.2 describes the initiation, accumulation and saturation of multiple transverse cracks as fatigue cycles increase for both cross-ply laminates ($[0/90_2]_s$ and $[0_2/90_4]_s$) under different stress levels. Then, in Section 4.3, the interaction among transverse cracks within a laminate is quantified by characterising independent and dependent cracks. Further, a strength-based probabilistic model is proposed in Section 4.4, to investigate the scattering evolution of transverse cracks for the $[0_2/90_4]_s$ laminates.

4.2. INITIATION, ACCUMULATION AND SATURATION

AMONG three different techniques employed in the fatigue tests, edge observation by digital cameras provides the most sufficient information about the generation of transverse cracks at 90 plies, while the strain distribution field at exterior 0 plies from DIC analysis is also found to be affected by the crack evolution. Section 4.2.1 summarises the analysis of crack-related results from these two techniques. Then, based on the monitoring from the edge cameras, AE results are interpreted and correlated to the crack evolution in Section 4.2.2. Further, the effect of stress levels and ply-block thicknesses on the accumulation and saturation of transverse cracks are discussed in Section 4.2.3 and 4.2.4 .

4.2.1. ANALYSIS BASED ON EDGE OBSERVATION AND DIC RESULTS

FOR both ply configurations, most of transverse cracks propagated through the width direction with 500 cycles, after initiating from edges. As observed by digital cameras, the number of transverse cracks and their location at 90 plies were almost the same for both left and right sides after every 500 cycles. Besides, when a transverse crack forms at inner 90 plies, the axial strain concentration, across the entire width of the laminate, is induced at the related position of the exterior 0 ply.

For the examples of both ply configurations tested under 70% of UTS, Figure 4.1 presents the distribution of axial strain concentrations within the gauge region at four different moments. Red arrows mark the location of new cracks generated at certain fatigue cycles.

A good correlation can be observed between the location of new cracks at 90 plies and newly formed concentration of the axial strain at the 0 ply. When the new crack closes to neighbouring cracks, an expansion of the original axial strain concentration can be observed at the related local region; otherwise, an extra axial strain concentration is formed at the gauge region.

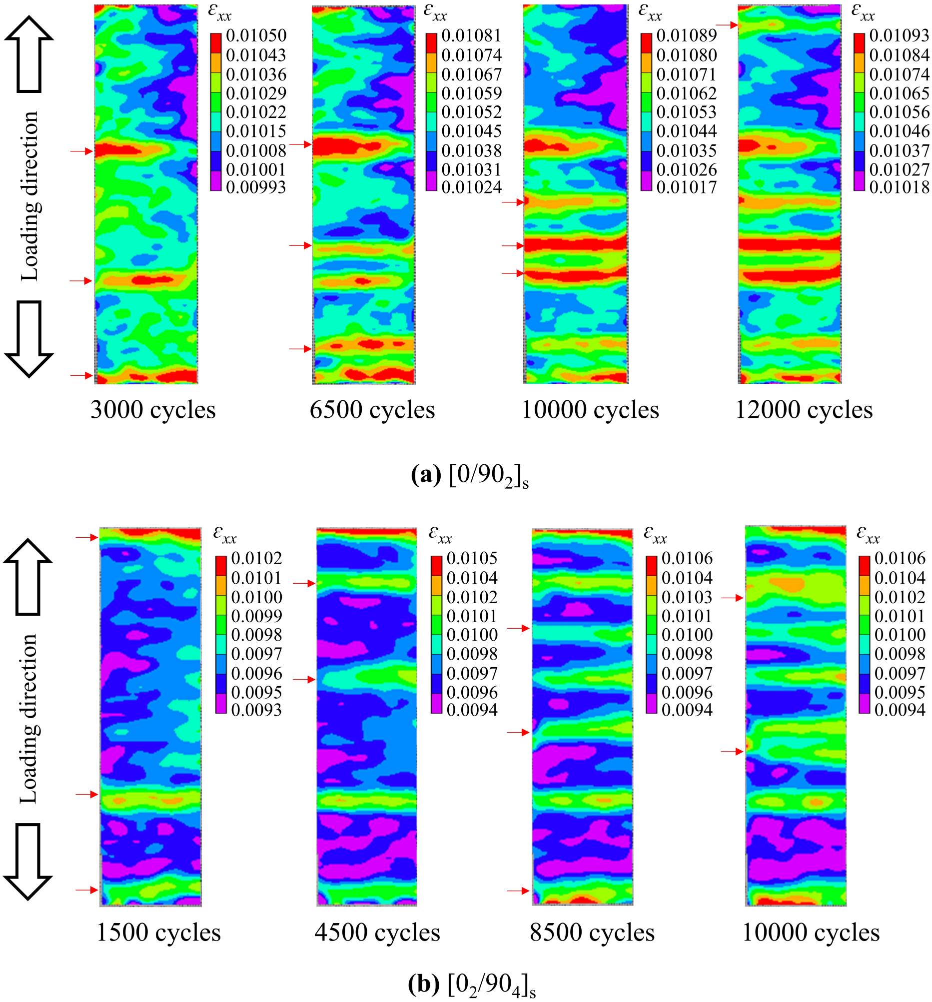

Figure 4.1: Evolution of axial strain distribution at the gauge region as fatigue cycles increases for both ply configurations.

To further quantify the accumulation process, crack density ρ is introduced. Based on a user-defined image processing algorithm as described in Section 3.3.1, ρ is calculated by the average number of transverse cracks counted from both left and right sides, which is then divided by the gauge length (~ 80 mm). Figure 4.2 and 4.3 show the increase of crack density as a function of fatigue cycles for both ply-configurations (see scatter plots).

For the $[0/90_2]_s$ laminates, bi-linear growing trends of crack density are presented in Figure 4.2, and they are similar between specimens tested under the same stress level. After the crack density reaches around 0.8 mm^{-1}, transverse cracks accumulate at a slower rate compared with that at the initial period. Eventually, a constant crack density is hard to achieve as fatigue cycles increase. Therefore, the saturation of transverse cracks (or CDS) here is defined as the moment when the crack density approaches 1 mm^{-1}.

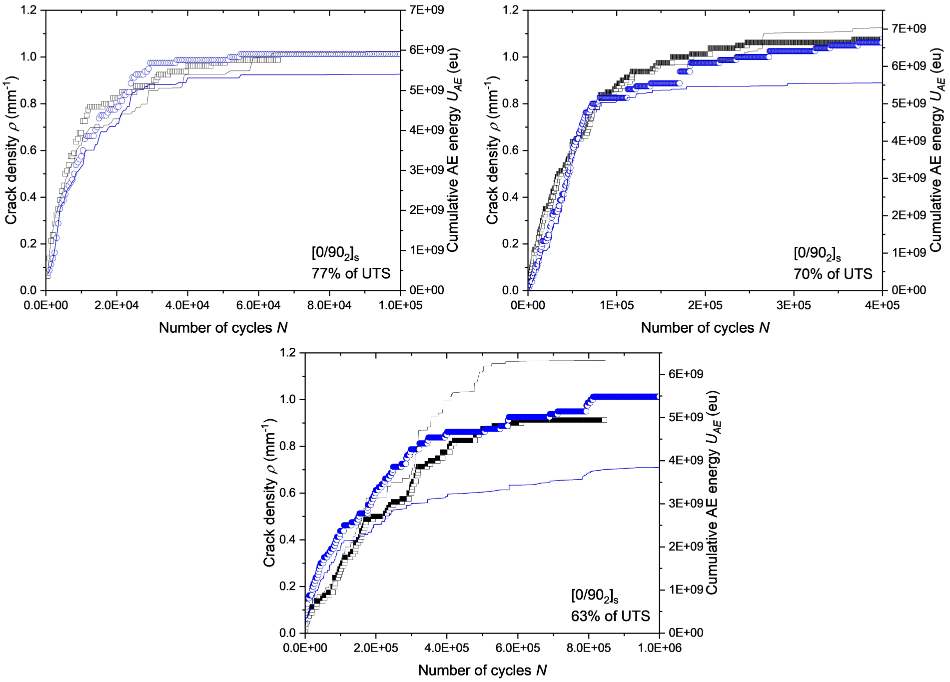

Figure 4.2: The evolution of crack density (scatter plots) and cumulative AE energy (line plots) as a function of fatigue cycles for $[0/90_2]_s$ laminates.

Different from the $[0/90_2]_s$ laminates, the evolution of crack density scatters among specimens with a similar stiffness degradation trend for the $[0_2/90_4]_s$ laminates, as presented in Figure 4.3. A linear increase of crack density can be observed at the very early fatigue life. Once reaching a certain threshold, which differs among specimens, a gradual decrease of the growth rate is observed, till the occurrence of characteristic damage state. As shown in Figure 4.3, transverse cracks saturate at the density ranging from ~0.2 to ~0.4 mm^{-1} for each group of specimens, regardless of stress levels, as also reported by Pakdel and Mohammadi [1]. In addition, a negative correlation between saturated crack density and fatigue cycles to reach CDS is found for each stress level. Specimens which spend more time to reach CDS have a lower saturated crack density, and vice versa. These similarities indicate that the characteristic damage state is independent of stress levels for the $[0_2/90_4]_s$ laminates.

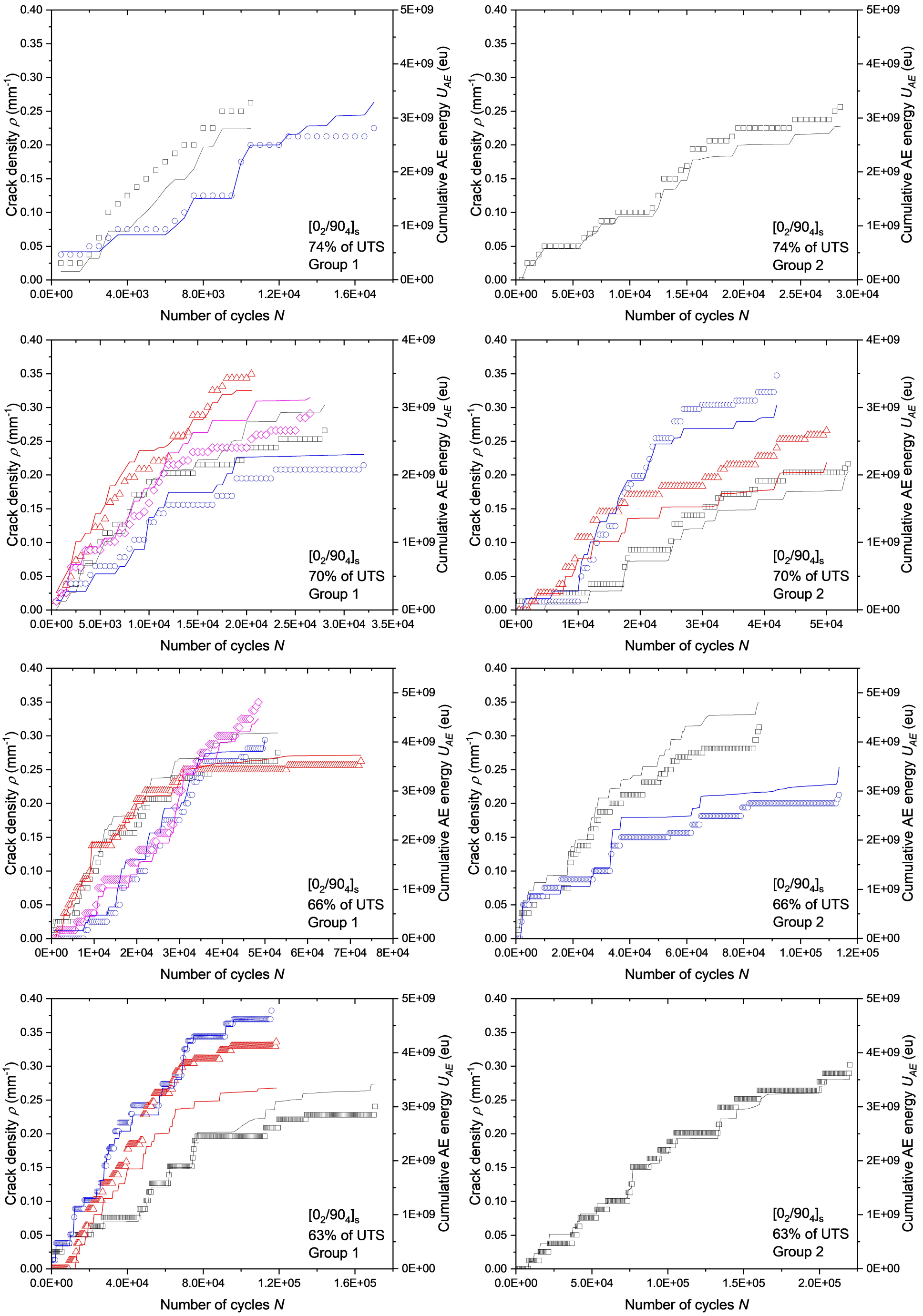

Figure 4.3: The evolution of crack density (scatter plots) and cumulative AE energy (line plots) as a function of fatigue cycles for two groups of $[0_2/90_4]_s$ laminates.

4.2.2. ANALYSIS BASED ON AE RESULTS

ACOUSTIC emission has shown its potentials for monitoring the progressive accumulation process of composites based on the extensive efforts of interpreting AE activities [2]. Literature [3–5] has showed that cumulative AE hits, counts and energy with the increase of number of cycles could signify different stages of damage accumulation under fatigue loading. In view that the increase of cumulative AE energy has showed the similar trend compared with accumulation of transverse cracks under static tensile loading [6], the relation between cumulative AE energy and crack density is further explored here for fatigue loading.

A localisation algorithm is firstly applied to filter out AE signals which are out of the gauge region. Then, cumulative energy U_{AE} of recorded AE signals is calculated as a function of fatigue cycles, as shown in Figure 4.2 and 4.3 (see line plots). Here, the AE energy of each signal is defined as the area under the squared signal envelope, as shown in Figure 2.5 [2]. As observed, the growing trends of cumulative AE energy are well correlated to those of crack density, especially the sudden jumps. This indicates that transverse cracks are the main damage source to produce AE signals carrying high released energy for two types of cross-ply laminates. Furthermore, a linear relation between crack density and cumulative AE energy until the saturation of transverse cracks is presented in Figure 4.4 and 4.5 for both ply configurations.

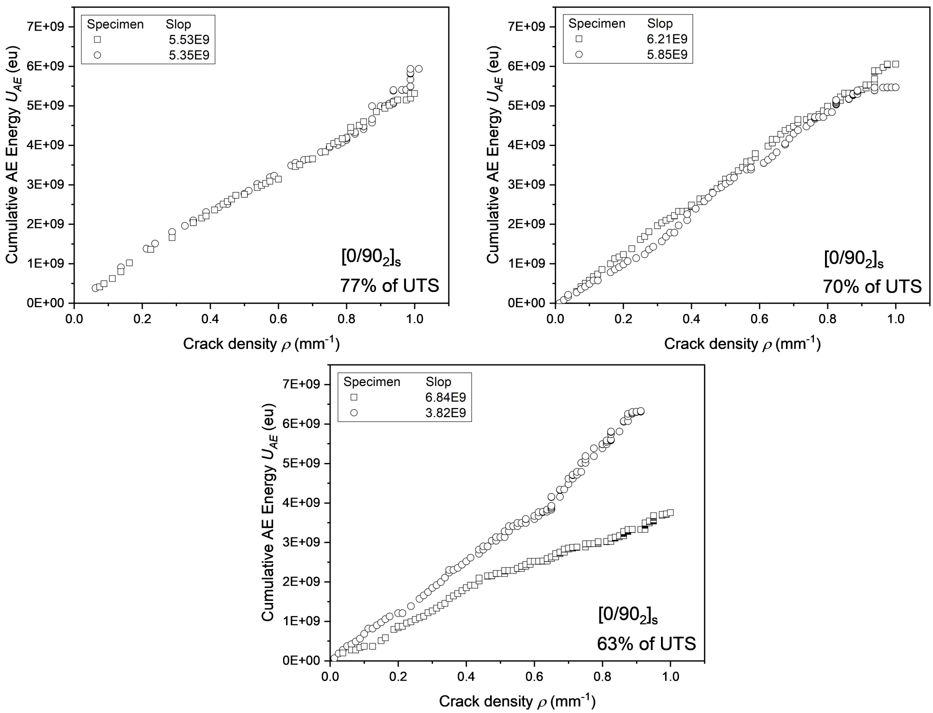

Figure 4.4: The linear relation between crack density and cumulative AE energy for $[0/90_2]_s$ laminates under different stress levels.

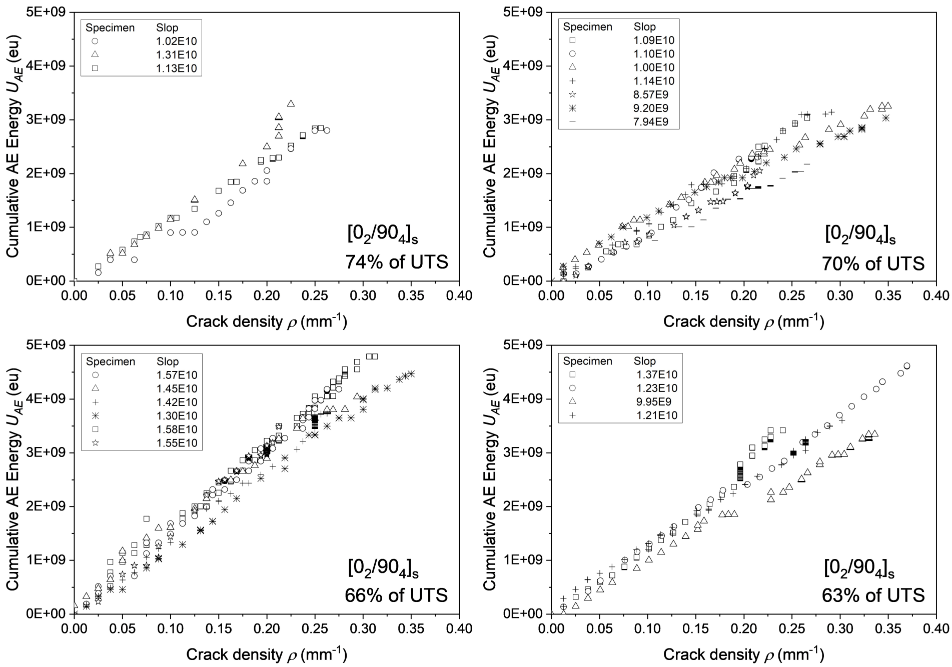

Figure 4.5: The linear relation between crack density and cumulative AE energy for $[0_2/90_4]_s$ laminates under different stress levels.

The slop of $U_{AE} - \rho$ curves for the $[0_2/90_4]_s$ laminates is about twice of that for the $[0/90_2]_s$ laminates. This phenomenon implies that the released energy from a transverse crack at thick 90 plies is higher than that at thin 90 plies for the same material system, as the crack surface is different for both types of laminates. Overall, cumulative AE energy can be regarded as an indicator of crack density for cross-ply laminates.

4.2.3. PLY-BLOCK THICKNESS EFFECT

THE saturated crack density of $[0/90_2]_s$ laminates is approximately 2-5 times larger than that of $[0_2/90_4]_s$ laminates. Carraro et al. [7] and Pakdel and Mohammadi [1] also found that the crack density at the saturated state is higher for cross-ply laminates with thinner 90 plies. As stress relaxation around a transverse crack is narrower for thinner cracking plies [8, 9], more high-stress region exists at the cracking plies to support the transverse crack initiation. In addition, local delamination is easier to emerge for thicker cracking plies [7]. This fact further widens the region of stress relaxation and restrains the transverse crack initiation at thick plies. Therefore, $[0/90_2]_s$ laminates present higher chances to form transverse cracks with a larger number presented at the saturated state, in comparison with $[0_2/90_4]_s$ laminates.

In view that different stress levels were involved during the fatigue tests, Figure 4.6 compares the evolution of crack density as a function of fatigue cycles under the same stress levels. Although sharing the same initial stiffness, UTS is slightly higher for the thinner ply configuration. Therefore, it might not be proper to compare both ply configurations under the stress level which has the same percentage of UTS. Instead, the stress at 90 plies when the first transverse crack occurred in laminates, denoted as σ_{90_i}, is involved here, as mentioned in Section 3.5.2. The maximum cyclic stress of 90 plies divided by σ_{90_i}, also named as the percentage of σ_{90_i} listed in Table 3.6, could be used to reflect how severe the applied stress is on the 90 plies, rather than the whole laminate. If the percentage of σ_{90_i} is more than one, then the first transverse crack initiates at the very first cycle; otherwise, the transverse crack initiation delays [10]. Therefore, it would also be interesting to compare both laminates under the stress level which has the similar percentage of σ_{90_i}.

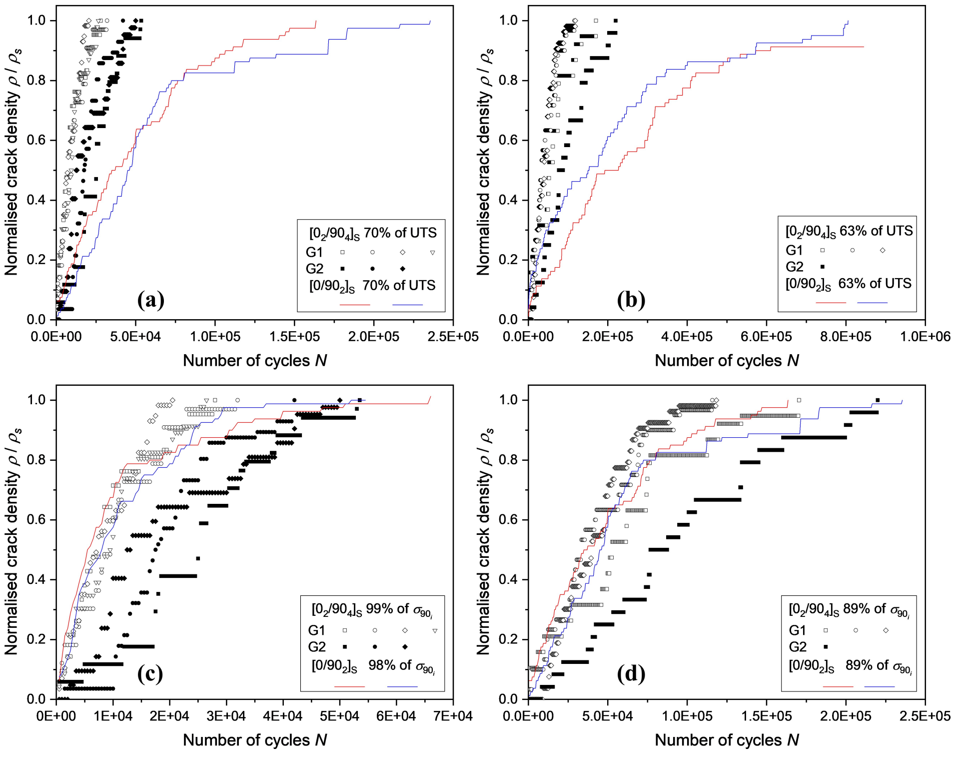

Figure 4.6: Comparison about the increase of normalised crack density as a function of fatigue cycles for both ply configurations: (a) stress level at the 70% of UTS; (b) stress level at the 63% of UTS; (c) stress level at 98-99% of σ_{90_i}; (d) stress level at 89% of σ_{90_i}). (G1-Group 1; G2-Group 2).

Overall, two different ways are used to calculate the stress level: one refers to the whole laminate and the other refers to the 90 plies. Crack density of each specimen is normalised by its saturated crack density. When the stress level for the whole laminates is the same, a slow accumulation of transverse cracks is presented for $[0/90_2]_s$ laminates (see Figure 4.6 (a) and (b)). Besides, the consumed fatigue cycles to reach the saturation of transverse cracks is about five times longer than that of $[0_2/90_4]_s$ laminates. As listed in Table 3.6, under the stress level at either 70% or 63% of UTS, the corresponding stress level for 90 plies of $[0/90_2]_s$ laminates is 9-10% lower than that of $[0_2/90_4]_s$ laminates, thus increasing their resistance to the initiation of transverse cracks. When the comparison about the evolution of normalised crack density is under a similar stress level for 90 plies, a new insight can be provided to bridge the evolution of transverse cracks for both cross-ply laminates; it is the stress level for 90 plies that mainly controls how fast the saturation of transverse cracks occurs. As presented in Figure 4.6 (c) and (d), the growing rate of normalised crack density for $[0/90_2]_s$ laminates is close to that of $[0_2/90_4]_s$ laminates in the Group 1. In particular, the first linear increase of normalised crack density with the increase of fatigue cycles is almost the same for both ply configurations.

As the initial stiffness is the same for both cross-ply laminates, how transverse cracks affect stiffness for each type of laminates is further investigated. Figure 4.7 presents the decrease of normalised longitudinal stiffness as crack density increases. For the $[0/90_2]_s$ laminates, the degrading trend of stiffness remains linear during the entire process of transverse crack accumulation. However, for the $[0_2/90_4]_s$ laminates, a linear relation between crack density and degraded stiffness is presented at the beginning of crack accumulation. When crack density reaches a certain threshold, which differs from specimen to specimen, the deceasing rate of stiffness suddenly increases and becomes more and more aggressive for the remaining fatigue cycles. It is inferred that another damage mechanism, delamination, starts to play a role in degrading the stiffness. On the contrary, the linear trend of E_N/E_0-ρ for the $[0/90_2]_s$ laminates indicates that no significant delamination grew at the 0/90 interfaces during the early fatigue life to degrade stiffness. By fitting the linear parts of plots in Figure 4.7, it is observed that the decrease of stiffness caused by transverse cracks shows a slow rate for $[0/90_2]_s$ laminates, which is about half of that for $[0_2/90_4]_s$ laminates. This difference is because that area of a transverse crack surface for $[0/90_2]_s$ laminates is smaller that of $[0_2/90_4]_s$laminates [11].

4.2.4. STRESS LEVEL EFFECT

THE effect of stress levels on the accumulation of transverse cracks is reflected on the growth rate of crack density, in accordance with the conclusion from Hosoi et al. [12]. The higher the stress level is, the faster the growth rate of crack density presents. Except this, the accumulation of transverse cracks is similar among different stress levels for both cross-ply configurations. When the accumulation of transverse cracks reaches CDS, the saturated crack density is found to be independent of stress levels, as presented in Figure 4.2 and 4.3. Especially for the $[0_2/90_4]_s$ laminates, specimens with lower saturated crack density tend to consume more fatigue cycles to reach CDS, which is observed under all stress levels. Besides, the stress level effect on the stiffness degradation as a function of crack density is also explored. As presented in Figure 4.7, for both cross-ply laminates, the normalised longitudinal stiffness degraded by transverse cracks shows a similar decreasing trend with the increase of crack density, irrespective of applied stress levels. In particular, the nonlinear decease of E_N/E_0 plotted in Figure 4.7(a), is also similar among specimens with a similar saturated crack density.

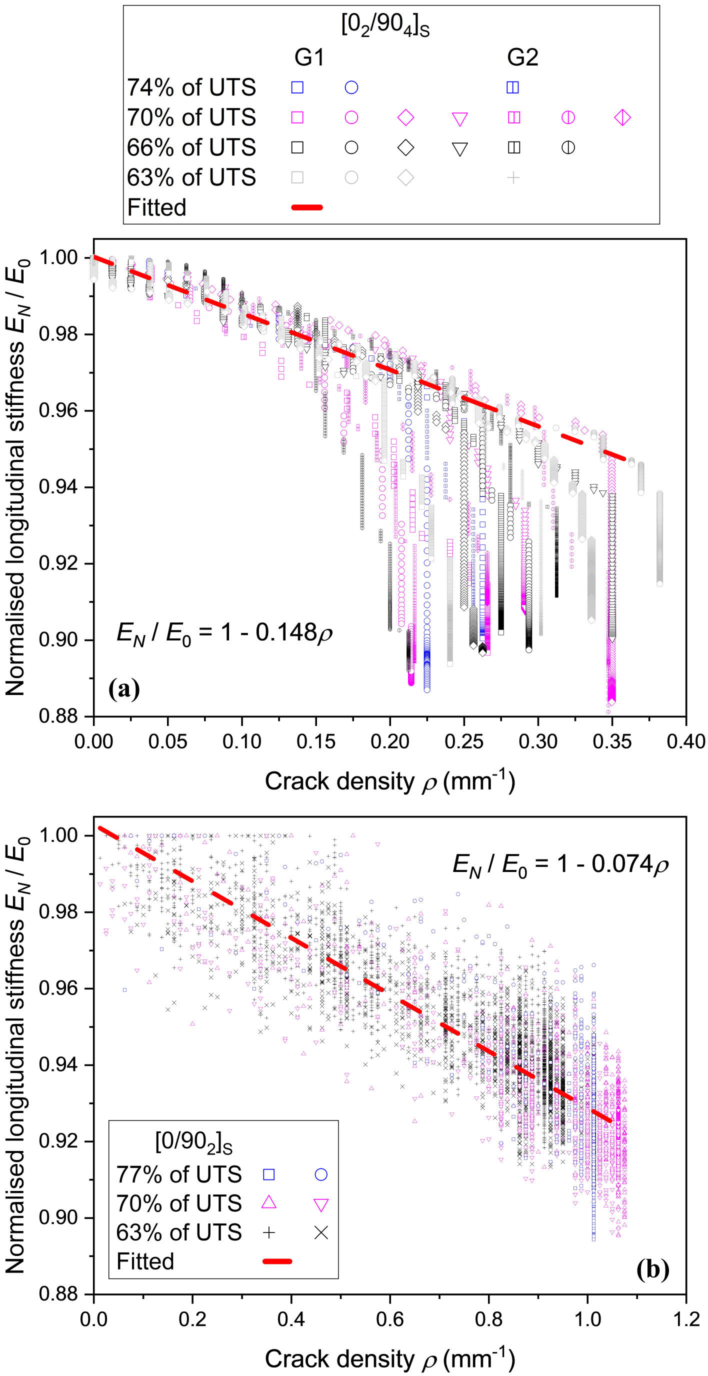

Figure 4.7: Crack density versus normalised longitudinal stiffness for $[0_2/90_4]_s$ (a) and $[0/90_2]_s$ (b) laminates. (G1-Group 1; G2-Group 2).

4.3. CHARACTERISATION OF INDEPENDENT AND DEPENDENT CRACKS

DURING the early fatigue life, the growing trend of crack density for both types of cross-ply laminates initiates from a linear increase, followed by a decrease of the growth rate. Regarding the decrease of the growth rate of crack density, it could be attributed to either the accumulation of other damage mechanisms like delamination or the interaction among different transverse cracks. In terms of the latter, literature has reported that off-axis matrix cracks with high local density are prone to interact with their neighbours, accompanying with stress redistribution at local off-axis plies [13–16]. Therefore, to gain a better understanding about the growing trend of crack density, the interaction among transverse cracks should be further quantified. Here, the concept of independent and dependent cracks is introduced: the former locate far from neighbours where the local stress remains at a uniform stress level inside the 90 plies, while the latter initiate close to existing cracks where a redistributed stress state exists.

To identify whether a transverse matrix crack is independent or dependent, a critical crack spacing for each ply configuration is determined by using finite element modelling, as described in Section 4.3.1. Then, dependent crack ratio is proposed in Section 4.3.2 to investigate the interaction among transverse cracks.

4.3.1. CRITICAL CRACK SPACING

FOR each cross-ply configuration, a parametric finite element analysis was performed to calculate the stress state between two cracks at various distances. As shown in Figure 4.8(a) and 4.9(a), two-dimensional model with 10 mm length, using CPS4R (4-node bilinear plane strain quadrilateral, reduced integration) elements, was built from the edge view for the $[0/90_2]_s$ laminate and the $[0_2/90_4]_s$ laminate, respectively. The mesh size was set to 0.05 mm based on a sensitivity analysis. Linear-elastic material properties of unidirectional lamina as listed in Table 3.1 were assigned to both 0 and 90 plies. To simulate the cracked region, seam cracks were applied to the red locations marked in Figure 4.8(a) and 4.9(a). In ABAQUS, a seam crack defines an edge or a face with overlapping nodes that can separate during an analysis [17]. The displacement of nodes at the left end of the model was constrained along the loading direction. Considering that transverse matrix cracks are supposed to generate at the loading process within a cycle, modelling the load can be simplified by introducing a linearly increasing force up to a maximum cyclic load. The force was imposed on a reference point where all nodes at the right end were coupled.

The axial normal stress state at 90 plies as a function of the position between two cracks is presented in Figure 4.8(b) and 4.9(b) for the $[0/90_2]_s$ laminate and the $[0_2/90_4]_s$ laminate, respectively. Here, the axial stress state is averaged along the thickness, denoted as $\overline{\sigma}$, and then normalised by the average of maximum applied stress at 90 plies $\overline{\sigma}_{applied}$. $\overline{\sigma}_{applied}$ can be regarded as the maximum cyclic stress as listed in Table 3.6. The position X is normalised by the crack spacing d, which ranges from 0.5 to 3.5 mm for the $[0/90_2]_s$ laminate and ranges from 0.5 to 5 mm for the $[0_2/90_4]_s$ laminate.

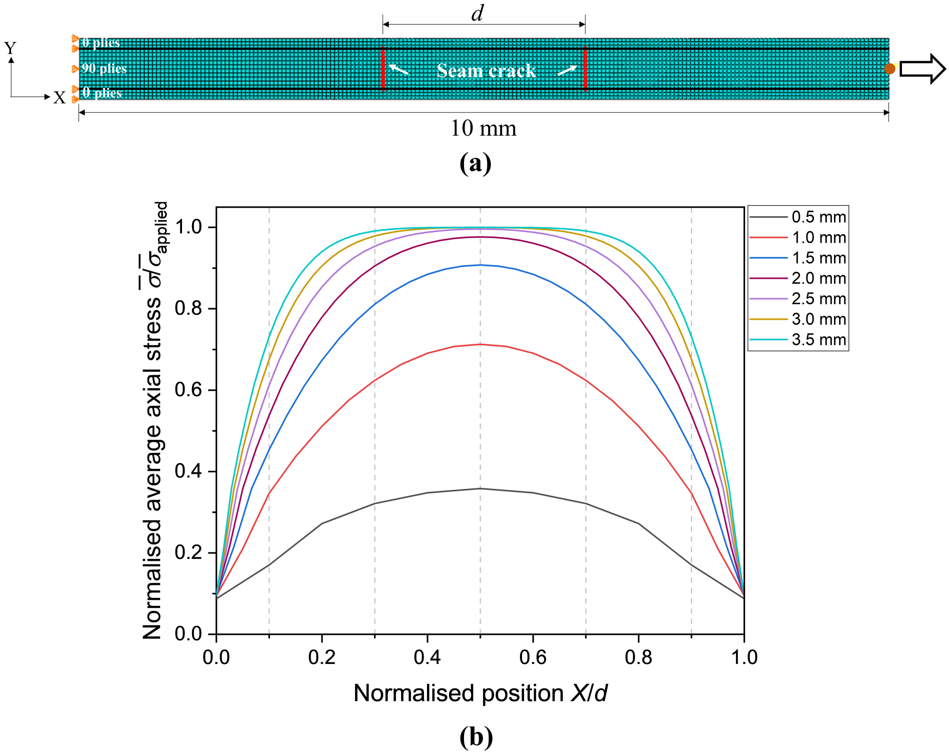

Figure 4.8: Schematic diagram of the finite element model for a cracked laminate, including boundary and loading conditions, ply configuration and geometry dimensions (a); The normalised average axial stress versus normalised position along x-axis (b) for the $[0/90_2]_s$ laminate.

For the $[0/90_2]_s$ laminate, the average axial stress at the middle of two cracks is lower than the applied level when the crack spacing is $d < 2.5$ mm, as observed in Figure 4.8(b). This observation indicates that stress redistribution is triggered between two cracks with a distance smaller than 2.5 mm and the driving force to initiate a new crack in the middle will be affected by the occurrence of prior cracks. In the case of $d \geq 2.5$ mm, the average axial stress is equal to the applied level at $X/d = 0.5$, where the new crack will not interact with its neighbours. Therefore, the critical crack spacing for the $[0/90_2]_s$ laminate is found to be $2.5/2 = 1.25$ mm. Similarly, for the $[0_2/90_4]_s$ laminate, when the crack spacing is $d < 4.5$ mm, the new crack generating in the middle will interact with its neighbours at $X/d = 0.5$ where the stress level is lower than the applied level (see Figure 4.9(b)). Therefore, the critical crack spacing for the $[0_2/90_4]_s$ laminate is found to be $4.5/2 = 2.25$ mm.

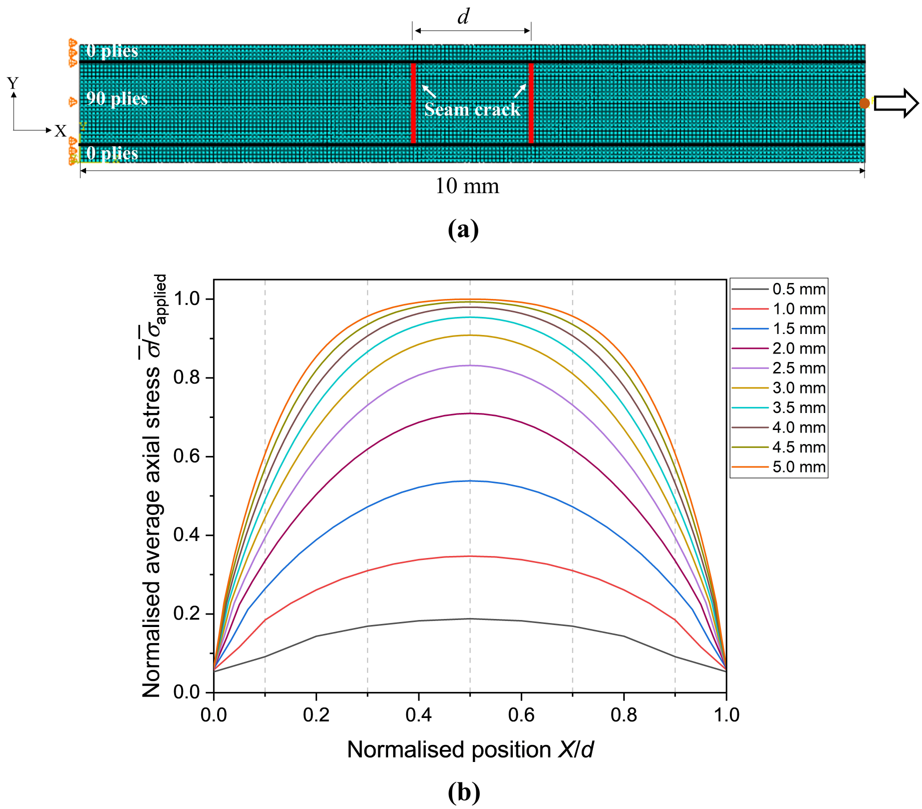

Figure 4.9: Schematic diagram of the finite element model for a cracked laminate, including boundary and loading conditions, ply configuration and geometry dimensions (a); The normalised average axial stress versus normalised position along x-axis (b) for the $[0_2/90_4]_s$ laminate.

4.3.2. DEPENDENT CRACK RATIO

HAVING estimated the critical crack spacing, the dependent and independent transverse cracks can be grouped accordingly. For the $[0/90_2]_s$ laminates, the number of independent cracks T_{amax} at the saturated state scatters in a certain range, as summarised in Figure 4.10; the mean value of T_{amax} is 35 (see the blue dash line). Regarding the $[0_2/90_4]_s$ laminates, the number of independent cracks T_{amax} at the saturated state also shows a scatter range in Figure 4.11, and its mean value is 17 among different stress levels (see the blue dash line).

Additionally, a dependent crack ratio r_d is introduced to represent the proportion of dependent cracks generated in one specimen. It is calculated as the number of dependent cracks T_b at a fatigue cycle N divided by the number of independent cracks T_{amax} at CDS. In the analysis of crack evolution, dependent crack ratio can be used to quantify the initial fatigue resistance to cracking and the severity of interaction among cracks for one specimen, especially when assuming that the maximum number of independent cracks is constant at 90 plies, within the present study 35 and 17 independent cracks for the $[0/90_2]_s$ and $[0_2/90_4]_s$ laminates.

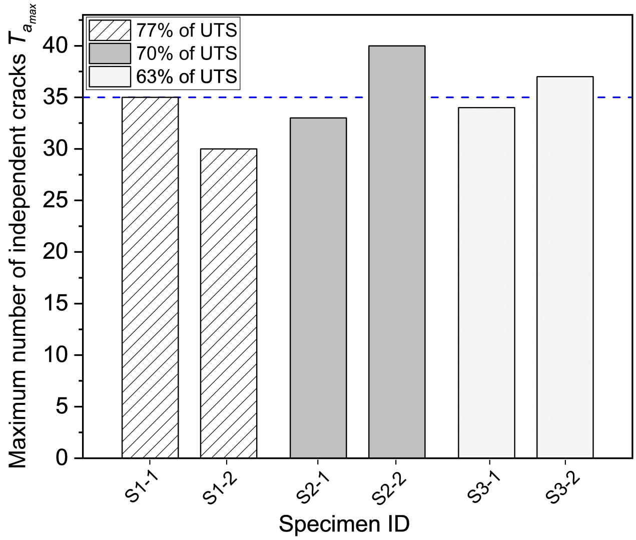

Figure 4.10: The maximum number of independent cracks at the saturated state for the $[0/90_2]_s$ laminates.

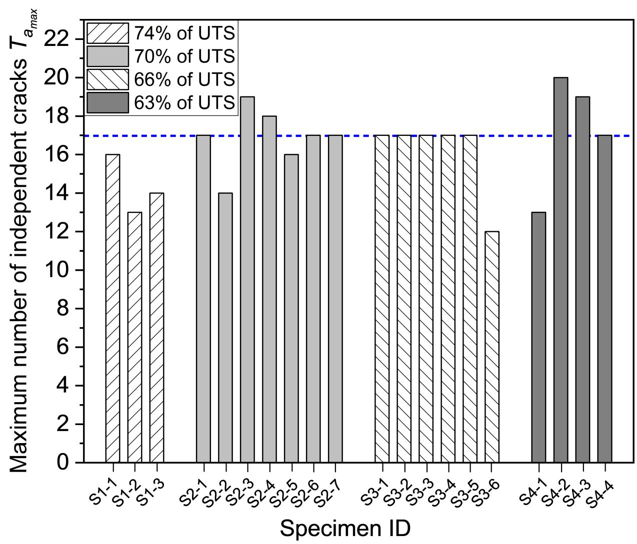

Figure 4.11: The maximum number of independent cracks at the saturated state for the $[0_2/90_4]_s$ laminates.

For the $[0/90_2]_s$ laminates, Figure 4.12 presents the increase of r_d as fatigue cycles increase (see line plots). Besides, the bi-linear increase of crack density is also showed in Figure 4.12 (see scatter plots), where the transition of the growth rate of crack density is marked as the red dash line. At this transition point, the related dependent crack ratio is about 0.8 to 1.0 for most specimens. Afterwards, dependent cracks seems to become dominant and high chances are provided to induce interaction among cracks, which delays the generation of new cracks and thus reduces the growth rate of crack density. At the saturated state, the dependent crack ratio is about 1.2 to 1.6 for all stress levels.

Considering the relatively low crack density of the $[0_2/90_4]_s$ laminates, the interaction among cracks is less severe than that of the $[0/90_2]_s$ laminates. Thus, the decrease of growth rate of crack density as fatigue cycles increase might be attributed to the occurrence of delamination which is prone to grow at thick off-axis plies [16]. However, the interactive level among transverse cracks is different from specimens tested under the same stress level, as shown in Figure 4.13. Dependent crack ratio $r_{d\,max}$ ranges from 0.1 to 0.7 at the saturated state. For each stress level, a higher dependent crack ratio $r_{d\,max}$ is produced for specimens with the larger crack density, reflecting severer interaction between independent and dependent cracks. This finding also indicates the scatter of saturated crack density for the $[0_2/90_4]_s$ laminates could be related to the fact that the interaction among transverse cracks is different from specimens tested under the same stress level.

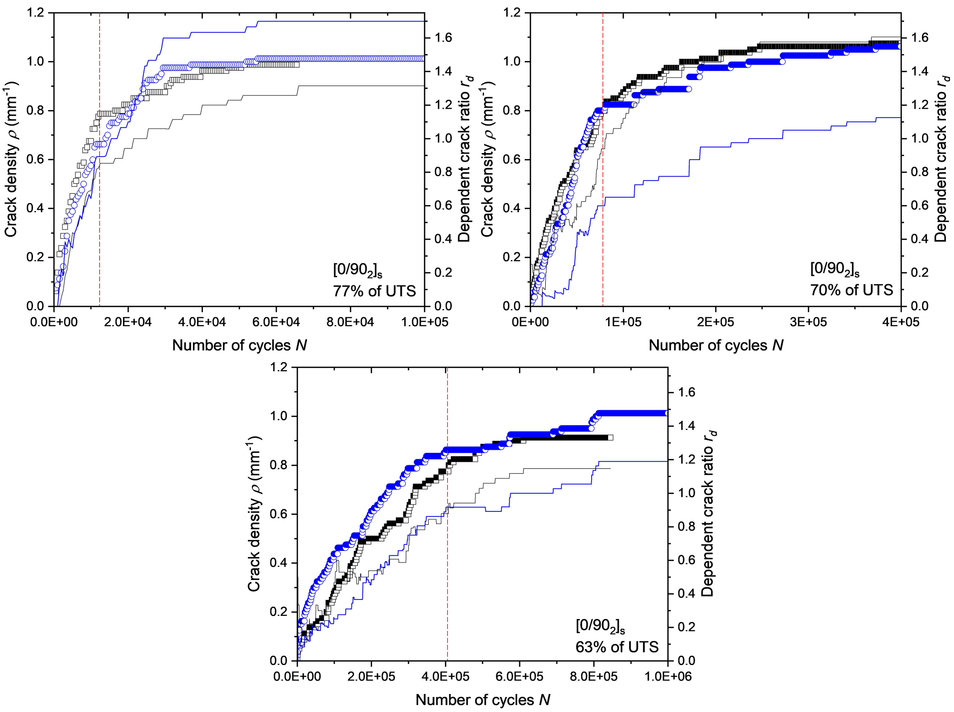

Figure 4.12: The increase of crack density (scatter plots) and dependent crack ratio (line plots) as a function of fatigue cycles for the $[0/90_2]_s$ laminates.

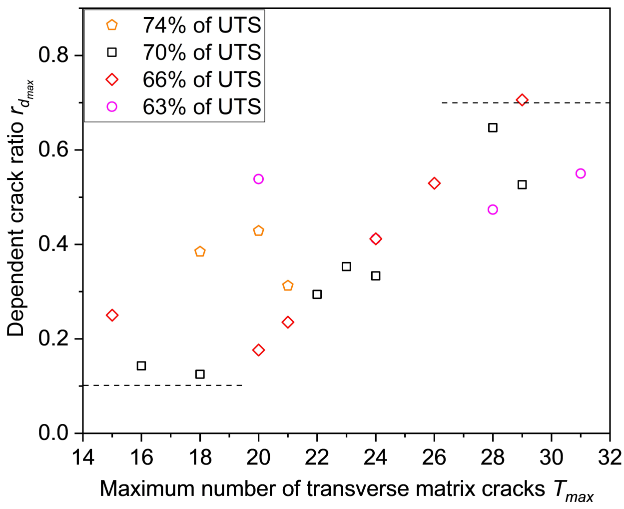

Figure 4.13: The dependent crack ratio versus the maximum number of transverse cracks at the saturated state for the $[0_2/90_4]_s$ laminates.

4.4. SCATTER ANALYSIS BASED ON A PROBABILISTIC MODEL

CONSIDERING the scatter phenomena of crack evolution among specimens in Figure 4.3, it is assumed that each specimen should have the certain strength variation at local region of 90 plies which governs the initial fatigue resistance to the formation of transverse cracks. It could also determine the accumulation and interaction of transverse cracks. Therefore, a strength-based probabilistic framework is proposed hereafter so as to explore further and understand better the scattering crack evolution for the $[0_2/90_4]_s$ laminates.

This strength-based model contains two parts: one is the modelling of independent crack accumulation in a non-interactive scheme (see Section 4.4.1) and the other is the modelling of dependent crack accumulation in an interactive scheme (see Section 4.4.2). Both parts need data input from fatigue tests at 70%, 63% and 55% of UTS to calibrate related empirical parameters. In Section 4.4.3, the model is validated by the crack evolution measured from tests under stress levels at 74% and 66% of UTS. The purpose is to gain a better understanding about the capability of the model on mimicking the crack evolution. Although delamination could grow at the 0/90 interfaces , it is assumed that delamination does not affect the corresponding local stress state when either independent or dependent cracks initiate. This assumption is based on the fact that transverse cracks will hardly generate at or close to the delaminated region where the driving force to produce new cracks is significantly reduced [18].

4.4.1. INDEPENDENT CRACK ACCUMULATION

IN view that the generation of independent cracks mainly depends on the local strength of 90 plies, it is necessary to obtain the statistical distribution of local strength and then relate the local strength to fatigue life of independent crack initiation.

1. COLLECTION OF LOCAL STRENGTH AT 90 PLIES

To obtain the local strength variations of 90 plies, crack evolution during static tests at the loading rate of 1 mm/min was monitored among five specimens, following the experimental methods reported in Section 3.3 and 3.4. Afterwards, the generated independent cracks were identified by the critical crack spacing as presented in Section 4.3.1. The axial stresses, where the independent cracks initiate, were used to form the data for the local strength of 90 plies S. Then, a Weibull distribution was used to fit the experimental data with the scale factor η =113.72 and the shape factor β =14.85. The Weibull distribution represents the local variations of strength for 90 plies among specimens tested under fatigue loading (see the red dash line in Figure 4.14).

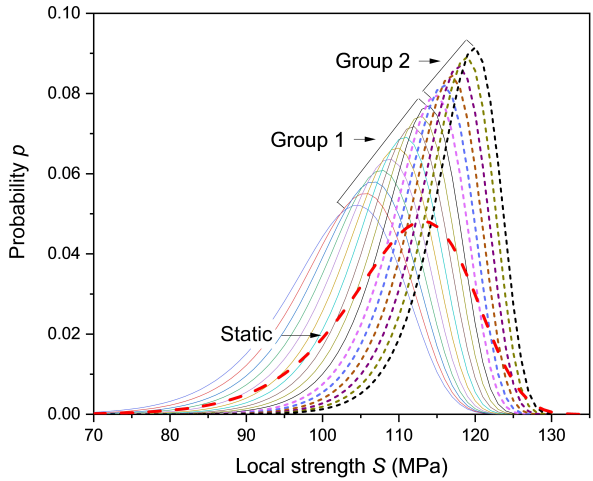

Figure 4.14: Two groups of Weibull distributions about the local strength of 90 plies generated based on the Weibull distribution of strength at 90 plies collected from static tests (red dash line).

2. LOCAL STRENGTH - FATIGUE LIFE RELATION

The number of cycles N_a when the independent cracks initiate was also measured during fatigue tests under the stress level at 70% of UTS. It was then fitted by a Weibull distribution (η: 13554.41; β: 1.18). Furthermore, the Strength Life Equal Rank Assumption (SLERA) [19] is introduced here, which is based on the correspondence that samples with higher static strength present longer fatigue life [20, 21]. It also states that one sample should have the same rank in all probability distributions of static strength, fatigue life and residual strength [22, 23]. According to SLERA, each pair of local strength S_a and fatigue life N_a under the same cumulative probability was correlated for the independent crack initiation at 70% of UTS, as expressed by:

$$S_a = 53.36408 \times N_a{}^{0.07952} \tag{4.1}$$

To expand this local strength - fatigue life relation from 70% of UTS to other stress levels, the number of cycles N_a for independent crack initiation was also measured for the stress levels at 63% and 55% of UTS. Then, P-S-N curves can be created at the cumulative probabilities of 1%, 50% and 99.7% for all the statistical distributions of fatigue life obtained at 70%, 63% and 55% of UTS, as presented in Figure 4.15. Based on the P-S-N curves, the relation between applied stress level σ_{pi} and fatigue life to initiate an independent crack N_a for a local region was established by the Basquin's power law equation:

$$\sigma_{pi} = A \times {N_a}^B \tag{4.2}$$

where B is set to -0.0647, which is the slope of the P-S-N curve at the cumulative probability 99.7%; A can be derived in the combination with Equation 4.1. In this way, if local strength S_a is known, the number of cycles N_a, needed to initiate an independent crack, can be calculated for an arbitrary stress level σ_{pi}.

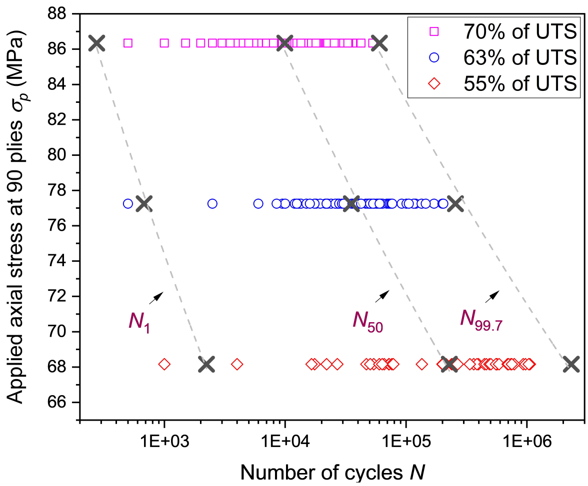

Figure 4.15: Scatter of fatigue life related to the initiation of independent cracks collected from fatigue tests under the three different stress levels, and the fitted P-S-N curves.

3. Fatigue life of independent crack initiation

As the local strength - fatigue life relation has been obtained, the next step is to describe the differences of local strength variations among specimens, after which the scatter of independent crack evolution as a function of fatigue cycles can be modelled.

For specimens with lower initial fatigue resistance to cracking (i.e. larger number of cracks at the saturated state), more significant manufacturing-induced inhomogeneity is presented, which could contribute to averagely low local strength of 90 plies with a wide scatter band. It should be the opposite for specimens with higher initial fatigue resistance to cracking. Accordingly, a variety of Weibull distributions, based on the reference distribution of local strength from static tests (see the red dash line in Figure 4.14), can be generated to represent different variations of local strength at 90 plies and different initial fatigue resistance to cracking from specimen to specimen. As shown in Figure 4.14, among Weibull distributions positioning along the x-axis, both scale factors ($\eta \in$ [105, 120]) and shape factors ($\beta \in$ [14.85, 29.85]) increase monotonically, and the higher peak is along with a narrower scatter band.

By providing a generated distribution of local strength (see Figure 4.14) as an input, the statistical distribution of fatigue cycles for independent crack initiation under a certain stress level can be obtained according to Equation 4.1 and 4.2. The related cumulative probability of this fatigue life distribution for an arbitrary cycle can be regarded as the probability of an independent crack formation at this cycle. The maximum of the cumulative probability was fixed to 0.997 to avoid the infinite fatigue life. Then, by assuming the maximum number of independent cracks at the saturation T_{amax} is constant, the increase of the number of independent cracks as a function of fatigue cycles can be modelled. Here, T_{amax} is set to 17, same as the mean value among specimens from fatigue tests (see Figure 4.11). Figure 4.16 presents the correlation between modelling and test results for the accumulation of independent cracks under stress levels at 70% and 63% of UTS, according to which the range of scale and shape factors as well as the grouping of generated Weibull distributions plotted in Figure 4.14 are validated. Thus, these two groups of generated Weibull distributions appropriately reflect the local variations at 90 plies for two groups of specimens with different trends of stiffness degradation (see Figure 3.12).

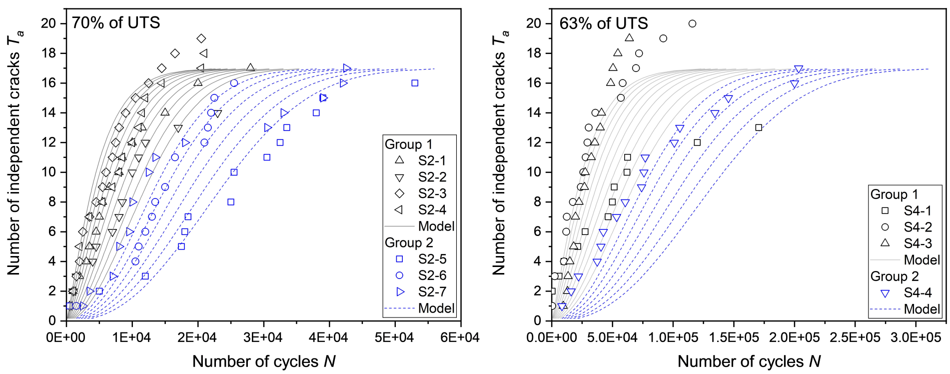

Figure 4.16: Comparison between the experimental and modelling results about the evolution of independent cracks as a function of fatigue life under the stress levels at 70% and 63% of UTS.

4.4.2. DEPENDENT CRACK ACCUMULATION

THE initiation of dependent cracks is controlled by both local strength of 90 plies and variations of stress state around the independent cracks. To describe the dependent crack accumulation in the model, their interaction with independent cracks should be firstly clarified.

1. SEVERITY OF INTERACTION

As the maximum number of independent cracks T_{amax} is constant in the model, the dependent crack ratio at the saturated sate r_{dmax} can be assigned to each generated Weibull distribution (see Figure 4.14). In this way, the severity of interaction among cracks is determined from specimen to specimen. In Section 4.3.2, it is found that r_{dmax} ranges from 0.1 to 0.7 and it increases with the decrease of fatigue resistance to cracking. Based on these observations, a Weibull distribution of local strength (in Figure 4.14) at each group are matched with a dependent crack ratio r_{dmax}, in a way that r_{dmax} decreases proportionally from 0.7 to 0.1 when the peak of the Weibull distribution increases. As a result, the maximum number of dependent cracks can be determined.

$$T_{bmax} = T_{amax} \times r_{dmax} \tag{4.3}$$

2. Interactive region

Once the total number of dependent cracks T_{bmax} is known, interactive regions can be formulated in the model by matching dependent cracks with independent ones. Due to the relatively low crack density in the present study, the severity and complexity of crack interactions are alleviated in comparison with the very high-density cases. As a result, two dependent cracks initiating at both sides of an independent crack was not frequently occurred during tests. Therefore, one-time interaction is considered for an independent crack, which means that an interactive region contains only one pair of independent and dependent cracks. To obtain the number of fatigue cycles that a dependent crack initiates, the local strength S_a for the independent crack, local strength S_b for the dependent crack and the crack spacing d need to be determined. The following steps illustrate the collecting and matching of S_a, S_b, and d for all interactive regions in a specimen.

4

Step 1: Local strength $S_a(i)$ for the i^{th} independent crack is collected at the cumulative probability of the selected Weibull distribution $P_i = i/T_{amax}$ when $i \in [1, T_{amax}-1]$ and $P_i = 0.997$ when $i = T_{amax}$, as shown in Figure 4.17(a). In this way, a group of S_a which scatters in a certain band and concentrates around the peak of probabilistic density function (PDF) is created.

Step 2: The collection of local strength $S_b(j)$ for the j^{th} dependent crack is moved to the decreasing part of the PDF, as shown in Figure 4.17(b), since the local region where dependent cracks initiate generally possesses high initial fatigue resistance to cracking than those of independent cracks. Then, $S_b(j)$ is selected at the cumulative probability level $P_j = j \times (1 - P_{peak})/(T_{bmax} + 1)(j \in [1, T_{bmax}])$, where P_{peak} is the cumulative probability at the peak of PDF. Consequently, a group of S_b is produced to represent the local strength for dependent cracks.

Step 3: Provided the collections of local strength for both independent cracks and dependent cracks, the j^{th} dependent crack with the local strength $S_b(j)$ can be matched to an independent crack with a local strength $S_a(i)$. $S_a(i)$ should be less than $S_b(j)$ in view that the independent crack initiates earlier than the dependent crack at an interactive region. After being matched with a dependent crack, $S_a(i)$ is removed from the group of S_a to guarantee one-time interaction among cracks.

Step 4: As the local strength is known for independent and dependent cracks at an interactive region, the range of crack spacing $[d_{min}, d_{max}]$ between two cracks should be determined. Here, d_{max} is equal to the critical crack spacing 2.25 mm, while d_{min} is initially set to 0.05 mm as the minimum crack spacing observed during fatigue tests. Given a pair of $S_a(i)$ and $S_b(j)$, d_{min} should be re-calibrated to avoid the fatigue cycles for dependent crack initiation exceeds an expected limit.

Step 5: Considering the spatial randomness of transverse cracks, the matching of local strength for a pair of independent and dependent cracks (**Step 3**), and the determination of the crack spacing (**Step 4**), are supposed to be a random process. Therefore, given a local strength $S_b(j)$ for the j^{th} dependent crack, 100-time Monte Carlo simulations are performed to pick up a $S_a(i)$ and d in the limited ranges.

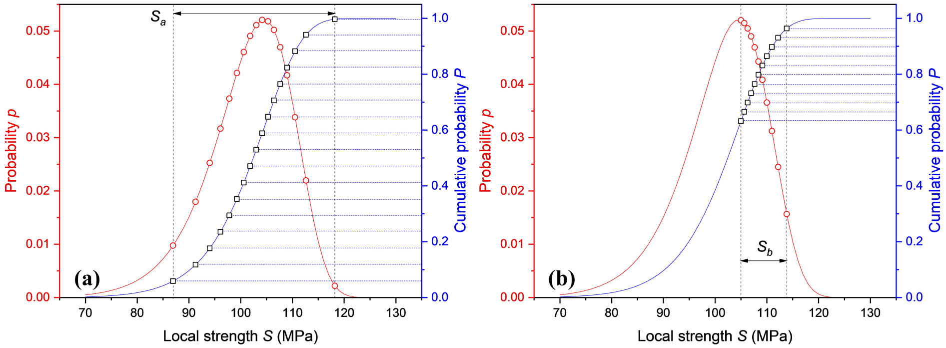

Figure 4.17: Collections of local strength for independent cracks (a) and dependent cracks (b), given a statistical distribution of local strength.

3. FATIGUE LIFE OF DEPENDENT CRACK INITIATION

As the local strength and distance about independent and dependent cracks can be determined, the number of fatigue cycles for a dependent crack initiation is further explored. At an interactive region, the local position of the dependent crack at 90 plies experiences a stress redistribution where the maximum cyclic stress is presented as two consecutive blocks under stress levels of σ_{p1} and σ_{p2} (see Figure 4.18).

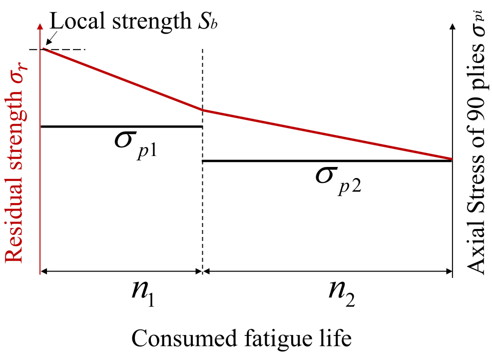

Figure 4.18: Variations of axial stress and the degradation of residual strength at the local region of 90 plies before the initiation of a dependent crack.

Prior to the independent crack initiation, the maximum stress at this local position remains constant and is the same as the applied maximum stress on the 90 plies, denoted as σ_{p1}. So, the consumed fatigue cycles n_1 under σ_{p1} is the same as the fatigue life of the independent crack initiation N_a. Once the independent crack initiates, this maximum stress redistributes, and it can be calculated by:

$$\sigma_{p2} = a_0 - a_1 \times {a_2}^d \tag{4.4}$$

Equation 4.4 is obtained from the finite element model shown in Section 4.3.1. The fitted parameters a_0, a_1, a_2 are listed in Table 4.1 for different stress levels, where d is the distance of this local position from the independent crack.

Table 4.1: The fitted parameters in the function of axial stress state at the cracked region of 90 plies for different stress levels.

Stress level	a_0	a_1	a_2
74% of UTS	91.3933	86.3079	
70% of UTS	86.8237	81.9925	0.1660
66% of UTS	82.2540	77.6771	
63% of UTS	77.6843	73.3617	

The consumed fatigue cycles n_2, under σ_{p2}, can be derived based on a strength-based failure criterion that the residual strength σ_r of the local position should degrade to σ_{p2} when the dependent crack initiates. Therefore, Broutman-Sahu model is adopted here to calculate the residual strength of this local position, as expressed by Equation 4.5.

$$\sigma_r = \sigma_{ult} - \sum_i (\sigma_{ult} - \sigma_{pi}) \times \frac{n_i}{N_i} \tag{4.5}$$

where σ_{ult} is the local strength; n_i is the consumed fatigue cycles at the applied stress level σ_{pi}; N_i is the fatigue life up to final failure of this local position given a constant stress level σ_{pi}, and can be calculated from Equation 4.1 and 4.2. The reason to use Broutman-Sahu model here is that it excludes the extra residual strength tests. Based on this residual strength model, the related n_2 calculated from 100-time Monte Carlo simulations (Step 5 in Section 4.4.2) was averaged and then summed with n_1 to obtain the fatigue cycles consumed at this interactive region for a dependent crack initiation.

Overall, the prediction about the number of cracks as fatigue life increases showed in Figure 4.16 should be improved with the consideration of interaction among cracks. For each statistical distribution of local strength plotted in Figure 4.14, the interactive region and related fatigue cycles of dependent crack initiation were determined. Then, the number of transverse matrix cracks including both independent and dependent ones as fatigue cycles increase was updated. Based on the gauge length 80 mm, the updated crack number can be converted to the crack density, in accordance with the damage monitoring region during tests. Figure 4.19 presents two groups of crack density evolution with the increase of fatigue cycles from both the modelling (area plots) and experiments (dot plots) for the stress levels at 70% and 63% of UTS. As observed, the modelled scatter area covers the most of test data. The negative correlation between crack density and the number of fatigue cycles consumed at the saturation is also achieved by the model. Therefore, the empirical parameters involved in the model and the proposed modelling strategy are appropriate to explain the scatter phenomena of crack evolution.

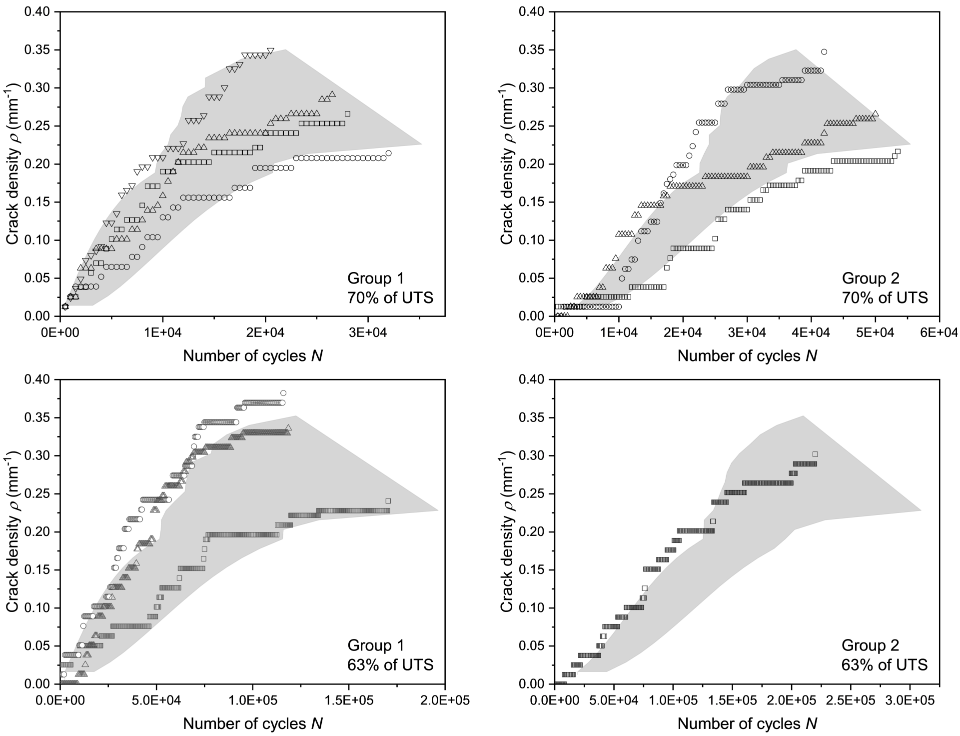

Figure 4.19: Comparisons between the experimental results (dot plots) and modelling results (area plots) about the evolution of crack density for the two groups of specimens under stress levels at 70% and 63% of UTS.

4.4.3. VALIDATION

To further check the applicability of the proposed model, stress levels at 74% and 66% of UTS, which are not included in the data input for the model calibration, are selected here. Figure 4.20 shows both modelling results (area plots) and test data (dot plots) about the evolution of crack density as the number of cycles increases. As observed, the modelled scatter area here seems less qualified than that in Figure 4.19. When compared with Group 2, more test data is covered at the modelled scatter area for Group 1. These results could be attributed to the availability of more data from specimens of Group 1 than that of Group 2 during the model calibration. Despite some mismatch between modelling and tests regarding the history of crack evolution, the model does capture a proper scatter range of saturated crack density and the predicted error about the limits of fatigue life at the saturation of cracks is less than 15%. Therefore, the modelling results correspond to test data in an acceptable way, indicating that the proposed model can provide guidance for experimental design and probabilistic analysis under diverse stress levels.

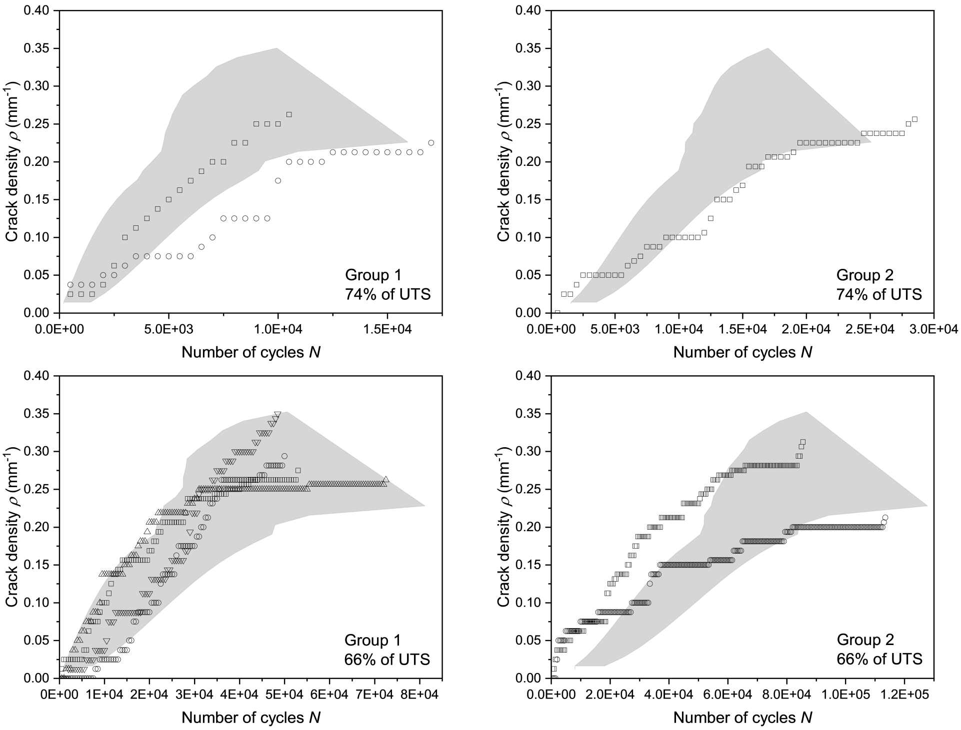

Figure 4.20: Comparisons between the experimental results (scatter plots) and modelling results (area plots) about the evolution of crack density for the two groups of specimens under stress levels at 74% and 66% of UTS.

4.4.4. DISCUSSIONS

IN the model, given a local strength distribution of 90 plies, the severity of interaction among cracks and the fatigue cycles for crack initiation can be determined according to the local strength distribution-dependent crack ratio relation and the local strength-fatigue life relation which were calibrated from test data. Therefore, the statistical distributions of local strength generated in Figure 4.14 behave as the scatter input of the model to produce the variations of crack evolution among specimens. The agreement between the modelling and test data about the scatter area of crack evolution (see Figure 4.19 and 4.20) indicates that the simulated scatter input (local strength distribution of 90 plies) is reasonable to quantify the initial fatigue resistance to cracking and to describe the stochastic crack evolution with the increase of fatigue cycles among specimens. When move to load conditions with high frequency and stress ratio, the model should consider other fatigue-induced factors like cyclic creep and hysteresis heat which could become significant to affect the fatigue resistance to cracking [24–27]. Overall, the assumption that local strength variations are the dominant scatter source to control the fatigue life for crack initiation at 90 plies among specimens, is verified by the present probabilistic modelling under low frequency (5 Hz) and stress ratio (R=0.1).

As the local strength distribution of 90 plies is the dominant scatter source here, the approach to relate the local strength with fatigue cycles for the initiation of an independent crack becomes a key point of the model. The local strength refers to the initial fatigue strength, and it can be related to the in-situ strength of 90 plies collected from static tests. So, the question converts to how to obtain the static strength-fatigue life relation. In view that both static strength and fatigue life for a local region of 90 plies cannot be experimentally obtained at the same time, this relation is hard to be derived. As a result, the Strength Life Equal Rank Assumption (SLERA) applied in Section 4.4.1 is not easy to be proved. D'Amore and Grassia [23] proposed that the SLERA can be applied if the scatter of fatigue life is mainly dominated by the scatter of static strength and other scatter sources induced during the fatigue tests remain negligible. As a final note, it would be meaningful to figure out how to verify this assumption and comprehensively recognise under which load conditions it may hold true.

4.5. CONCLUSIONS

WHAT needs to be stressed here is the obvious ply-block thickness effect on the accumulation and saturation of transverse cracks. Due to to the suppression of manufacturing inhomogeneity, transverse crack evolution at the thin 90-ply block of $[0/90_2]_s$ laminates is similar between specimens. Besides, because of the smaller critical crack spacing, about twice of number of independent cracks generates at the saturated state. Thus, the interactive level among transverse cracks is higher than that of $[0_2/90_4]_s$ laminates, according to the quantification of dependent crack ratio. As for $[0_2/90_4]_s$ laminates, significant scatter of transverse crack evolution is presented at the thick 90 ply-block. This scatter phenomenon has been further revealed by the differences of interaction among cracks for multiple specimens. Severe interaction among cracks is presented for the specimen with a fast growing trend of crack density and consequently a high saturated crack density. A strength-based probabilistic model is established to describe the scattering evolution of transverse cracks among specimens with a similar degrading trend of stiffness. It is found that the distribution of local strength at 90 plies reliably represents the scatter source to produce differences of crack density evolution among multiple specimens.

However, based on the above-mentioned understandings, one may come up with the question that why specimens with different growing trends of crack evolution and saturated crack density share a similar trend of stiffness degradation. This is going to be answered in the next chapter with the analysis of delamination involved.

REFERENCES

[1] H. Pakdel and B. Mohammadi, *Characteristic damage state of symmetric laminates subject to uniaxial monotonic-fatigue loading,* Engineering Fracture Mechanics **199**, 86 (2018).

[2] M. Saeedifar and D. Zarouchas, *Damage characterization of laminated compos-*

ites using acoustic emission: A review, Composites Part B: Engineering **195**, 108039 (2020).

[3] M. Naderi, A. Kahirdeh, and M. M. Khonsari, *Dissipated thermal energy and damage evolution of Glass / Epoxy using infrared thermography and acoustic emission,* Composites Part B **43**, 1613 (2012).

[4] Z. Zhang, G. Yang, and K. Hu, *Prediction of fatigue crack growth in gas turbine engine blades using acoustic emission,* Sensors (Switzerland) **18**, 1321 (2018).

[5] C. Chen, X. Chen, and S. Guo, *Experimental study on acoustic emission characteristic of fatigue crack growth of self-compacting concrete,* Structural Control and Health Monitoring **26**, 1 (2019).

[6] C. Baker, G. N. Morscher, V. V. Pujar, and J. R. Lemanski, *Transverse cracking in carbon fiber reinforced polymer composites: Modal acoustic emission and peak frequency analysis,* Composites Science and Technology **116**, 26 (2015).

[7] P. A. Carraro, L. Maragoni, and M. Quaresimin, *Characterisation and analysis of transverse crack-induced delamination in cross-ply composite laminates under fatigue loadings,* International Journal of Fatigue **129**, 105217 (2019).

[8] H. Shen, W. Yao, W. Qi, and J. Zong, *Experimental investigation on damage evolution in cross-ply laminates subjected to quasi-static and fatigue loading,* Composites Part B: Engineering **120**, 10 (2017).

[9] H. Pakdel, B. Mohammadi, and H. Hosseini-toudeshky, *Stress and energy based prediction of crack distribution pattern in general cross-ply laminates,* Engineering Fracture Mechanics **223**, 106769 (2020).

[10] J. M. Berthelot, A. El Mahi, and J. F. Le Corre, *Development of transverse cracking in cross-ply laminates during fatigue tests,* Composites Science and Technology **61**, 1711 (2001).

[11] J. Montesano and C. V. Singh, *Predicting evolution of ply cracks in composite laminates subjected to biaxial loading,* Composites Part B: Engineering **75**, 264 (2015).

[12] A. Hosoi, K. Takamura, N. Sato, and H. Kawada, *Quantitative evaluation of fatigue damage growth in CFRP laminates that changes due to applied stress level,* International Journal of Fatigue **33**, 781 (2011).

[13] J. A. Glud, J. M. Dulieu-barton, O. T. Thomsen, and L. C. T. Overgaard, *Fatigue damage evolution in GFRP laminates with constrained off-axis plies,* Composites Part A **95**, 359 (2017).

[14] M. Quaresimin, P. A. Carraro, L. P. Mikkelsen, N. Lucato, L. Vivian, P. Brøndsted, B. F. Sørensen, J. Varna, and R. Talreja, *Damage evolution under cyclic multiaxial stress state : A comparative analysis between glass / epoxy laminates and tubes,* Compoistes: Part B **61**, 282 (2014).

[15] H. B. Kahla, Z. Ayadi, F. Edgren, A. Pupurs, and J. Varna, *Statistical model for initiation governed intralaminar cracking in composite laminates during tensile quasi-static and cyclic tests,* International Journal of Fatigue **116**, 1 (2018).

[16] P. A. Carraro, L. Maragoni, and M. Quaresimin, *Prediction of the crack density evolution in multidirectional laminates under fatigue loadings,* Composites Science and Technology **145**, 24 (2017).

[17] Abaqus, *User documentation,* in *Fatigue Life Prediction of Composites and Composite Structures* (Dassault Systemes Simulia Corp, 2017).

[18] R. Talreja, *Damage and fatigue in composites - A personal account,* Composites Science and Technology **68**, 2585 (2008).

[19] P. Chou and R. Croman, *Residual Strength in Fatigue Based on the Strength-Life Equal Rank Assumption**, Journal of Composite Materials **12**, 177 (1978).

[20] H. Hahn and R. Y. Kim, *Proof Testing of Composite Materials,* Journal of Composite Materials **9**, 297 (1975).

[21] A. D'Amore and L. Grassia, *A method to predict the fatigue life and the residual strength of composite materials subjected to variable amplitude (VA) loadings,* Composite Structures **228**, 111338 (2019).

[22] V. Passipoularidis and T. Philippidis, *Strength Degradation due to Fatigue in Fiber Dominated Glass/Epoxy Composites: A Statistical Approach,* Journal of Composite Materials **43**, 997 (2009).

[23] A. D'Amore and L. Grassia, *Principal Features of Fatigue and Residual Strength of Composite Materials Subjected to Constant Amplitude (CA) Loading,* Materials **12**, 2586 (2019).

[24] R. Růžek, M. Kadlec, and L. Petrusová, *Effect of fatigue loading rate on lifespan and temperature of tailored blank C/PPS thermoplastic composite,* International Journal of Fatigue **113**, 253 (2018).

[25] A. V. Movahedi-Rad, T. Keller, and A. P. Vassilopoulos, *Creep effects on tension-tension fatigue behavior of angle-ply GFRP composite laminates,* International Journal of Fatigue **123**, 144 (2019).

[26] A. V. Movahedi-Rad, T. Keller, and A. P. Vassilopoulos, *Stress ratio effect on tension-tension fatigue behavior of angle-ply GFRP laminates,* International Journal of Fatigue **126**, 103 (2019).

[27] M. Eftekhari and A. Fatemi, *On the strengthening effect of increasing cycling frequency on fatigue behavior of some polymers and their composites: Experiments and modeling,* International Journal of Fatigue **87**, 153 (2016).

5

Delamination under fatigue loading

5.1. INTRODUCTION

BASED on the linear relation between stiffness degradation and crack density presented in Figure 4.7(b), it has been inferred that no significant delamination grows inside the $[0/90_2]_s$ laminates to degrade stiffness during the testing. To further confirm this statement, specimens were C-scanned after testing. As shown in Figure 5.1, at the region between two tabs, almost no delamination was detected inside the tested specimens in comparison with the intact one. Therefore, in the present study, the 90-block (0.5mm thickness) used for the $[0/90_2]_s$ laminates completely restrains the growth of delamination due to its low energy release rate for thin plies [1], and the suppression of delamination with thinner plies was also observed by Kötter et al [2]. As a result, transverse cracks are the only dominant damage mechanism during the testing for the $[0/90_2]_s$ laminates.

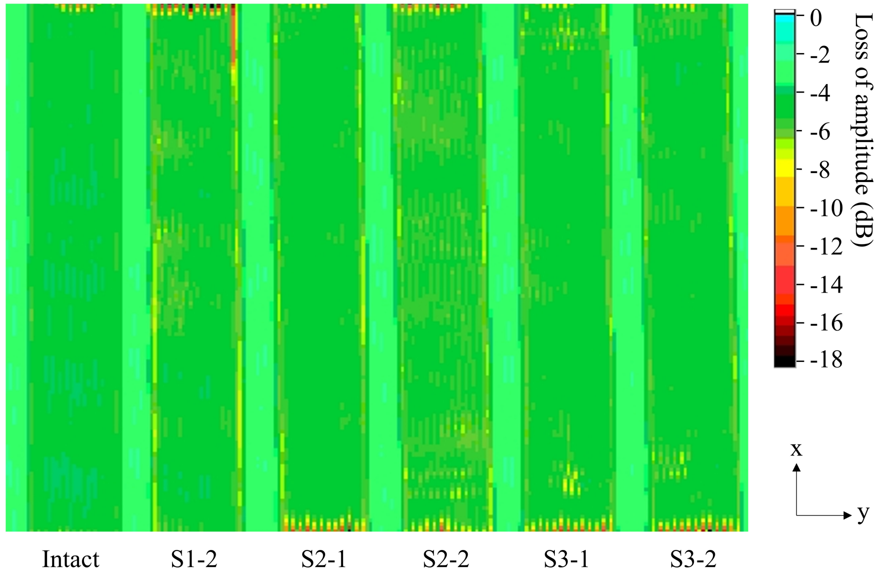

Figure 5.1: C-scanning results for the $[0/90_2]_s$ laminates after testing (S1 - 77% of UTS; S2 - 70% of UTS; S3 - 63% of UTS).Note: a clear visualisation is provided by the digital version of this thesis.

Regarding the $[0_2/90_4]_s$ laminates, it is found that the stiffness degradation does not reach the plateau when transverse cracks saturate. As shown in Figure 5.2, the stiffness reduction at CDS accounts for 43% to 97% of the overall stiffness reduction within Stage I. This phenomenon means that both transverse crack saturation and delamination initiation occurred before the transition moment from Stage I to Stage II. Further, the non-linear relation between stiffness degradation and crack density, as presented in Figure 4.7(a), indicates delamination initiates even before the saturation of transverse cracks to degrade stiffness. Based on the C-scanning results, almost all specimens were locally delaminated after being tested. Therefore, both transverse cracks and delamination should be the dominant damage mechanisms during the early fatigue life for the $[0_2/90_4]_s$ laminates.

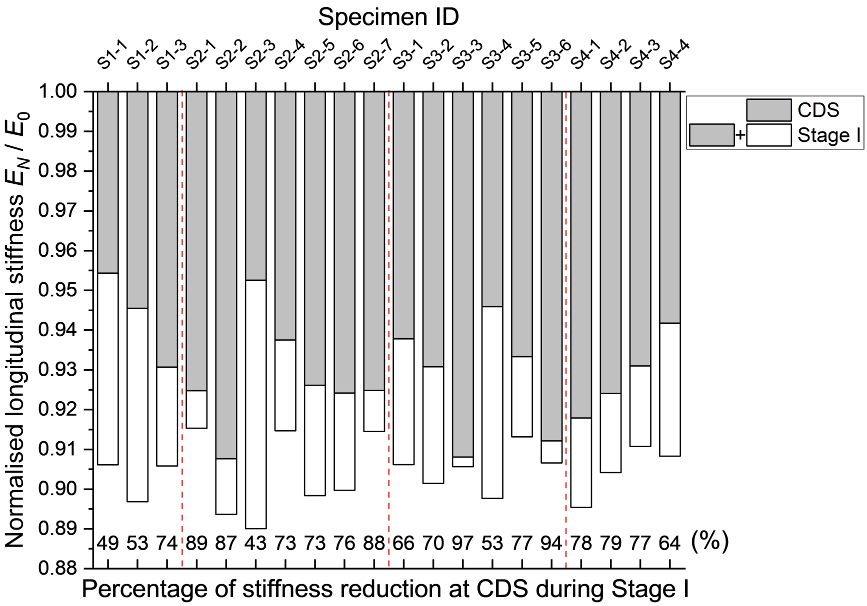

Figure 5.2: Normalised stiffness degradation at CDS and at the end of Stage I, and the percentage of stiffness reduction during Stage I for the $[0_2/90_4]_s$ laminates (S1 - 74% of UTS; S2 - 70% of UTS; S3 - 66% of UTS; S4 - 63% of UTS).

In this chapter, the propagation of delamination for the $[0_2/90_4]_s$ laminates is investigated under different stress levels (see Section 5.2), and further the interaction between delamination and transverse cracks is explored (see Section 5.3).

5.2. DELAMINATION PROPAGATION

IN view of the two-dimensional propagation of delamination at the 0/90 interfaces along both the length and width direction of a laminate, the analysis about delamination growth inside the $[0_2/90_4]_s$ laminates is divided into two parts: Section 5.2.1 describes the propagation from the edge view by image analysis and Section 5.2.2 describes the propagation based on DIC analysis from the front view.

5.2.1. EDGE VIEW

FROM the edge view, it is observed that interlaminar cracks initiated at tips of transverse cracks and then propagated at 0/90 interfaces along the length direction. Interlaminar crack ratio I_r, obtained as the ratio of interlaminar crack length to the gauge length (~ 80 mm), is used to quantify the delamination propagation along edges. Here, interlaminar crack length is obtained by the average of $max\{L_{r1}, L_{r2}\}$ and $max\{L_{l1}, L_{l2}\}$, where L_{r1}, L_{r2} are the total length of inter-laminar cracks located at each interface of the right edge and similarly L_{l1}, L_{l2} are for the left edge. Figure 5.3 plots the evolution of interlaminar crack ratio as a function of fatigue cycles under different stress levels. To further check the proportion of delaminated region at the crucial moments of fatigue damage accumulation process of laminates, i.e. CDS and the end of Stage I of stiffness degradation, a bar chart is plotted in Figure 5.4.

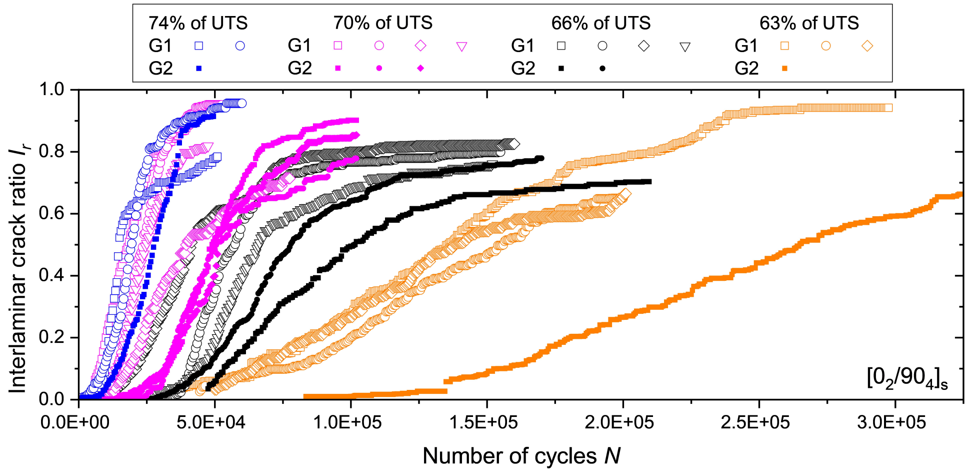

Figure 5.3: The evolution of interlaminar crack ratio as a function of fatigue cycles for the $[0_2/90_4]_s$ laminates (G1-Group 1; G2-Group 2).

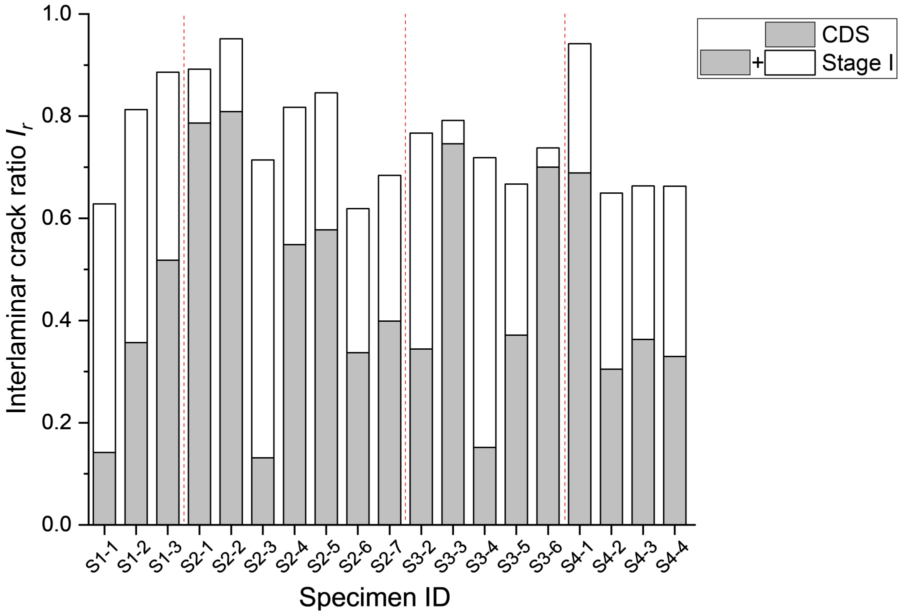

Figure 5.4: Interlaminar crack ratio at CDS and at the end of Stage I for the $[0_2/90_4]_s$ laminates (S1 - 74% of UTS; S2 - 70% of UTS; S3 - 66% of UTS; S4 - 63% of UTS).

As shown in Figure 5.3, the increase of I_r experiences a slow-rapid-slow process during the fatigue loading. At the saturation of transverse cracks (CDS), visible interlaminar cracks can be observed, and some of specimens even show 70% - 80% delaminated region at edges, as presented in Figure 5.4. When the stiffness degradation approaches the second stage, all specimens delaminated more than 60% of the gauge region along edges, and the growth rate of I_r starts to become slowly. Until the end of testing, specimens were almost fully delaminated along the length. Beside the growth rate, the stress level seems to have less effect on the delamination propagation along the edges [3].

5.2.2. FRONT VIEW

CONSIDERING the delamination propagation towards the width direction, the in-situ monitoring remains a challenge for CFRP laminates. Oz et al. observed Poisson contraction and transverse strain concentrations through DIC at the exterior surface of quasi-isotropic CFRP laminates when delamination was generated at interfaces [4]. Following this observation and aiming at developing a DIC-based parameter to describe the delamination growth inside the CFRP laminates, the relations among transverse strain concentration, Poisson contraction and delamination are further explored hereafter.

Figure 5.5 shows a linear growth of Poisson's ratio υ with the normalised area of transverse strain concentration A_C at the DIC interest area for all specimens. A_C is obtained by the total area of transverse strain concentration divided by the DIC measurement area. To quantify the delamination area according to the transverse strain concentration area, the maximum value of transverse strain contour at the gauge region should be fixed for the DIC post-analysis during all fatigue cycles. Here, it is determined as the value of transverse strain when Poisson's ratio starts to increase. As observed, the slop of υ-A_C is nearly the same under all stress levels.

Moreover, the relation between delaminated region from C-scan results and transverse strain concentration region from DIC analysis is explored. For the examples of the specimen S2-1 and S2-2 tested under the stress level of 70% UTS, it is founded that the delamination can be correlated to the transverse strain concentration at numbered local regions in Figure 5.6. This is because more 90 plies are separate from 0 plies with the increase of delamination area. As a result, 0 plies become flexible and perform significant Poisson effect, and transverse strain concentration at the exterior 0 ply is created at delaminated region.

Based on all-mentioned above, Poisson's ratio and transverse strain concentration area can be used to describe the accumulation process of delamination inside the laminate. Hereafter, the normalised area of transverse strain concentration A_C is used to represent the normalised delamination area A_d within the gauge region.

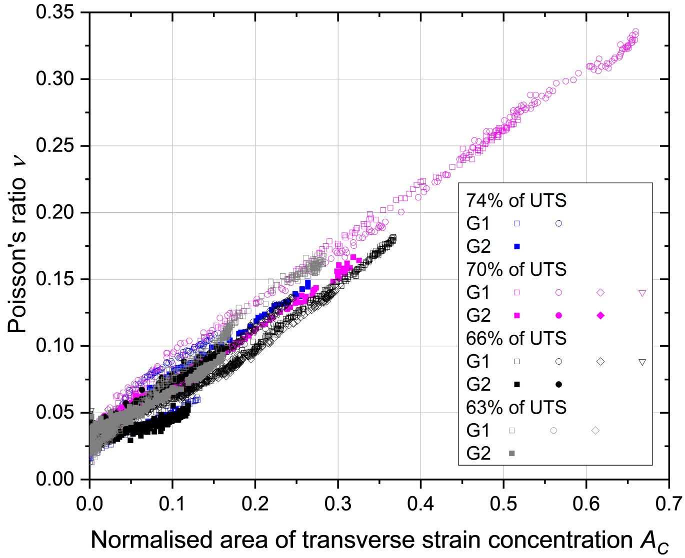

Figure 5.5: Poisson's ratio versus normalised area of transverse strain concentration for the $[0_2/90_4]_s$ laminates.

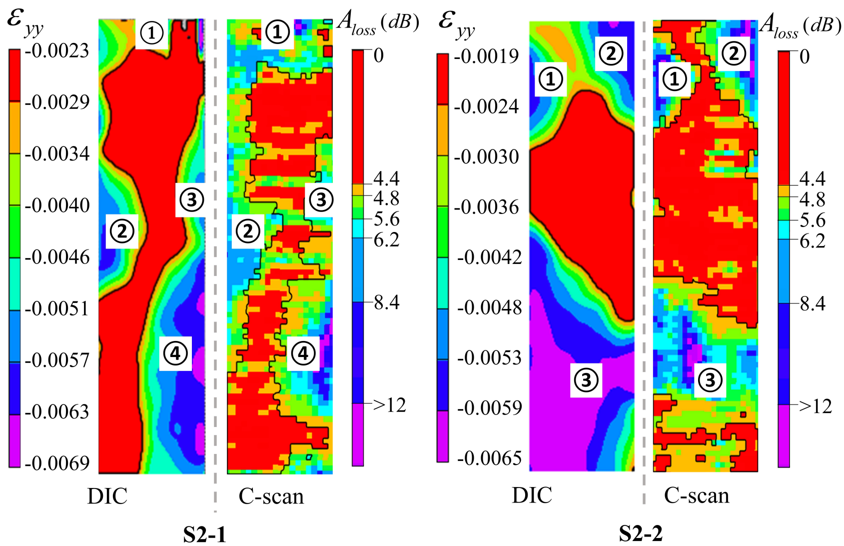

Figure 5.6: Correlation of transverse strain concentrations and delamination at numbered local regions at 1e5 cycles for the $[0_2/90_4]_s$ laminates under the stress level at 70% of UTS (A_{loss}-loss of amplitude).

Figure 5.7 presents the increase of normalised delamination area as a function of fatigue cycles. Unlike the growth along the length, delamination propagates less than the half of the area of the gauge region for most specimens when tests stopped. Besides, most of transverse strain concentrations locate near edges, further indicating that delamination propagated faster along the edges than though the width as reported by O'Brien [5].

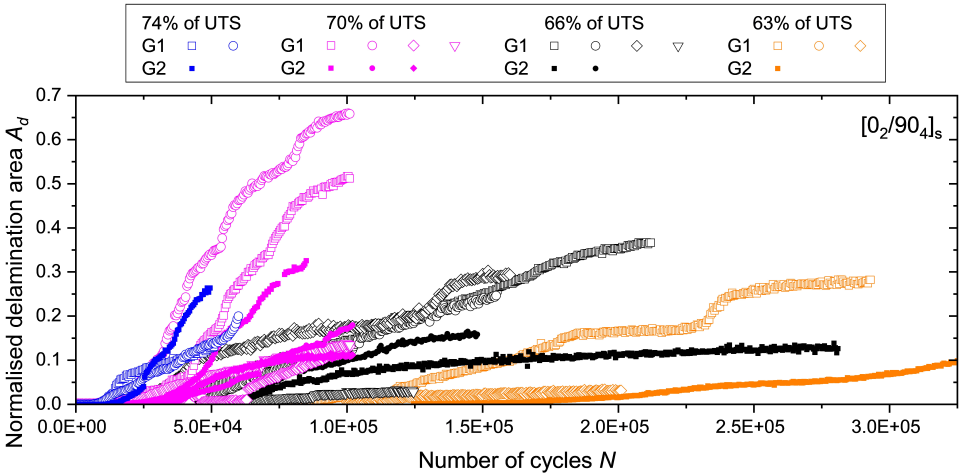

Figure 5.7: The evolution of normalised delamination area as a function of fatigue cycles for the $[0_2/90_4]_s$ laminates.

5.3. INTERACTION BETWEEN DELAMINATION AND TRANSVERSE CRACKING

LIKE the accumulation of transverse cracks, delamination growth scatters among each group of specimens during the early fatigue life for the $[0_2/90_4]_s$ laminates, indicating the existence of different levels of interaction between both damage mechanisms.

Figure 5.8 shows the propagation of delamination along edges and inside specimens as crack density increases. Based on the saturated crack density ρ_S, specimens with ρ_S equals to $0.21 \pm 0.01, 0.26 \pm 0.01, 0.3 \pm 0.01$ and 0.34 ± 0.01 mm^{-1} are classified into four groups for all stress levels. A faster increase of interlaminar crack ratio and normalised delamination area can be observed for specimens with lower saturated crack density, leading to larger delamination propagation along edges and inside specimens at the characteristic damage state. These phenomena indicate saturated crack density can reflect the severity of interaction between delamination and transverse cracks regardless of stress levels. The lower the saturated crack density is, the severer the interaction among both damage mechanisms exists for the $[0_2/90_4]_s$ laminates. Besides, the competitive relation between delamination propagation and crack evolution is also presented in Figure 5.8, as delamination could postpone or prevent further generation of transverse cracks at neighbouring regions [6–8].

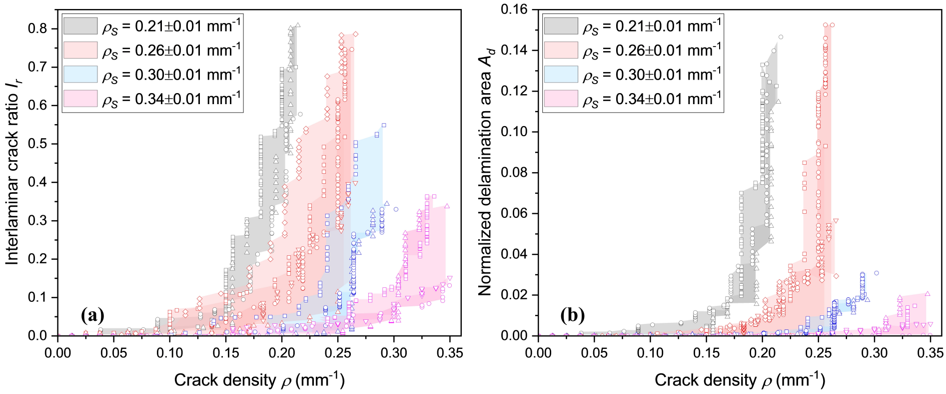

Figure 5.8: The increase of interlaminar crack ratio (a) and normalised delamination ratio (b) with the increase of crack density for the $[0_2/90_4]_s$ laminates.

To explore why the accumulation of these two damage mechanisms restrains each other, the spatial distribution of transverse cracks along edges and delamination within the gauge region is checked at the characteristic damage state and at the end of stage I of stiffness degradation. For an example, considering one of specimens tested under the stress level of 70% UTS, the position of transverse cracks is marked along the 80 mm gauge length, as shown in Figure 5.9(a). In addition, the transverse strain concentration obtained from DIC is also presented, where the red means no delamination and the rest means delaminated region.

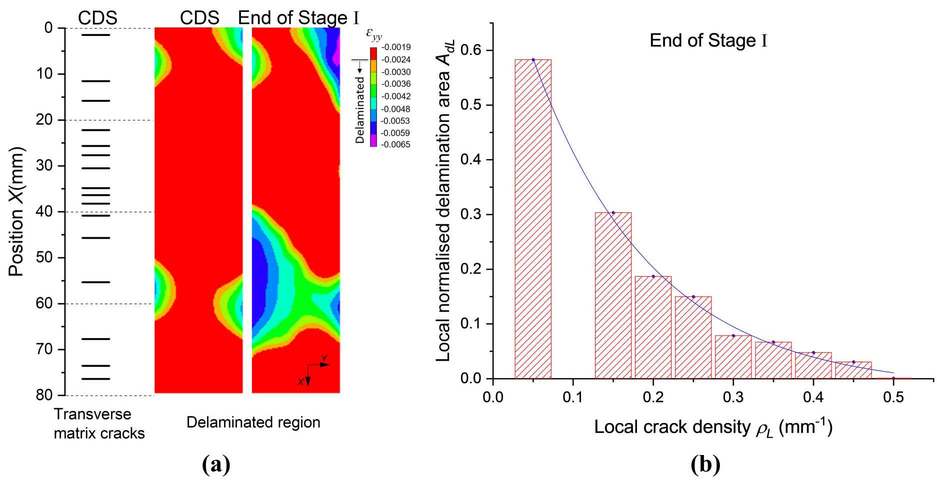

Figure 5.9: Spatial distributions of transverse cracks and delamination at CDS and end of Stage I of stiffness degradation for one of the $[0_2/90_4]_s$ specimens tested under the stress level of 70% UTS (a); local normalised delamination area versus local crack density at the end of Stage I for the $[0_2/90_4]_s$ laminates tested under all stress levels.

As observed, delamination is prone to initiate and propagate at the local region with a large crack spacing. Further, the gauge region of specimens tested under all stress levels is evenly divided into four parts with 20 mm length. Then, the local crack density ρ_L and local normalised delamination area A_{dL} at the end of Stage I are quantified and summarised in Figure 5.9(b), where A_{dL} is the mean value among all specimens. It is obvious that the relation between A_{dL} and ρ_L is nonlinear and the delaminated region is less than 10% when the local crack density is higher than 0.3 mm^{-1}.

5.4. CONCLUSIONS

WHILE only transverse cracks accumulate during the testing with almost non-existed delamination for the $[0/90_2]_s$ laminates, delamination inside the $[0_2/90_4]_s$ laminates initiates before the saturation of transverse cracks rather than at the transition moment from Stage I to Stage II of stiffness degradation. For specimens sharing a similar degrading trend of stiffness, different interactive levels between both damage mechanisms are founded which can be further represented by the saturated crack density. The specimen with a lower saturated crack density usually spends more fatigue cycles to reach CDS (transverse crack saturation), in view that larger delaminated area coexists to restrain the generation of new cracks. The competitive relation between transverse cracks and delamination means that the both damage mechanisms fight for contributing to the energy dissipation and stiffness degradation which can be regarded as constant for each group of specimens. As different competitive levels between these two damage mechanisms are presented in Figure 5.8, the portions of their contributions to the energy dissipation and stiffness degradation should be diverse, thus resulting in the scatter phenomena of the crack evolution and delamination growth among specimens with a similar trend of stiffness degradation.

5

REFERENCES

[1] P. A. Carraro, L. Maragoni, and M. Quaresimin, *Characterisation and analysis of transverse crack-induced delamination in cross-ply composite laminates under fatigue loadings,* International Journal of Fatigue **129**, 105217 (2019).

[2] B. Kötter, J. Endres, J. Körbelin, F. Bittner, H. J. Endres, and B. Fiedler, *Fatigue and fatigue after impact behaviour of Thin- and Thick-Ply composites observed by computed tomography,* Composites Part C: Open Access **5**, 100139 (2021).

[3] A. Hosoi, K. Takamura, N. Sato, and H. Kawada, *Quantitative evaluation of fatigue damage growth in CFRP laminates that changes due to applied stress level,* International Journal of Fatigue **33**, 781 (2011).

[4] F. E. Oz, N. Ersoy, M. Mehdikhani, and S. V. Lomov, *Multi-instrument in-situ damage monitoring in quasi-isotropic CFRP laminates under tension,* Composite Structures **196**, 163 (2018).

[5] T. O'brien, *Characterization of delamination onset and growth in a composite laminate,* in *Damage in composite materials: basic mechanisms, accumulation, tolerance, and characterization* (ASTM International, 1982).

[6] R. Talreja, *Damage and fatigue in composites – A personal account,* Composites Science and Technology **68**, 2585 (2008).

[7] H. Shen, W. Yao, W. Qi, and J. Zong, *Experimental investigation on damage evolution in cross-ply laminates subjected to quasi-static and fatigue loading,* Composites Part B:Engineering **120**, 10 (2017).

[8] H. Pakdel and B. Mohammadi, *Characteristic damage state of symmetric laminates subject to uniaxial monotonic-fatigue loading,* Engineering Fracture Mechanics **199**, 86 (2018).

6

Conclusions and Recommendations

6.1. Summary of main findings

As this thesis is titled, the aim is to unfold the progressive damage accumulation process of CFRP cross-ply laminates during the early fatigue life under tension-tension fatigue. Before the analysis under fatigue loading, $[0_2/90_4]_s$ laminates were studied under static tensile loading. The execution of static tests shows the capabilities of proposed experimental methods on the in-situ damage monitoring. Then, around 30 specimens were fatigued at different stress levels with two types of ply configurations involved (i.e. $[0/90_2]_s$ and $[0_2/90_4]_s$). Both experimental analysis and probabilistic modelling were performed to help achieve the research aim of this thesis. Section 6.1.1 and 6.1.2 summarise the main findings in two aspects: in-situ damage monitoring and early fatigue damage accumulation.

6.1.1. In-situ damage monitoring

Although the challenge is obvious to achieve the in-situ damage monitoring of non-transparent CFRP laminates, the three damage monitoring techniques employed in this thesis, i.e. edge observation by digital cameras, digital image correlation and acoustic emission, do provide sufficient damage-related information. Therefore, it is necessary to have multiple techniques involved for the in-situ damage monitoring of CFRP laminates. In this way, not only reliable monitoring can be guaranteed but also potentials of each technique can be explored in-depth. The highlights are listed as follows:

- The in-situ damage monitoring should be applied at a relatively large gauge region, in view that the damage accumulated at locally small region may not be representative considering the spatial randomness of damage distribution.
- Local strain concentration at the exterior 0 ply from DIC analysis can be used to identify the damaged region of cross-ply laminates. Narrow strips of axial strain concentration occurred at the exterior 0 ply once transverse matrix cracks initiated, and a correlation between the number of strips and the number of cracks was found. The strips, at a later stage, expanded or connected with one another to form wide concentration regions due to the generation of new cracks with a high density. Besides, transverse strain concentration was induced at the delaminated region, in view that the separation between 0 and 90 plies makes 0 plies more flexible to perform significant Poisson effect.
- Based on the correlation among transverse strain concentration area, delamination area and Poisson's ratio, the delamination growth during the fatigue loading can be represented by the increase of Poisson's ratio for cross-ply laminates. For laminates without significant delamination growth, Poisson's ratio decreases as the fatigue cycles increases. Therefore, Poisson's ratio could be considered to identify whether the early fatigue damage is dominant by transverse cracks or involves delamination.
- Cumulative AE energy is well-correlated to crack density with the increase of fatigue cycles for both ply-configurations, indicating it could be sensitive to the generation of transverse cracks for cross-ply laminates and could be used as an indicator of crack density.

6.1.2. EARLY FATIGUE DAMAGE ACCUMULATION

BASED on the experimental analysis and probabilistic modelling, the main findings about the early fatigue damage accumulation of cross-ply laminates are summarised as follows.

- For the $[0/90_2]_s$ laminates, the mechanical response and damage evolution with the increase of fatigue cycles are similar between specimens tested under the same stress level. Transverse cracks are the only dominant damage mechanism in the early fatigue life while almost no delamination was detected during the accumulation of transverse cracks. Consequently, a linear relation between the crack density and stiffness degradation is presented. Although the thin 90 ply-block restrains the initiation of delamination, severer interaction among transverse cracks is presented due to the high crack density compared with the thick 90 ply-block.

- For the $[0_2/90_4]_s$ laminates, significant scatter of mechanical response and damage evolution exits among specimens tested under the same stress level. The scattering crack evolution has been investigated by a strength-based probabilistic model and the variations of local strength distributions of 90 plies among specimens are found to be the main scatter source. Before the saturation of transverse cracks, delamination initiates and both damage mechanisms interact with each other in a competitive way. Different interactive levels between transverse cracks and delamination exist among specimens with a similar trend of stiffness degradation at Stage I. As a result of the interaction, the increase of stiffness degradation with crack density is linear at the beginning but gradually becomes more and more aggressive due to delamination growth for the $[0_2/90_4]_s$ laminates.

- It is necessary to take the ply-block(ply) thickness effect into account for the analysis of progressive fatigue damage accumulation of laminates, according to the differences of mechanical response and damage evolution presented by the $[0/90_2]_s$ and $[0_2/90_4]_s$ laminates. Regarding the mechanical response, the stiffness experienced a bi-linear decrease in a rapid-slow manner for the $[0/90_2]_s$ laminates which seems hardly to reach the plateau, opposite to the stiffness degrading trends of the $[0_2/90_4]_s$ laminates. Also, an increase of Poisson's ratio during the early fatigue life is presented for the $[0_2/90_4]_s$ laminates due to the growth of delamination, while the $[0/90_2]_s$ laminates show the exactly opposite trend caused by the accumulation of transverse cracks. As for the damage evolution, the fatigue cycles consumed to reach the saturation of transverse cracks is about five times longer for the $[0/90_2]_s$ laminates than that for the $[0_2/90_4]_s$ laminates under the stress level at the same percentage of UTS. Besides, the saturated crack density of the $[0/90_2]_s$ laminates is approximately 2-5 times larger than that of the $[0_2/90_4]_s$ laminates.

- The effect of stress levels on the early fatigue damage accumulation is reflected on the growth rates of transverse cracks and delamination. Except this, the accumulation of early fatigue damage is similar among different stress levels for both cross-ply configurations. For instance, the saturated crack density is found to be independent of stress levels.

- The interactive scheme which considers the significant interaction among transverse cracks and the interaction between both damage mechanisms (i.e. transverse cracks and delamination), should be proposed for describing process of early fatigue damage accumulation process rather than the non-interactive one. Dependent crack ratio proposed in this thesis could be used to quantify the interaction among independent and dependent cracks classified by a critical crack spacing. Besides, saturated crack density can reflect the severity of interaction between transverse cracks and delamination regardless of stress levels.

6.2. RECOMMENDATIONS FOR FUTURE WORK

THIS thesis has made some contributions to the understanding of progressive damage accumulation of CFRP laminates during the early fatigue life. However, more efforts are still needed to answer the following open questions.

- **What is the relation between static strength and fatigue life of a local region at off-axis plies of laminates?**
  The Strength Life Equal Rank Assumption (SLERA) has been used to link the static strength and fatigue life distributions at 90 plies, in order to establish the strength-based probabilistic model and predict the scattering crack evolution of $[0_2/90_4]_s$ laminates. It is necessary to verify this assumption under different fatigue loading conditions, where fatigue-induce phenomena like time-dependent creep and cyclic hysteresis heat might be significant.

- **How does the early fatigue damage affect the scatter of fatigue life of laminates?**
  Based on the understanding about the early fatigue damage accumulation, it would be of great interest to go one step further to the damage accumulation in the subsequent fatigue cycles until the failure of laminates. It is inferred that the differences of early fatigue damage accumulation, including the initiation of both damage mechanisms and their interaction, among specimens could affect further the accumulation and interaction of delamination and fibre damage, which later determines the fatigue life. In this way, it is very promising to understand and predict the significant scatter of fatigue life for laminates based on the analysis about their progressive damage accumulation process.

- **How can the stochastic damage initiation and the random microstructure of 90 plies be bridged?**
  The monitoring of damage performed in this thesis is at mesoscale and macroscale. A smaller monitoring scale like microscale would be helpful for exploring the relation between the stochastic nature of damage initiation and the randomness of microstructure. Further, a clear picture may be provided about the scatter sources of experimental results as presented for the $[0_2/90_4]_s$ laminates in this thesis.

- **How can the knowledge about the early fatigue damage accumulation of CFRP cross-ply laminates in this thesis be expanded to other laminate/loading cases?**
  The present analysis focuses on the cross-ply laminates under tension-tension fatigue loading with a constant stress ratio (R=0.1) and frequency (f=5Hz). How-

6

ever, different damage accumulation process is expected for laminates with different stacking sequences and fatigue tests under different loading conditions. For instance, matrix crack might not be the tunnelling ones like cross-ply laminates for laminates with angle piles; different damage mechanisms can be induced like fibre kinking under the compression stress state. Therefore, it is meaningful to expand our knowledge about early fatigue damage from the current study case to laminates with angle-plies and other fatigue loading types like different frequencies, different stress ratios especially for tension-compression and compression-compression fatigue loading.

Acknowledgements

What does a PhD journey mean? When I just started, I thought it means research efforts of some years plus a doctor degree. Gradually, I felt it is not just about research. I met and knew lots of 'you' from worldwide here in Delft. We worked together, chatted together, biked together... Many many nice memories were with 'you' that makes this four-year life wonderful and special.

First of all, great thanks go to my daily supervisor, Dr. Dimitiros Zarouchas. Thank you for guiding and helping when I am lost. Thank you for providing feedbacks, suggestions and answers when I need. Thank you for all the valuable discussions that enlightened me. Thank you also for expanding my limits and making me a better myself. I learnt a lot from you, not only about being professional in research, but also about having a wide eye sight about where to head in the near and far future. All in one sentence - Thank you, Dimitrios!

Besides, I would like to acknowledge my promotor Prof. Rinze Benedictus. Thank you for providing constructive advice on my research work and personal development. Thank you for placing trust in me and giving me the freedom to take my own decisions. Also, my second supervisor, Dr. Sofia Teixeira de Freitas, thank you for evoking my critical thinking, offering valuable suggestions and comments, giving me warm caring, about my work and life. You are my idol!

Then, I am very grateful to Gemma. You are always enthusiastic and efficient to offer help whenever I needed. Thank you for the fast reply of emails I sent to you. Thank you for all the paperwork that you did for me.

Experimental campaigns included in this thesis were conducted in Delft Aerospace Structures and Materials Laboratory in the Faculty of Aerospace Engineering. I am very appreciate for the well-organised lab operation and an amazing team here. I am extremely grateful to Alexander, Berthil, Casper, Dave, Durga, Frans, Fred, Gertjan, Johan, Marianne, Misja, and Victor. Your help and explanation are very important and useful for my research, and all chats and talks with you make more fun of my lab work. My special thanks go to Berthil and Gertjan, without your patient and knowledgeable helps, suggestions and discussions, especially on the fatigue machine and cameras, I cannot perform experiments as expected.

My NB0.42 office mates: Agnes, Aydin, Bram, Fabricio, Julian, Megan, Muhamad, Panos, Roberto, and Satya, thank you for all the nice, interesting, scientific talks. Also, thank you for delivering all the useful information and helps for me especially when I just arrived. Special thanks go to Agnes and Megan, our daily and warm girls' chat, and it is really nice to have you around during this four years; I would also express my special thanks to Julian for teaching and helping me about manufacturing laminates, and Bram for telling me lots of useful and detailed information like how to use overleaf which makes me write this thesis more efficiently.

I would also like to thank everyone (once) working in the Pythia team, Agnes, Christos, Demetrio, Daniele, Ferda, Fressisco, Georgios, Milad, Morteza, Nan Yue, Nick, Panos, Robert and Wangdong. It is such a nice experience to work with you. Special thanks go to Milad, thank you for all the valuable discussions about my research work, teaching me how to use acoustic emission and analyse AE data. Special thanks also go to Nan; It is really nice to meet you, and many nice chats, drinks, gatherings were with you!

Please also accept my appreciation to colleagues and friends I met from the Structural Integrity & Composites group: Ali, Andrei, Calvin, Chantal, Chirag, Davide, Eva, Hongwei, Jesse, John-Alan, Pedro, Lubin, Luigi, Luis, Nan Tao, Nakash, Nicolas, Nitesh, Niels, René, Romina, Roger, Tian, Wenjie, Xiang, Yuzhe and everyone I have forgotten to mention. Besides, I would like to thank colleagues and friends that I met outside the SIC group: Camila, Clemens, Chizoba, Deniz, Inés, Javier, Jingjing, Ozan, Marta, Silvia, Shichen, Ujala, Xiaodong, Yannos, Yuqian and everyone I have forgotten to mention. Thank you for all the nice talks, coffee-breaks, parties, lunches and dinners. Special thanks go to Camila, Romina and Yuqian, for all the closest chat and warm caring.

My boyfriend, Dayou: Lucky me to have you around when I was doing my master and PhD; Lucky me to have you understanding me and supporting me with the best you can. 爱你:)

最后，我想在我这里感谢我的父母。谢谢你们这么多年对我无条件的爱与支持，尊重我的决定与想法。因为有你们的爱与肯定，我才能走地这么远。爱你们:)

Curriculum Vitæ

Personal information

Name	Xi Li	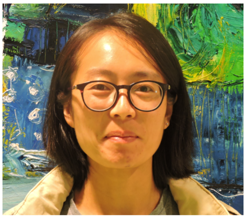
Date of birth	26-7-1993	
Nationality	Chinese	
Email	lixinwpu@foxmail.com	

Education

2011-2014	Honors College Northwestern Polytechnical University, Xi' an, China
2014-2015	**B. Eng**, School of Aeronautics Northwestern Polytechnical University, Xi' an, China Final graduation thesis (March-August 2015) Undergraduate International Exchange Program Institute of Aircraft and Lightweight Structures Technical University of Braunschweig, Braunschweig, German
2015-2018	**M. Eng**, School of Aeronautics Northwestern Polytechnical University, Xi' an, China *Supervisors:* Prof. dr. Yulong Li and Prof. dr. Chao Zhang
2018-2022	**Ph.D**, Faculty of Aerospace Engineering Delft University of Technology, Delft, the Netherlands *Promotor:* Prof. dr. ir. Rinze Benedicus *Copromotor(daily supervisor):* dr. ir. Dimitrios Zarouchas *Second supervisor:* dr. Sofia Teixeira de Freitas

List of Publications

4. **X. Li**, R. Benedictus, D. Zarouchas, *Early Fatigue Damage Accumulation of CFRP Cross-Ply Laminates Considering Size and Stress Level Effects*, International Journal of Fatigue **159**, 106811 (2022).

3. **X. Li**, R. Benedictus, D. Zarouchas, *Analysis of Stochastic Matrix Crack Evolution in CFRP Cross-Ply Laminates under Fatigue Loading*, under review at Journal of Composite Materials.

2. **X. Li**, J. Kupski, S. Teixeira De Freitas,R. Benedictus, D. Zarouchas, *Unfolding the early fatigue damage process for CFRP cross-ply laminates*, International Journal of Fatigue **140**, 105820 (2020).

1. **X. Li**, M. Saeedifar, R. Benedictus, D. Zarouchas, *Damage accumulation analysis of cfrp cross-ply laminates under different tensile loading rates*, Composites Part C **1**, 100005 (2020).